Stony Brook University

Design of Electromagnetic Shock Absorbers for Energy Harvesting from Vehicle Suspensions

A Thesis Presented

by

Pei Sheng Zhang

to

The Graduate School

in Partial Fulfillment of the

Requirements

for the Degree of

Master of Science

in

Mechanical Engineering

Stony Brook University

December 2010

Stony Brook University

The Graduate School

Pei Sheng Zhang

We, the thesis committee for the above candidate for the
Master of Science degree, hereby recommend
acceptance of this thesis.

***Zuo, Lei* – Thesis Advisor**
Assistant Professor in Mechanical Engineering

***Kao, Imin* – Chairperson of Defense**
Associate Dean in College of Engineering and Applied Sciences

***Kincaid, John* – Committee Member**
Professor in Mechanical Engineering

This thesis is accepted by the Graduate School

Lawrence Martin
Dean of the Graduate School

Abstract of the Thesis

Design of Electromagnetic Shock Absorbers for Energy Harvesting for Energy Harvesting from Vehicle Suspensions

by

Pei Sheng Zhang

Master of Science

in

Mechanical Engineering

Stony Brook University

2010

Transportation accounts for 70% of oil consumption, and yet only 10-20% the fuel energy is used for vehicle mobility. One of the important losses is the energy dissipation in suspension vibration. The objectives of this thesis are to investigate energy recovery from vehicle suspensions by answering two questions: (1) how much energy is available while meeting the primary functions of shock absorbers? (2) how can the wasted energy be converted efficiently to electricity?

To answer the first question, a vehicle-ground model, including the stochastic property of road roughness, vehicle parameters, travelling speed, is created with analysis of ride comfort, road safety, and vibration energy induced by road roughness. We found that the dissipative power from all four shock absorbers for a typical mid-size passenger car on ISO class B (good), C (average), and D (poor) roads are approximately 100, 400, 1600 Watts respectively. The sensitivity of the power generation, ride comfort and ride safety to various operational vehicle parameters are further analyzed. Results indicate the power generation is mainly depended on the tire stiffness in which the higher tire stiffness is, the more power generation. However, higher tire stiffness will cause a less comfort and more dangerous ride. Therefore, larger sprung mass will be preferred for achieving a more comfort and safer ride to compromise the negative effects of high tire stiffness. More importantly, the suspension damping also plays as an important role on ride comfort and safety aspects. A more comfortable ride can be accomplished with softer damper. As a tradeoff, the probability of losing ground contact increases which will cause

handling issues and safety hazards. In addition to numerical analysis, experiments are carried out to estimate the dissipated power by measuring the relative displacement of shock absorber on both campus road and highway at different vehicle speeds. Road profile in space domain is then revealed as the shock displacement profile in time domain. The mean power is calculated with the known velocity profile differentiated from displacement profile and the damping coefficient. Results validate the numerical results in which the higher vehicle speeds result in more dissipative power from vehicle suspension systems.

To answer the second question, we designed and compared different electromagnetic (EM) shock absorbers, potentially retrofitted into car suspensions. Two approaches are taken to increase power generation: to increase the flux density B [T] and to boost up the motion. The first type is linear EM harvesters with implementation of both axial and radial magnets. A double layered configuration is favored to increase the flux density inside the air gap. Electromagnetic finite element analysis indicates that we are able to increase the power generation 8 times and energy density by a factor of 5 comparing to the performance of initially designed linear EM. The second type is rotational harvesters with motion magnification mechanism. Two EM shock absorbers using rack pinion and ball screw mechanisms are designed and tested in lab to evaluate the harvester performances. Both rotational harvesters are able to generate more than 100 watts of power. However, there are other forces revealed in rotational harvesters besides damping force. The system is also experiencing frictional and stiffness forces in which further modeling works are needed to acquire better understanding on the harvester dynamics. The performances of all three electromagnetic harvesters are then compared and evaluated.

CONTENTS

LIST OF FIGURES

LIST OF TABLES

ACKNOWLEDGEMENTS

This thesis was started years ago and finally it comes to an end with the help from many people. Without them, I will not be able to accomplish this work. I would like to express my sincere thanks to everyone who helped, encouraged, and supported me throughout this journey.

First, I would like to give thanks to my advisor, Professor Lei Zuo. He is a knowledgeable and brilliant person who conveys his passion and enthusiasms wholeheartedly in his research areas. His creativity and hard-working attitude influent and encourage me to overcome all kinds of obstacles and to move forward with confidence. I am honored to have him as my advisor.

Next, I express my appreciation to my team and my lab mates for providing help and encouragement. Without my team, Zak, Hani, and Chris, I will not be able to build the rack and pinion prototype for my experiments. They stayed for further improving the design prototype. Their contributions on the design and manufacturing are meaningful. So does my lab mates, Xiudong, Xiaoming, Tao, Gopi, and Wanlu. Their encouragements give me strength to move on and finish my work. Especially, thanks to Xiudong and Tao for their help one road data acquisition.

Lastly, I would like to thank my loved one, Sissi. Her support and devotion makes my life easier and better, so I can devote myself in constituting the thesis.

CHAPTER 1 SUSPENSION OVERVIEW

1. SUSPENSION OVERVIEW

Vehicle suspension system is a mass-spring-damper system that isolates vehicle body frame from road random disturbance. Springs counter the weight of vehicle body. Dampers, also called shock absorber, undoubtedly they are the key components to damp the vibration which is transmitted from ground. More importantly, dampers are design to reduce the sudden effects of road disturbance such as hitting on a bump to achieve a smooth ride.

In general, dampers are categorized into three classes according to their functionalities which are passive damper, semi-active damper, and active damper. As a result, the suspension systems are also divided into passive, semi-active, and active suspension systems.

Conventionally, dampers are designed to dissipate vibration energy into heat via viscous fluids or dry frictions. Hydraulic passive dampers are common used in vehicle suspension system due to its simplicity and economic value. Nowadays, as the mechatronics and magnetic materials are well developed, the suspension systems tend toward to semi-active and active configurations to improve the vibration migration performance. Instead of dissipating the vibration energy into heat wastes, electromagnetic damper will transform the energy into electricity and store it for late use. The stored electricity can be used to tune the damping force of the damper to improve the suspension performance or to power car electronics to increase vehicle fuel efficiency. This is so called semi-active suspension and it has advantages over traditional suspension system. Active suspension system has great performance on vehicle body isolation and rider's comfort. However, the payoff of this great performance is the exclusive usage of energy. Moreover, the performance will not be achieved when the power is out. Thus, the safety issue is well considered for active suspension system.

Electromagnetic dampers are designed to harvest vibration energy as a vehicle travels on a road and at the same time achieve typical damping force. In addition, sensors and micro-controllers can be applied to calibrate damping force while vehicle experiences different road input such as hitting on a bump or rolling over a hole. The semi-active performance of electromagnetic damper will greatly improve rider's comfort in all kind of situations.

1.1. MOTIVATION AND THESIS OVERVIEW

Green energy is one of the most popular topics nowadays. The future of clean energy technology is foreseeable, especially on vehicle industry. U.S. Department of energy data [1] show the automobile consumes 70% of the total oil consumption in the United States. Department of Transportation [2] statistically analyzed the total oil consumption for automobiles are more than 175 billion gallons annually. However, the vehicle fuel efficiency is not desirable as Fueleconomy.gov [3] pointed out that only 16% of energy is actually used for driving. Therefore, the Department of Energy [1] has announced a 14 million dollars funding to increase vehicle fuel efficiency in 2005, and secretary Chu declare 187 million dollars to improve vehicle efficiency for heavy-duty trucks and passenger cars in January 2010. If only 16% of energy is actually used to drive, where does the rest amount of energy go? Figure 1.1 shows the typical energy flow of passenger cars on the road. Theoretical results show a maximum of 10 % fuel efficiency can be recovered from vehicle suspension system by implementing regenerative shock absorbers as illustrated in dashed square.

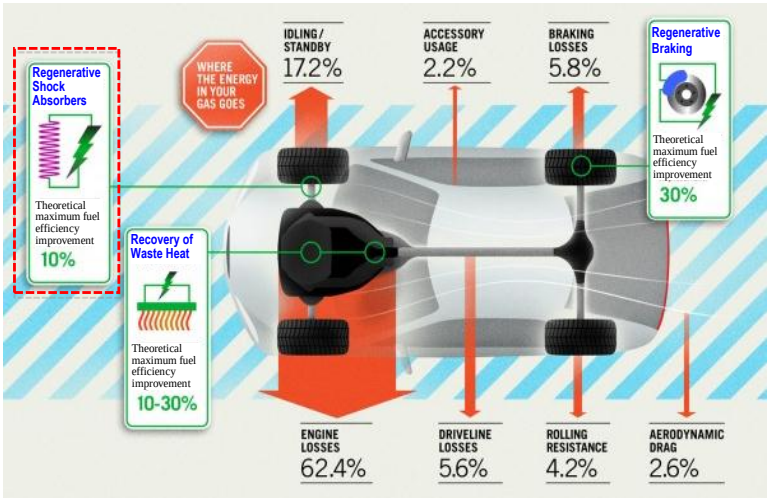

FIGURE 1.1 ENERGY FLOW OF A TYPICAL VEHICLE AND THE OPPORTUNITY OF ENERGY

One of the important mechanisms of energy loss for automobile is through vehicle vibration. For the past hundred years, the vibration energy of vehicle was dissipated into heat waste by frictional damper in suspension system. Assuming the vertical velocity of the damper's relative motion is from 0.15 - 0.4 m/s with a typical damping force of 1500 Ns/m, the power is defined as the product of the damping force and the velocity square, thus the amount of energy wasted by all four shock absorbers are from 100-1600 watts which is on the same order of the vehicle alternator (500-600 Watts, with 50-60% efficiency). Therefore, if the amount of energy wasted by all four shock absorbers is harvested for driving, we can increase the fuel efficiency by 1-8%. According to the US Bureau of Transit Statistics [4] for 2008 there are 255 million registered passenger vehicles in the US. Let us say on average vehicles are driven 1.5 hours per day. If we harvest the vehicle vibration energy at 400 Watts, we can continuously save the energy at power rate of

255,000,000 X 1.5 hours X 400 Watts/24 hours = 6.4 GWatts

This is half of the total installed wind turbine capacity in US, which is 11.6 GWatts by the end of 2006.

The potential of regenerative shock absorber is foreseeable and is the motivation for this thesis research. The first chapter of this thesis is the review of current vehicle

suspension systems and the literature works that have been done on regenerative shock absorbers. Chapter 2 compares the numeric and experiment results of road-vehicle dynamics including suspension performance and power. The tradeoff between ride comfort, ride safety, and dissipated power is discussed and the sensitivity is studied to understand the compromise of different vehicle parameters on energy harvesting and the primary suspension functions. Chapter 3 gives a visual understanding on the electromagnetic harvesters including linear electromagnetic harvester and rotational harvester. Linear harvester design is studied by Finite Elements Method using ANSYS. Both axial and radial magnets are implemented to understand the performance of linear harvester with different configurations and arrangements. Significant improvement from previous single layer harvester is revealed in new design. The evaluation of the performance of rack and pinion harvester is conducted thereafter. An electromagnetic harvester prototype is built using rack and pinion mechanism to validate the feasibility and advantage of motion magnification. In addition to rack and pinion design, a ball screw mechanism harvester is examined to compare the performance with rack and pinion design. Chapter 4 evaluates the performances of all three EM harvesters from different perspectives. Chapter 5 summarizes all the works have been done to achieve higher energy generation by introducing new configurations of linear electromagnetic harvester and motion magnification on rack & pinion and ball screw harvester. Future works on harvesting circuit and vibration control is briefly discussed.

1.2. VEHICLE SUSPENSION SYSTEM

The primary function of vehicle suspension system is to damp out vibration transmitted from road irregularities, therefore achieve a comfortable ride. The suspension system consists of a sprung mass (car body), unsprang masses (wheels), springs, and dampers. As the wheels roll on the road, the irregularity of road frame acts as displacements input. Vibration motions are transmitted from the wheels to car body at certain frequency range. At the same time, springs and dampers act as the vibration filters which stopping vibration transfer to the car body to distract the driver.

According to the level of controllability, suspension systems are classified as

passive, semi-active, and active suspension systems. Passive suspension system is commonly used in commercial passenger cars due to its market value. The damping force is tuned and fixed to a constant value. Semi-active suspension system utilizes the road input and provides better vibration isolation by changing damping force according to road profile. Active suspension system applies external force from actuator to counter the vibration from ground to achieve excellent vibration migration.

1.2.1. PASSIVE SUSPENSION SYSTEM

Passive suspension system is widely used in today's automobile industry. They are designed to dissipated vibration energy through fluid or dry friction, and they take advantage of economic value and simplicity. In general, the system is consisting of springs and single or twin-tube dampers. Generally softer damper provide better rider comfort, while stiffer damper achieve better stability. Thus, the damping force of the passive suspension system is tuned to its optimal condition which can successfully damp most road irregular input. However, the system experiences different road inputs with constant damping force. Therefore, the performance of isolation system will not be friendly when the road conditions shift constantly.

1.2.2. SEMI-ACTIVE SUSPENSION SYSTEM

Semi-active suspension system takes the advantage of changing the damping force by external power when vehicle experience different road irregular inputs. For example, when the vehicle hits a bump, the sensor and micro-controller take the input signal and vary the damper characteristic to eliminate the vibration in a short period of time. The performance of semi-active suspension system is better than passive suspension system, especially response to sudden effects such as hitting a bump. Moreover, if the controller fails to its function, the semi-active suspension system still can perform as passive suspension system. One typical semi-active suspension system is using MR-fluid damper, where the fluid viscosity can be tuned accordingly to achieve desired damping force to counter different road irregular input. However, the market value of MR-fluid dampers is expensive and the properties of MR degrade with time, temperature, and sealing problem.

1.2.3. ACTIVE SUSPENSION SYSTEM

Active suspension system relies on external power to isolate the car body from ground. The performance of active suspension system using feedback control is certainly outstanding. In active suspension system, an actuator acts as the external force to suppress the vibration. However, active suspension system is only implemented for certain vehicles due to the matters on size, weight, power consumption, and price. Moreover, if the power is down on suspension system, the vehicle will experience zero damping force. Therefore, safety issue is also concerned for active suspension system.

1.3. DAMPERS IN VEHICLE SUSPENSION SYSTEM

Dampers in vehicle suspension system are also known as shock absorbers. Conventionally, dampers are designed to dissipate vibration energy through fluid, air, or dry frictions. Commonly seen passive dampers are mono-tube and twin-tube oil damper in today's commercial passenger cars. Semi-active dampers receive more attention nowadays because they can achieve better isolation performance. Several concepts of semi-control strategies are explored and applied to vehicle suspension system such as solenoid-valve, ER-fluid, MR-fluid, Eddy current and electromagnetic dampers. Active damper is simply an actuator. They are designed to achieve the best isolation performance with the tradeoff of power consumption, price, and size.

Among all the semi-active dampers, they can be subdivided into regenerative and non-regenerative damper. Non-regenerative dampers consume external power as active damper. Without external power source, the semi-active damper has the same properties as passive damper. Regenerative dampers harvest vibration energy while achieving expected damping force. The vibration energy is then transformed into other forms such as electricity and stored. The energy is used for powering sensors and micro-controllers to tune the damping forces to control the vehicle body isolation. At the same time, the unused power can be inserted to vehicle power circulation to reduce the car generator's duty; thus, increase the vehicle fuel efficiency. Regenerative semi-active damper receives more attention on its advantage of self-powering and energy generation.

1.3.1. PASSIVE DAMPERS

Passive damper is often referred to passive hydraulic damper. It is the conventional type of damper used in most automobile industry nowadays. Thus, passive hydraulic damper occupies the major proportional share in damper market due to its market value and simplicity. The damper suppresses vehicle vibration by a piston with holes moving through oil. The viscosity of oil resists the flow from moving through holes. In addition, holes are covered by valves to create extra resistible force and unidirectional flow.

There are two basic configurations of passive hydraulic dampers as shown in Figure 1.2, single tube and twin-tube dampers. A single tube damper consists of a piston moving in a sealed cylindrical tube. The tube is further divided in three chambers: compression oil chamber, extension oil chamber, and gas chamber. As the piston moves inside the tube, the liquid inside the tube is compressed and pushed to corresponding side through the holes on piston. The size of holes determines the damping force of a damper. Moreover, valves inside the holes provide one-way flow direction therefore achieve different damping forces on compression and extension. The gas chamber allows the volume of piston rod to enter a damper. In addition, gas chamber also carries spring effects.

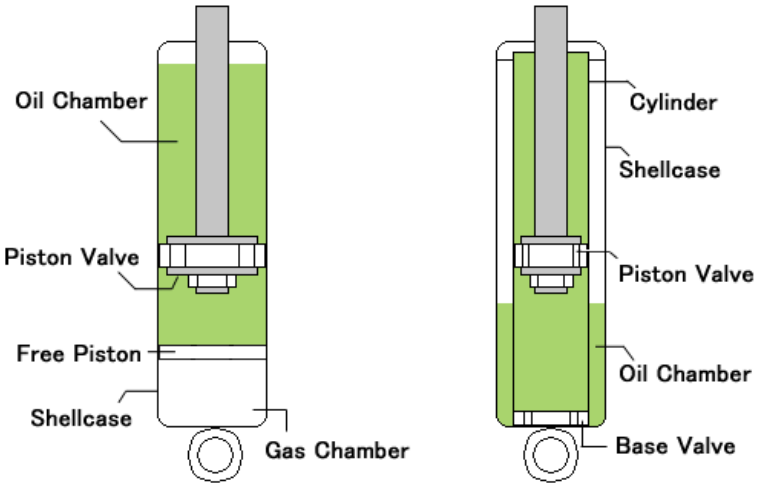

FIGURE 1.2 PASSIVE HYDRAULIC DAMPERS, SINGLE TUBE AND TWIN-TUBE SHOCK

Similar to single tube damper, twin-tube damper also has three chambers but it is more complicated. The compression chamber is interconnected with gas chamber. Instead of having holes only on piston, twin-tube damper also carries hole on the bottom wall of the inner tube. When the damper is experiencing compression, both holes on piston and inner tube determine damping force. When the damper is under extensional force, holes on piston will have major effects of damping force.

Single tube dampers are simpler in design and manufacturing. Thus, they are cheaper and have higher market share. However, the gas pressure inside the gas chamber experiences wider range. In contrast to single tube damper, twin-tube dampers are more complex, the designs of interconnected compression and gas chamber constraint the placement of the damper to be only in one orientation, and they often have difficulty on dissipating heat energy. In addition, the advantage is that the gas pressure is relatively smaller inside the gas chamber compare to single tube damper.

1.3.2. SEMI-ACTIVE DAMPER

Semi-active damper uses technique of adjusting valves or changing the viscosity of fluid inside the damper to achieve desired damping force. Similar to passive hydraulic dampers, they are designed to have damping force proportional to the relative velocity of the damper. Nowadays, solenoid-valves and MR-fluid dampers are commercialized to achieve semi-active control over vehicle vibration isolation.

Solenoid-valve semi-active damper works by tuning the valves to achieve desired damping. The basic principle of solenoid-valve damper is shown in Figure 1.3. When the power is on, the valve is open, thus the damping force is decreased to have softer ride. When the power is off, valves are closed, there are less fluid moving through holes in the same time period, therefore larger damping force achieve. In addition, solenoid-valve damper can provide high speed, accurate flow control.

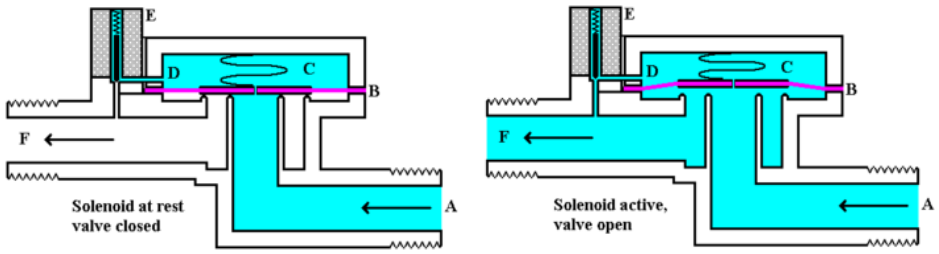

FIGURE 1.3 SOLENOID VALVES WORKING PRINCIPLE, OPEN AND CLOSED STATES

MR-fluid has the characteristics of changing fluid viscosity when it experiences magnetic fields. In a MR-fluid damper, the oil is surrounded with electromagnets. As shown in Figure 1.4, the particles in MR fluid are free to move in unmagnified state. However, they are quickly aligned in certain geometry when the magnetic field is applied, thus the fluid becomes thicker which make it more difficult to pass through holes and higher damping force achieved.

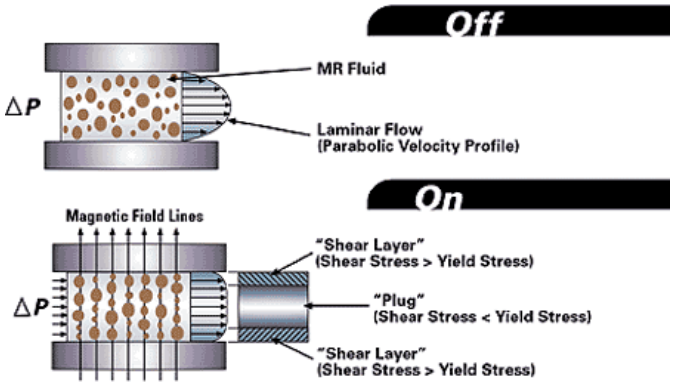

FIGURE 1.4 MR DAMPER WORKING PRINCIPLES, ON AND OFF STATES

The thickness of fluid depends on the applied magnetic fields. The stronger the magnetic field is applied; the oil will have higher viscosity corresponding to higher damping force. Moreover, the magnetic field is adjusted by the current pass through wires. Therefore, the reaction time to adjust different damping force becomes significantly short which is on the order of millisecond.

Both solenoid-valve and MR-fluid dampers have accurate adjustment of damping force. Solenoid-valve damper involves physical actions on opening and closing valves which create delay on reaction time and resolution is relatively smaller than MR-fluid

damper. The increase in number of valves will achieve higher resolution. MR-fluid damper has smoother damping variance. However, the power consumption becomes an issue when higher damping force is in demand.

1.3.3. ACTIVE DAMPER

Active damper also refer to electromagnetic actuator. It relies on external power source to drive the actuator to counter the disturbance transmitted from ground irregularities. In general, they have the best ability to achieve vibration isolation. Unlike conventional hydraulic damper, the damping force is generated by the motor inside electromagnetic damper. There are several types of active approaches for vibration isolation. Mostly commonly seen are linear electromagnetic actuator, ball screw electromagnetic damper, and rack-pinion based electromagnetic damper.

Linear electromagnetic actuator is the first concept introduced to achieve active control. The working principle is based on Faraday's law. When there is current passing through wire coil, magnetic field is generated, the magnetic field generated by current will react to the magnetic field of permanent magnets. The direction on force depends on the direction of current flow. There are two types of linear actuators, moving coil and moving magnets. They are named after the moving parts of the linear actuator. Anyway, the linear actuators are simple to design and manufacture, but the stroke is limited and output force is relatively small.

Since a linear electromagnetic actuator can only provide limited amount of force, ball screw electromagnetic actuator is introduced to solve the shortage of force. The linear motion is provided by a rotatory motor, where ball screw acts as the linear-rotatory transmission. A gearbox in between the ball screw and motor provide magnification function to amplify motion, thus shorten reaction time. Although ball screw provides enough counter force, the resistant force of transmitting rotational to linear motion is significant, system efficiency is considerable, and the actuator's life time is also a concern.

Rack-pinion damper is similar to ball screw electromagnetic damper; they both rely on motion transmission from rotational to linear. Differently, the motion is transmitted by rack and pinion design, and a bevel gear is implemented for 90 degree transmission. However, the acting force on the rack and pinion is off-centered which will affect the life time of the damper and the integration of rack & pinion mechanism is a concern.

Based on the concepts of electromagnetic actuators, Bose Corporation [5] has proposed an active electromagnetic suspension system as shown in Figure 1.5. The amount of electrical power delivered to its motor is determined by using closed loop feedback control. However, the system is too expensive to be commercialized.

FIGURE 1.5 ACTIVE SUSPENSION SYSTEM BY BOSE

The Michelin Company [6] also illustrates its active wheel driving system in late 2008. Michelin investigated an active suspension system on the wheel as shown in Figure 1.6. The new design of active control will achieve 3ms response time as Michelin claims. However, the design does not fit current vehicle structure, and it won't be feasible to replace the current suspension system.

FIGURE 1.6 ACTIVE WHEEL BY MICHELIN

1.4. OVERVIEW OF LITERATURE ON REGENERATIVE SUSPENSION

Due to global energy concern, new forms of clean energy technologies are favored. However, the dependence on gasoline to power our daily life won't fade away in short future. Nowadays, the world's daily consumption on oil is 85220000 barrels said Department of Energy [1]. More importantly, Department of Transportation [2] points out that U.S. account for ¼ of world oil usage and 70% of oil are used for transportation. One the other word, if we can improve the efficiency of running vehicles, we can greatly save oil consumptions, thus enhances environmental protection. Energy is partially converted to move vehicles, the rest of them are lost in other forms of waste such as heat, light, etc. As previously discussed, energy lost due to vibration through suspension system is on the order of hundred to thousand watts. By recovering the dissipative energy, we can improve the fuel efficiency by 2-8 %, thus we make the vehicles cleaner. The potential of energy regeneration from shock absorbers caught researchers' attention. More and more research studies have been done on regenerative shock absorbers.

The objective of the section is to gain an understanding on the field of regenerative shock absorber and works have been done previously. The theoretical research on the regeneration feasibility of vehicle suspension vibration energy has begun since late 1970s. Karnopp [7] made a considerable contribution on suspension power requirement and active suspension system. He analyzed the energy loss on damper system. Energy dissipated by shock absorbers are calculated and modeled by Hammad [8] to verify the existence of energy who claims 1.5 kW of dissipative energy from shock absorbers. However, Hsu [17] claims only 400 Watts of power are dissipated from all four shock absorbers on the same condition. Suda and Nakano [9] experimentally validate the feasibility of performing active suspension control using regenerated energy from shock absorber. This section will review the researches on regenerative suspension system and different regenerative harvester prototypes built by researchers will be briefly discussed. Knowing other's work on this field is a great source and reference for my thesis and contribution in this area.

There are two types of regenerative suspension mechanisms; they are mechanical and electromagnetic regenerative suspension systems. The mechanical type converses the vibration energy into hydraulic or pneumatic energy by mechanical transmission, and energy then can be stored in the accumulators. The electromagnetic type converts vibration energy into electrical energy and stores to a battery to power car electronics.

1.4.1. MECHANICAL REGENERATIVE SUSPENSIONS

Fodor and Redfield [10] proposed the variable linear transmission (VLT) mechanism to harvest vibration energy by mechanical transmission. It is proposed to meet the barrier potential of a storage device while maintaining required damping force. The power stored is the product of force and velocity input. A piston forces fluid into a large hydro pneumatic accumulator where a regenerative damper employs the power and convert the input force into a desired damping force. The VLT is analyzed using a quarter car model as shown in Figure 1.7. The function of the lever beam is to magnify input force and velocity to overcome the storage device's barrier potential.

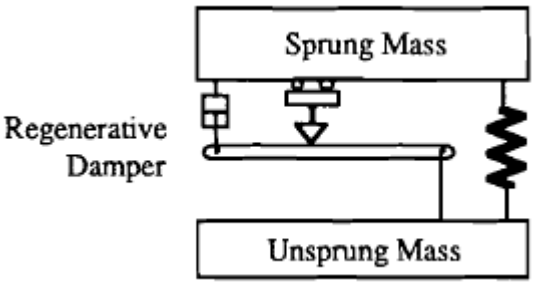

FIGURE 1.7 VLT SYSTEM FOR MECHANICAL ENERGY STORING

The input force necessary to provide storage is a function of the fulcrum position which can vary from zero to infinity regardless the direction of force. The movable fulcrum makes the system variable and to adjust the desired damping force.

The ideal fulcrum actuation acts as a passive viscous damper since the force is direct proportional to fulcrum's position with a constant viscous damping coefficient. However, the ideal case cannot be achieved in reality. Thus the non-ideal fulcrum actuation is considered. Force actuators typically act as low pass filter of control input

and adding phase lag. Slow fulcrum actuation exists to position the fulcrum in which average position will occur and the damper will behave as a coulomb friction damper. The VLT regenerative damper can generate constant force to achieve desired performance. However, some constraints show to stop the condition to be ideal. Moreover, the feasibility of VLT system is the main concern. Result shown that to perfectly control the random vibration induced by road roughness, some mechanical system need to be reduced to single degree of freedom. More importantly, the energy required to control the position of fulcrum is much larger than energy generated in reality.

James A. Stansbury [11] patented a regenerative suspension with accumulator systems. A pump attaches via a hose to a central accumulator cylinder that is mounted along the frame rails underneath the vehicle. Pressurized fluid, air, or other material charges the accumulator. The Pressurized fluid, air, or other material is controllably released via a valve in order to perform work. He also claims a hydraulic pump can be installed to harvest electricity when flow is in motion and the energy can be used to recharge car battery or power car electronics.

The advantage of mechanical regenerative suspension is that the accumulator can be added to the current hydraulic or pneumatic suspension and reduce the energy demand on actively controlling vibration. However, the low frequency and slow response are the primary drawbacks. In addition, VLT does not act ideally in reality in which it cannot control vibration desirably.

1.4.2. ELECTROMAGNETIC REGENERATIVE SUSPENSION

Since 1980s, permanent magnets were favored in electromagnetic suspension to provide semi-active force. The damping force can be simply changed by tuning the shunt resistances. In addition, electromagnetic shock absorbers utilize vibration energy and convert it into electrical energy by linear motors or rotatory motors to perform self-control. Furthermore electromagnetic suspension system can be modeled as passive, semi-active, or active suspension system.

1.4.2.1. LINEAR-MOTOR REGENERATIVE SUSPENSION

In 1997, Okada, Harada, and Suzuki [12] studied the active and regenerative vibration control using linear actuator. The linear actuator acts as damper and generator respectively as shown in Figure 1.8. When the shock is oscillating at high velocity, the shock is on regenerative state. Otherwise, at low suspension velocity, the generated energy is not enough to overcome the barrier potential and the system will be shunted with a resistor and acts as passive damper.

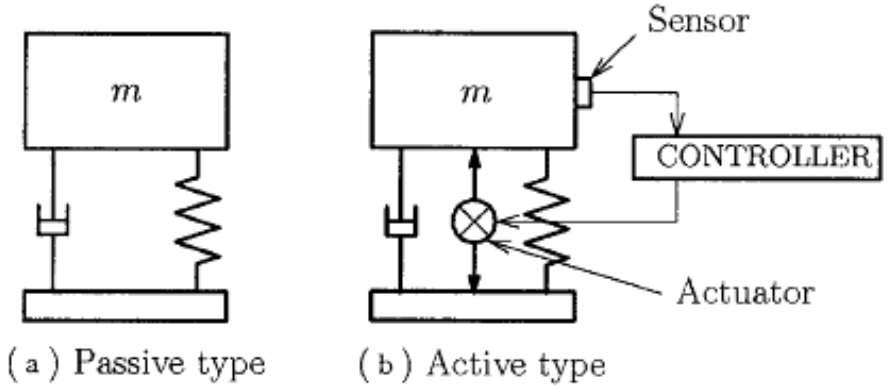

FIGURE 1.8 REGENERATIVE VIBRATION CONTROL, PASSIVE AND ACTIVE

In 2003, Nakano, Suda, and Nakadai [13] investigated the research on self-powered regenerative shock absorber by using linear motor. The actuation power is estimated by evaluating the suspension displacement, velocity, linear motor modeling and sensing system. Thereafter, the regenerative power is studied with shock dynamics. A power balance analysis is conducted to study the feasibility of achieving active control. Furthermore, Figure 1.9 shows a two-degree-of-freedom of quarter car prototype that is built with integrated linear actuator and sensors to verify theoretical results on self-powered active control.

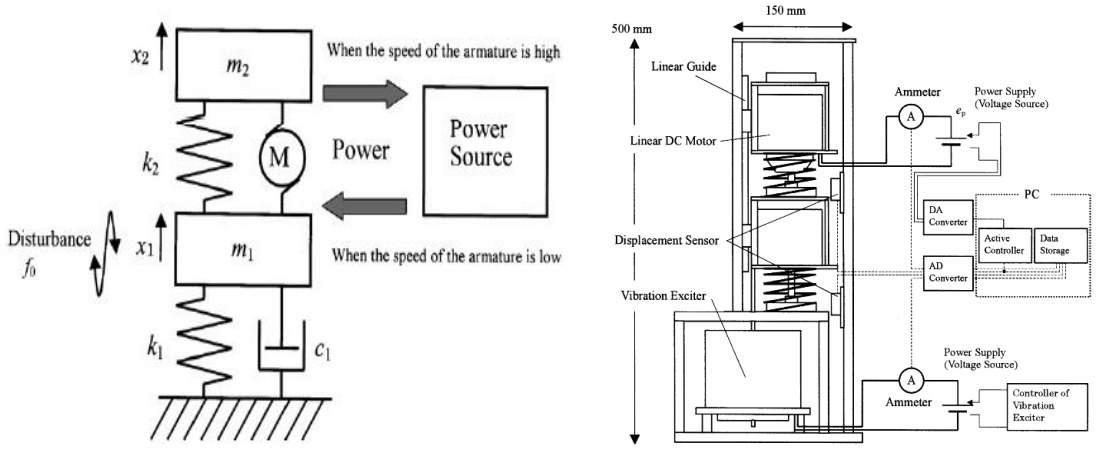

FIGURE 1.9 QUARTER CAR MODEL AND CONTROL USING LINEAR ACTUATOR

The ground excitation is modeled as the white noise input which is driven by a shaker. A circuit is designed to harvester energy when the speed of the armature is high, or the suspension acts actively by shunt the circuit with a resistor. The regenerative circuit is shown in Figure 1.10. The alternative current is converted into direct current to charge the battery. Vice versa, battery is used for providing alternative actuating force to counter road-induced vibration.

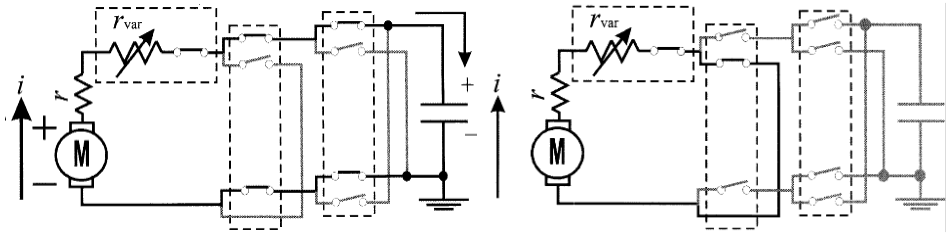

FIGURE 1.10 CIRCUIT DESIGN FOR CHARGING AND PASSIVE STATES

Sensors are applied for feedback control. The experimental result validates the theoretical prediction. The system is able to do self-active control. However, the actuator cannot generate enough force at certain condition.

In 2009, Zuo [14] built a linear regenerative energy harvester to test the amount of energy which can be harvested. The prototype he made is half scaled and is single layer permanent magnets with wire coils surrounded shown in Figure 1.11.

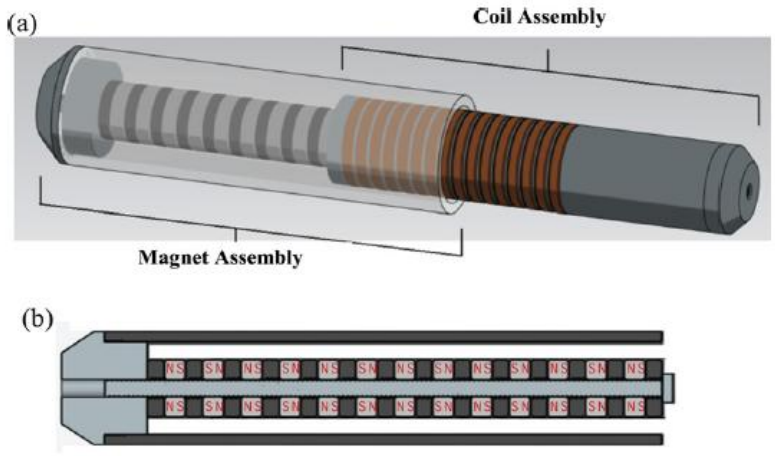

FIGURE 1.11 LINEAR ELECTROMAGNETIC HARVESTER DESIGN OVERVIEW

The orientation of the axial magnets alternates and are divided by iron space. Electricity will be generated when the wire coil cut the magnetic flux. Zuo claimed the steel shell will guide the flux and greatly increase the power density. The prototype is tested on a shaker. Experimental results match the theoretical result very much. If the prototype in made in full scale, he argues that there will be 16 watts of electrical energy generated at shock root mean square velocity of 0.25 m/s.

Linear regenerative damper can be designed the same size of actual shock absorber. The friction loss is significantly small since there is no contact between wire and magnets. However, the power and force generated are relatively smaller. Thus not much energy is harvested. Passive and semi-active suspension systems are more preferred.

1.4.2.2. ROTATORY REGENERATIVE DAMPER

In 1996, Suda and Shiiba [15] proposed a regenerative suspension system consists of a rotatory DC motor as actuator. The linear motion of the damper is converted into rotatory motion by rack and pinion mechanism. Both single-degree-of-freedom and two-degree-of-freedom prototypes are designed and examined experimentally. DC motor with gear box amplification will provide sufficient power for active control and vice versa. However, the prototypes are not design as the way the conventional dampers are as shown in Figure 1.12. Self-powered active vibration control is favored using this prototype.

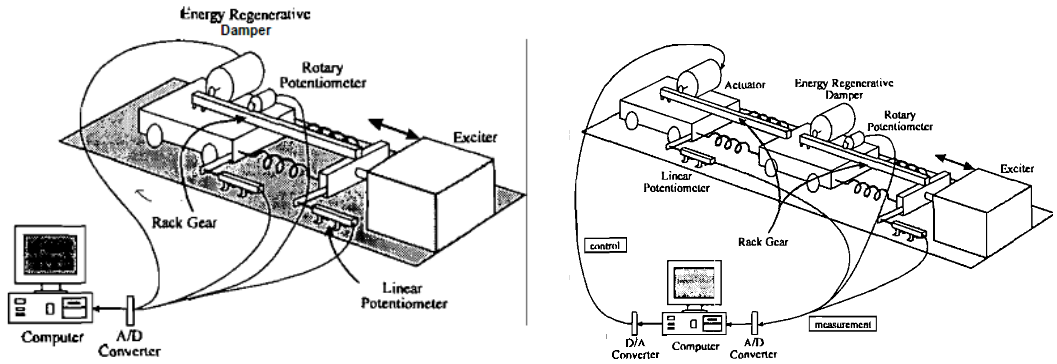

FIGURE 1.12 SYSTEMATIC VIEW OF RACK AND PINION DESIGN, SINGLE DEGREE OF FREEDOM AND 2 DEGREE OF FREEDOM

In 2004, Nakano and Suda [16] simulated the self-powered regenerative suspension system by using ball screw mechanism. Ball screw damper is modeled in Figure 1.13 to provide active suspension control of a truck.

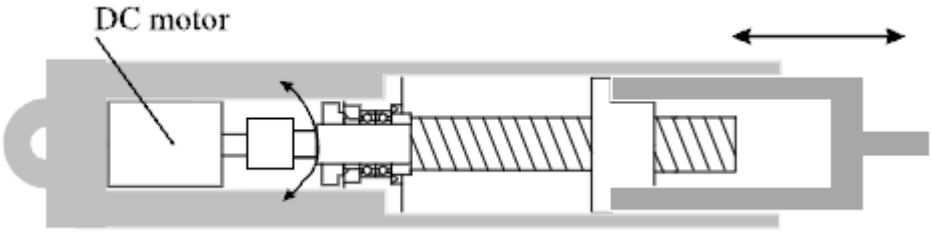

FIGURE 1.13 BALL SCREW HARVESTER OVERVIEW

As the DC motor turns, the ball screw turns and the ball nut will provide tensile or compressive force. Theoretical result shows the validation of self-active control using ball screw mechanism except actuator force does not meet the desired actuator force at certain state.

DC rotatory motor can provide sufficient actuating force to achieve active vibration control. However, size, weight, and transmission are the primary drawbacks. The rack and pinion prototype is not made accordingly. Moreover, friction due to transmission is also very considerable. The experiments are mostly done on self-powered regenerative active control but not on energy harvesting aspects. These researchers do not mainly consider the size, regenerated power and road induced vibration energy.

1.4.3. THE DIFFERENTIATION OF THE THESIS WORK

The regenerative suspension system has been favored for more than three decades. Different approaches and methods are developed to study the feasibility of power regeneration and vibration control as described above. Different laboratory prototypes are developed to verify the theoretical predictions such as linear electromagnetic harvester, rack & pinion harvester and ball screw harvester. Although many researches have been done on regenerative suspension as mentioned above, the results on shock dissipative energy are inconsistent and only a few works have shown the design of EM harvesters for energy harvesting. Therefore, this thesis shows experimentally validated numerical results on shock dissipative energy on different ISO classed roads at varies speeds. In addition, significant improvement on power regeneration from the design and performance aspects will be discussed thoroughly.

Some people may question on the amount of road induced vibration energy to vehicle when speaking shock dissipative energy on kW scale. The results of shock dissipative energies from different researchers vary on a large range. Therefore, it is important to understand the road-induced vibration energy both numerically and experimentally. After understanding the shock dissipative energy numerically, on road experiments on shock displacement profiles are conducted to validate the numerical results on different road conditions at varies speeds. Aside from energy harvesting, the primary function of shock absorber is to create a comfort and safe ride, which will also be discussed. Furthermore, the tradeoff between power generation, ride comfort and ride safety will be analyzed. A sensitivity study on vehicle parameters and performances is conducted thereafter.

Different from the linear harvester built in Zuo's research [14], in this thesis the radial magnets are implemented with double layer configuration to increase the magnetic flux density inside the air gap thus increase power generation. Finite elements analysis results show a great shift in power generation and energy density. Rack and pinion design is favored in this thesis because the whole transmission mechanism is completely integrated inside a cylindrical shock absorber and gearbox is implemented to boost power

generation. The size and design of rack and pinion harvester have great improvement compares the prototype built by Suda in Figure 1.12 [15], whose design cannot be integrated into the vehicle suspension system. Aside from linear and rack & pinion harvesters, the ball screw harvester is also evaluated in this thesis. Geared motor is replaced with traditional motor to improve the power generation.

1.5. SUMMARY

The primary function of vehicle suspension is to migration the vibration disturbance transmitted from road irregularity for better ride comfort and to maintain the good tire-ground contact force for better vehicle handling or road safety. Due to the simplicity and economical market value, passive viscous dampers are favored and used in most vehicle suspension system nowadays. As level of satisfaction and technology become more advanced, semi-active and active suspension systems are favored for the excellence in vibration isolation and vehicle handling. However, power consumption and fuel efficiency hit the concern. To counter the exclusive usage of external power, regenerative shock absorbers caught researchers' attentions. Not only regenerative shock absorbers may provide sufficient power to perform semi-active and active suspension control, but also they can reduce car engine's work load by charging the battery or powering vehicle power electronics using the regenerated electricity, thus increase vehicle fuel efficiency.

Theoretical works on vibration energy due to road roughness, suspension dissipative power and self-powered active control are investigated by some researchers, inconsistent results have been presented. Mechanical and electromagnetic mechanisms on regenerative suspension systems are studied by a few researchers. Different prototypes are built to examine and verify the research of power regeneration. Different from the works done by other researchers, the significances of this thesis are (1) to systematically evaluate the vibration energy, ride comfort, and road safety and experimentally verify it by road testing; (2) to present a new design of linear electromagnetic harvester with improved flux density inside the air gap; (3) to integrate rack & pinion and ball screw mechanisms into a likely sized shock absorber to verify the harvestable energy.

CHAPTER 2 GROUND-VEHICLE DYNAMICS AND VIBRATION ENERGY POTENTIAL

2. ROAD INDUCED ENERGY AND VEHICLE PERFORMANCE

Road is not flat in reality. When a vehicle is traveling on a road, it always experiences different kinds of disturbances, which will induce vehicle vibration. Different roads have different road roughness, thus energy dissipated by shock absorbers varies. Therefore, it is very important to understand the possible amount to energy dissipated by shock absorbers when a car is traveling on different ISO classified roads at different speeds. Many researchers have examined shock-dissipated energies which are reviewed in this section. Then a road-vehicle model is created to examine the vehicle dynamics and energy potential, and experiments are conducted on different road conditions to verify the prediction. In addition, the parameters that influence the shock dissipative energy and vehicle performance are studied. It is interesting to find that higher shock energy does not correspond to better vehicle control.

2.1. LITERATURE SURVEY ABOUT SHOCK ABSORBER ENERGY ON THE ROAD

Hsu [17] used a quarter car model and road roughness as white noise input to model the power dissipation on vehicle shock absorber. He claimed over 400 watts of energy can be recovered from all four shock absorbers at vehicle speed of 60mph. Moreover, under highway driving condition, 5% of the propulsion power can be potentially recovered. Velinsky and White [18] investigated the vehicle energy dissipation at different road roughness, vehicle speed, damping and stiffness. Results indicate a direct proportionality between vehicle speed and tire pressure corresponding to power dissipation. Zuo [19] also utilized the road roughness into account to simulate suspension deformation and velocity at different vehicle speeds and similar result are acquired. In addition to energy dissipation, Zuo also took rider comforts and road handling into account to evaluate the optimal performance.

Although much initial work has been done in regenerative vehicle suspension, the amount of harvestable energy on road varies from hundred watts to kilowatts as carried out by researchers. More importantly, there is no systematic analysis with considering the road roughness, vehicle dynamics, ride comfort and potential of power at the same time. The section will present the study on the road and vehicle dynamics analysis and the estimation of the power that is harvestable with the regenerative shock absorber. The influence of the parameters to the performance is also discussed. Since the energy harvesting performance conflicts with the vibration mitigation performance, a compromised solution will be suggested by tune vehicle hardware system such as tire and suspension stiffness, sprung and unspring mass, and damping.

2.2. MODELING OF ROAD AND VEHICLE DYNAMICS

Quarter car can be simply viewed as a two-degree-of-freedom system. Figure 2.1 shows the quarter car modeling of vehicle with viscous damper, while Figure 2.2 show the modeling of regenerative suspension where the dashpot is replaced with an electromagnetic transducer. Electromagnetic transducer is able to harvester vibration energy and at the same time provides desired damping force as viscous damper. The electricity is stored in a battery after regulation of power electronics.

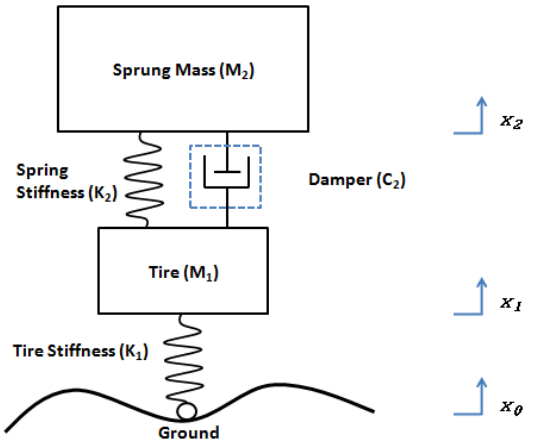

FIGURE 2.1 QUARTER-CAR MODEL WITH VISCOUS DAMPER

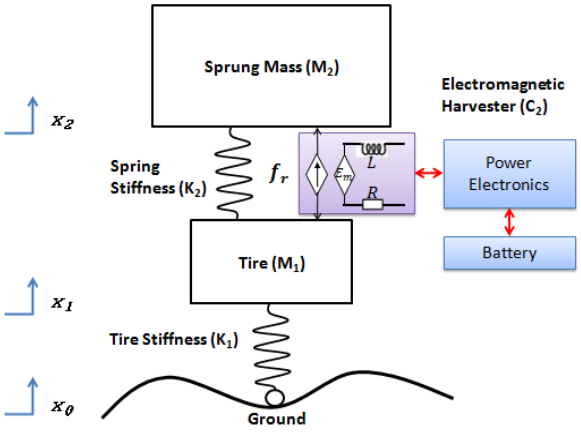

FIGURE 2.2 QUARTER-CAR MODEL WITH ELECTROMAGNETIC HARVESTER

Road roughness and vehicle dynamics not only have influence on the vibration performance of the vehicle but also affect the power we can harvest from the regenerative suspension. This section will discuss the modeling of the road roughness and vehicle dynamics and the relations of these parameters with the vibration and energy harvesting performance.

2.2.1. ROAD ROUGHNESS

As the vehicle travels on road, the wheel follows the trajectory of the irregularity of road surface. Therefore, road roughness can be modeled as ground displacement input. The road roughness is in space domain which has to be converted into time domain for input modeling through transformation. Variable vehicle speeds will affect the precision of transformation, thus constant vehicle speed is assumed.

The road irregularity is very random. Road condition varies in a wide range as well. Throughout numerous measurements and conditionings, international standard of road roughness is set for reference. ISO 2631 proposed a set of road roughness indices R_r for different levels of road conditions as shown in Table 2.1[20]. Since the classification is based on a set of roughness indices, selective values are chosen as presentation of different classes. The displacement power spectral density (PSD) in Gaussian stochastic process is expressed as

$$S_{PSD} = \frac{R_r}{2\pi} * v^{\beta}, \left[\frac{m^3}{cycle}\right] \tag{2.1}$$

where v stands for spatial frequency, β is usually taken as -2. The disturbance of displacement input now can be modeled as white noise input through a first order filter.

$$G_S = \frac{(R_r V)^{0.5}}{s + \omega_0} \tag{2.2}$$

here, ω_0 is the cutoff frequency or excitation frequency in time domain.

TABLE 2.1 ROAD ROUGHNESS INDICES, R_R X 10^{-6} [M^3/RAD]

Road Class	Range	Selective Mean
A (Excellent)	< 8	4
B (Good)	8 - 32	16
C (Average)	32 - 128	64
D (Poor)	128 - 512	256
E (Very Poor)	512 - 2048	1024
F (Very^2 Poor)	2048 - 8192	4096
G (Very^3 Poor)	8192 - 32768	16384
H (Very^4 Poor)	32768<	

2.2.2. RIDE COMFORT

Ride comfort is subjective to human perception. Study has shown that human perception greatly depends on acceleration.

$$K = K(a) \tag{2.3}$$

where K is non-dimensional perception quantity, and a is the absolute acceleration. More refined relationship between K and a is given in international standard referring to ISO 2631. Filters are required to set human perception respect to ISO 2631. The purpose of ISO 2631 is to evaluate the vibration exposed to human body by weighting the root mean square acceleration to human sensitivity curve in Figure 2.3. Human are mostly sensitive between 4 Hz to 8 Hz as shown in shaded area. According to Zuo [21], a third order filter with wider frequency range is chosen as

$$\frac{80.03\,s^2 + 989\,s + 0.02108}{s^3 + 78.92\,s^2 + 2412\,s + 5614} \tag{2.4}$$

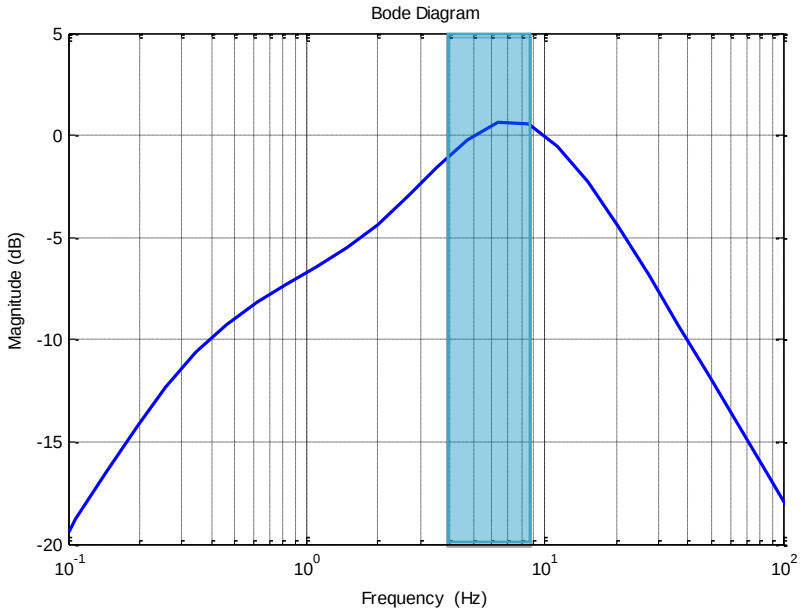

FIGURE 2.3 HUMAN SENSITIVITY CURVE

Therefore, the ride comfort can be evaluated as the *root mean square* value of the acceleration of the vehicle body weighted by the ISO2631 filter.

2.2.3. RIDE SAFETY AND HANDLING

Ride safety also refers to road handling. During the serve vibration, wheel may not experience enough contact force with ground or even lose contact, which will cause the vehicle losing control. Hence, the ride safety and handling is also considered as one of the performance index. It is the relationship between tire's static force and dynamic force. When the vehicle is under driving condition, the total load on wheel is consisting of static and dynamic loads; else only static force is applied when the vehicle is stationary.

The handling margin H is defined as the ratio between dynamic loads to static load. The higher the dynamic force the vehicle wheel experiences, the vehicle is unlikely to be handled easily. All wheels will lose ground contact when H=1. Furthermore, wheel dynamic forces are taken as variances with time. Here, H is a statistical quantity. Mean value of H is applied on road handling issue.

2.2.4. SUSPENSION POWER

The energy that is available for harvesting is estimated indirectly by examine the amount of the energy that is dissipated by the traditional viscous damping. Power dissipation is proportional to damping and shock velocity square.

$$P_{Shock} = C(\dot{x}_2 - \dot{x}_1)^2 \tag{2.5}$$

In reality C (ω) is a function of frequency, which varies at different frequency. In regular driving, different frequencies are imposed by road roughness. For simplicity, C is generally taken as a constant value since energy harvesting only falls in certain frequency range. Here, $\dot{x}(t)$ is also a function of time. Due to road irregularity, $\dot{x}$ ranges from 0.15 to 0.4 m/s typically. Hence, power recorded is a function of time. Mean value of power is used to estimate energy dissipated by shock absorber.

2.2.5. QUARTER CAR MODEL

A two-degree-of-freedom quarter car system is modeled to estimate the power dissipated by shock absorber while maintaining ride comfort and safety. Typical vehicle parameters are used to simulate the system.

$$\begin{bmatrix} M_1 & 0 \\ 0 & M_2 \end{bmatrix} \begin{pmatrix} \ddot{x_1} \\ \ddot{x_2} \end{pmatrix} + \begin{bmatrix} C_2 & -C_2 \\ -C_2 & C_2 \end{bmatrix} \begin{pmatrix} \dot{x_1} \\ \dot{x_2} \end{pmatrix} + \begin{bmatrix} k_1 + k_2 & -k_2 \\ -k_2 & k_2 \end{bmatrix} \begin{pmatrix} x_1 \\ x_2 \end{pmatrix} = \begin{bmatrix} k_1 \\ 0 \end{bmatrix} x_0 \tag{2.6}$$

The dynamic system can be expressed in state space form

$$\dot{Z} = AZ + Bx_0 \tag{2.7}$$

$$Y = CZ + Dx_0 \tag{2.8}$$

where Z are the states, Y is the output, and A, B, C, D are state space parameters.

$$A = \begin{bmatrix} 0 & I \\ -M^{-1}K & -M^{-1}C \end{bmatrix} \tag{2.9}$$

$$B = [0\ ;\ M^{-1}B_0] \tag{2.10}$$

$$C = \begin{bmatrix} C_1 \\ C_2 \\ C_3 \\ C_4 \end{bmatrix} = \begin{bmatrix} k_2/m_2 & -k_2/m_2 & c_2/m_2 & -c_2/m_2 \\ 0 & 0 & -1 & 1 \\ -1 & 1 & 0 & 0 \\ 1 & 0 & 0 & 0 \end{bmatrix} \tag{2.11}$$

$$D = [0; 0; 0; -1] \tag{2.12}$$

Here $B_0 = [k_1; 0]$ for force input acting on tire, $C_1, C_2, C_3, and\ C_4$ give weighted acceleration, suspension velocity, suspension stroke, and tire position respectively.

Figure 2.4 illustrates the block diagram of input-output relation. Matlab command *normh2* is used to evaluate output parameters. The power spectral density curves of velocity profile and displacement profile follow the same trajectory. Since, ground velocity input can be modeled as white noise input, the ground displacement input can also be modeled as white noise input. The weighting function is used to transform spatial frequency to time domain. ISO 2631 filter is applied to weight the vehicle vertical acceleration corresponding to human sensitivity.

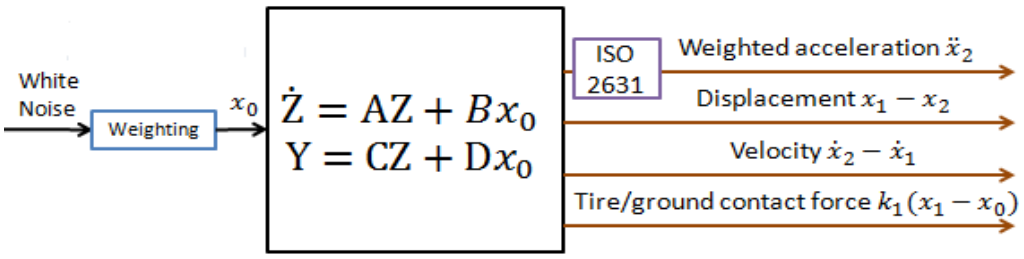

FIGURE 2.4 BLOCK DIAGRAM VIEW OF INPUT-OUTPUT PERFORMANCE

H2 norm returns the root mean square value of the given output parameters corresponding to white noise input. In state space realization, h2 norm is computed by solving Lyapnuvo equation

$$H_2\ Norm = \ trace[CPC']^{\frac{1}{2}} \ = \ trace[B'QB]^{\frac{1}{2}}$$

where P is the controllability grammian, and Q is the observability grammian. Hence, C is not the same as in our system because of multiple outputs.

2.3. NUMERIC RESULTS

In this section simulations based on a typical passenger car will be presented. Since most of the U.S, highways and local ways fall into average and good road category, R_r values are chosen as 64 and 16 respectively according to the ISO road roughness standard. The sensitivity of performances respect to vehicle parameters will also be discussed.

2.3.1. SUSPENSION DISPLACEMENT AND VELOCITY

Road disturbance is modeled as displacement input from ground, and the numerical results based on mid-sized car are shown in Figure 2.5. As the vehicle speed increases the root mean square (RMS) value of displacement increases. Similar trends are found in vertical suspension velocity curve in Figure 2.6. At regular driving of 60mph on average road, 0.25 m/s RMS suspension velocity can be achieved.

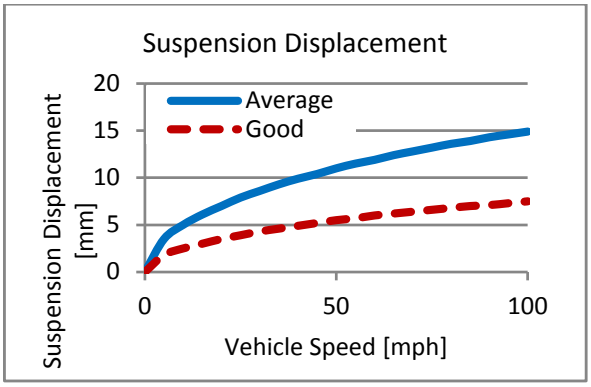

FIGURE 2.5 DISPLACEMENT ANALYSIS OVER VEHICLE SPEED

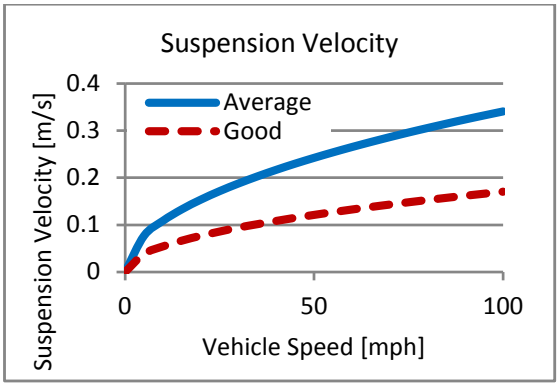

FIGURE 2.6 VELOCITY ANALYSIS OVER VEHICLE SPEED

2.3.2. RIDE COMFORT& RIDE SAFETY

The weighted vehicle body acceleration is shown in Figure 2.7. It indicates the higher the vehicle speed, the larger weighted vertical acceleration will be. Note that the numeric results of weighted accelerations are falling in extremely uncomfortable zone. This is because the weighted acceleration curve corresponds to vehicle body acceleration; the actual acceleration transmitted to human is much smaller due to the stiffness and damping of seats. Figure 2.8 illustrates the tire-ground contact force curves which also

refer to the safety curves. The ratio of tire dynamic force over tire static force increase as vehicle speed increases. Hence, tires experience less contact force or even likely losing contact with ground at higher vehicle speed which will cause handling and safety hazards. Therefore, it is more risky when a car is driving at higher speed.

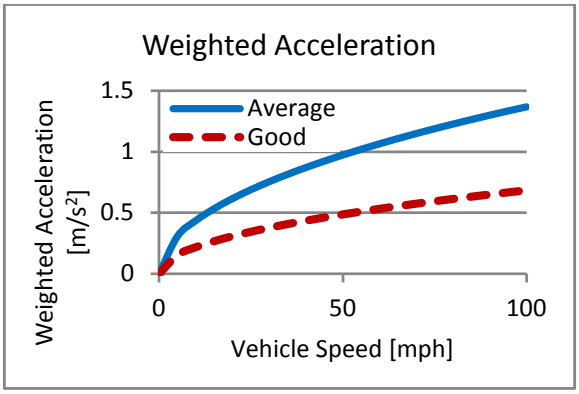

FIGURE 2.7 ACCELERATION ANALYSIS

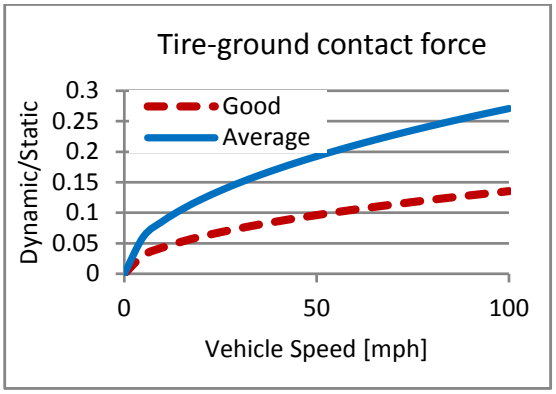

FIGURE 2.8 FORCE PROFILES ANALYSIS

2.3.3. POWER GENERATION

From energy harvesting standpoint, regenerative power is the primary quantity to consider. Since power is proportional to square of vehicle vertical velocity, the output power will increase with vehicle speed as shown in Figure 2.9. More than 400 watts of energy can be generated through all four shock absorbers when the vehicle is traveling on a class C (average) road at 65 mph. Hence, regenerative shock absorbers will considerably increase fuel efficiency.

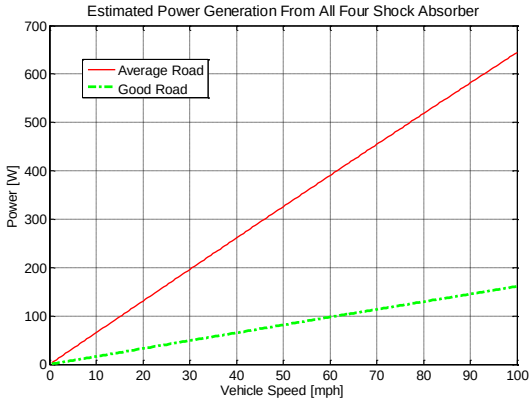

FIGURE 2.9 POWER GENERATION IN SUSPENSION SYSTEM

2.4. SENSITIVITY

Further studies are investigated on sensitivities of vehicle parameters in this section. The effects of changing in sprung & unsprung mass, tire & suspension stiffness, and damping on primary issues are further explored. Consider the initial results of mid-sized car as the reference, results of power, ride comfort, and ride safety sensitivity curves subject to parameter changes are plotted in Figure 2.10, 2.11, 2.12, 2.13, 2.14. As we can see, the change of tire stiffness has most significant effects on the change on regenerated power. However, stiffer tire contributes negative effects of ride comfort and handling. On the other hand, larger sprung mass will have positive effects on acceleration and safety. Lastly, size of suspension damping contributes certain level of security to vehicle body. Smaller or no shock absorber will cause handling problems.

The tradeoffs between power, handling, and ride comfort are illustrated vividly. For instant, according to Figure 2.13, the optimal damping for ride comfort is shown at 0.4 C_2 while it is 1.6 C_2 for best ride safety concern. Figure 2.12 shows the desired suspension stiffness for ride comfort is 0.2 K_2, but best safety index happens at 0.75 K_2. Overall, we really have to consider tuning tire stiffness for power, sprung mass for comfort and sprung mass, suspension damping for safety. Increasing tire stiffness by pumping more air is worth it since power increment is significantly larger than its opportunity costs. Adding car body mass will have considerable inferences on ride safety and ride comfort.

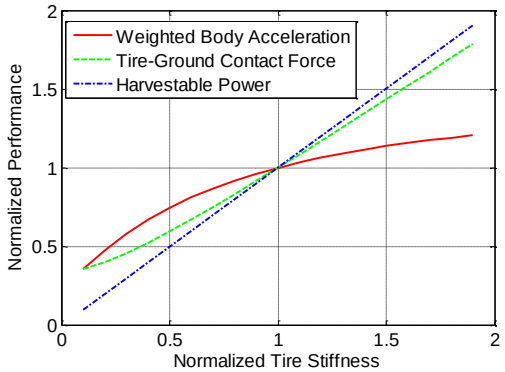

FIGURE 2.10 EFFECTS OF TIRE STIFFNESS ON VEHICLE PERFORMANCE

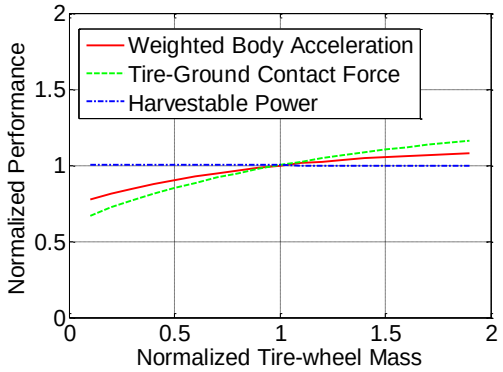

FIGURE 2.11 EFFECTS OF TIRE-WHEEL MASS ON VEHICLE PERFORMANCE

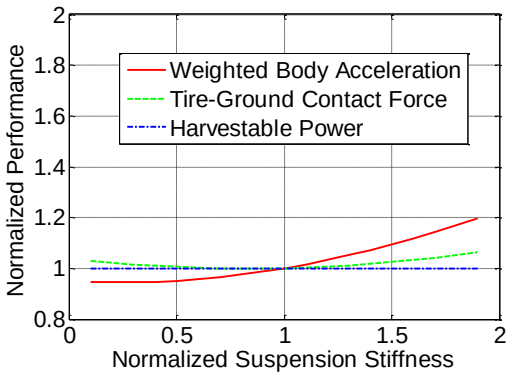

FIGURE 2.12 EFFECTS OF SUSPENSION STIFFNESS ON VEHICLE PERFORMANCE

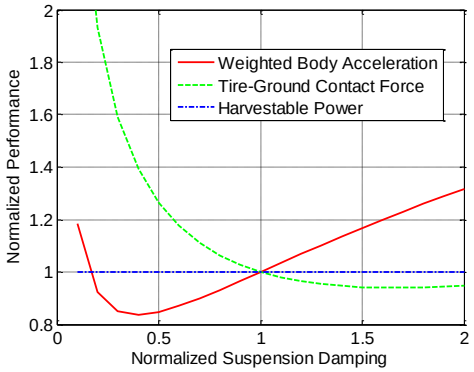

FIGURE 2.13 EFFECTS OF SUSPENSION DAMPING ON VEHICLE PERFORMANCE

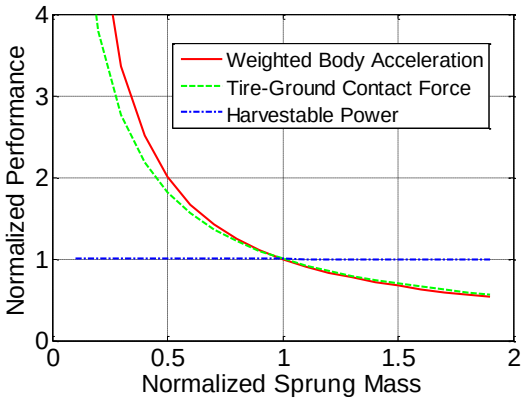

FIGURE 2.14 EFFECTS OF SPRUNG MASS ON VEHICLE PERFORMANCE

Another type of analysis is shown in Figure 2.15, 2.16, 2.17. Here, each component of vehicle performance is studied respect to vehicle parameters. Both Figure 2.15, and 2.16 show the negative effects of decreasing sprung mass which will make vehicle harder to handle and less comfortable. Moreover, suspension damping contributes great influence on a safe ride by increasing damping but adding negative effects on ride comfort. More importantly, only tire stiffness contributes great change on power as seen from Figure 2.17. This is because of the tradeoffs between parameters and performances. For example, increasing damping will have negative effect on suspension velocity; power is the product on damping and velocity square. Therefore, there is not great improvement on power output.

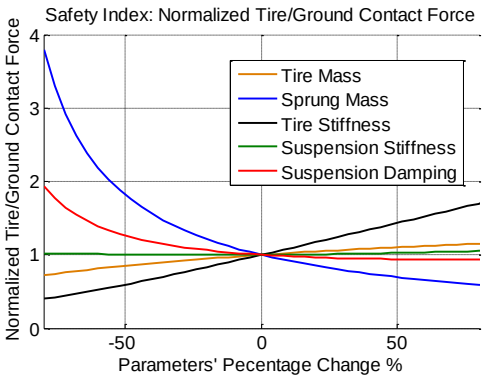

FIGURE 2.15 CHANGE OF TIRE/GROUND CONTACT FORCE RESPECT TO DIFFERENT VEHICLE PARAMETERS

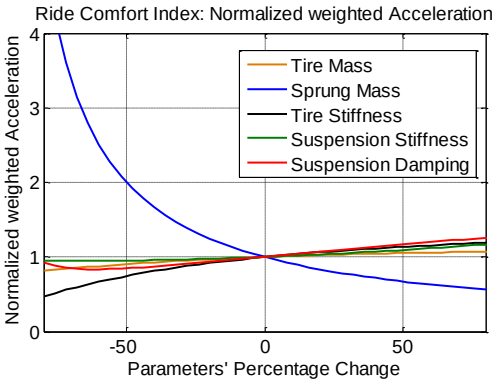

FIGURE 2.16 ACCELERATION CHANGE RESPECT TO DIFFERENT VEHICLE PARAMETERS

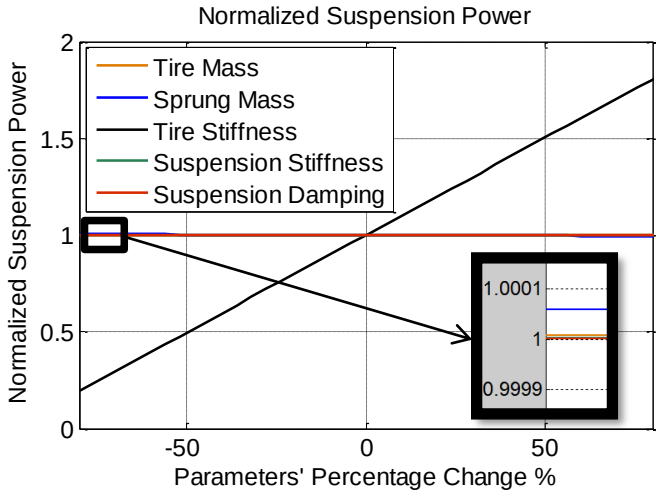

FIGURE 2.17 SUSPENSION POWER CHANGE RESPECT TO PARAMETERS' CHANGES

2.5. EXPERIMENTAL RESULT

Theoretical road modeling is conducted in the previous section. Power dissipation through shock absorbers is studied at different ISO standard road roughness and vehicle speeds. Results show more harvestable energy from vehicle suspension system on rougher roads and higher speeds. Approximately 400 watts of energy from all shock absorbers is harvestable when a vehicle is running on class C road at 65 mph. Concurrently, ride comfort and safety were also reviewed by considering practical real life situations. Although rougher road and higher speed can result more harvestable

energy from shock absorbers, it also creates uncomfortable riding conditions and even an unsafe ride. This is because human are sensitive to absolute acceleration and vehicle body acceleration increases as vehicle speed increase or road roughness increases. On the other hand, the dynamic contact force will also increases which result handling problem and set safety hazards at higher risk. Another mean to increase power dissipation from shock absorbers is to increase the tire stiffness which will also result in an uncomfortable and unsafe ride. The disadvantage of increasing tire stiffness can be compromised by increasing vehicle body mass at optimal damping. In order to validate the theoretical prediction about the energy from shock absorber, real time data acquisition on sample ride is gathered. The following sections will give an overview about experimental setup, result and discussion.

2.5.1. EXPERIMENT SETUP

A systematic view of experiment setup is shown in Figure 2.18. An electrical car is used for on-road data collecting on campus. The basic parameters of the electrical car are shown in Table 2.2. Since there is no actual specification shown for this electrical car, all the parameters are estimated. The damping is higher because the rear shock absorbers are mounted at an angle. Displacement of the rear shock absorber is then recorded by laser displacement sensor from Micro-Epsilon at sample rate of 1000 point per second. Thereafter, shock displacement profile is stored on a PC via Micro-Epsilon to process. Besides conducting experiments for the low vehicle speed on campus road, a set of high vehicle speed data of shock displacement profiles are also considered in this thesis research. A BMW x5 series SUV is used to test high-speed conditions on Long Island Expressway from Exit 62 to Exit 65. The parameters of BMW X5 series SUV is different from super compact electrical car and is also shown in Table 2.2. The SUV have larger car body mass and stiffer suspension springs with slightly higher natural frequency. Moreover, the rear damper is vertically installed in suspension system; thus damping is smaller than super compact electrical car.

FIGURE 2.18 SYSTEMATIC VIEW OF EXPERIMENT SETUP

The shock displacement profiles will be recorded at different vehicle speeds on the same section of campus road and LIE to assure the accuracy and precision of experiments.

TABLE 2.2 PARAMETERS OF TESTED VEHICLES

Tested Vehicle	Body Mass	Tire Mass	Spring Stiffness	Shock Damping	Tire Stiffness
Electrical	1300 kg	30 kg	20000N/m	1995 Ns/m	180000N/m
BMW X5	2358 kg	52 kg	52363N/m	1700 Ns/m	180000N/m

2.5.2. SUSPENSION DISPLACEMENT

Shock displacement is modeled at different vehicle speeds. Figure 2.19 show a typical displacement profile we obtain the experiment at vehicle speed of 25 mph. The instant peak to peak shock displacement can be as high as 40 mm, but root mean square value of the set of data is 4.6 mm. Figure 2.20 shows the displacement profile on LIE at 70 mph using BMW X5. The road is smoother than campus road since most of the displacement data falls in between ±10mm and there is no sudden changes revealed on the graph. The rms value of displacement is shown to be 4.1mm this is because the properties of vehicle parameters changes in which the spring stiffness is much higher.

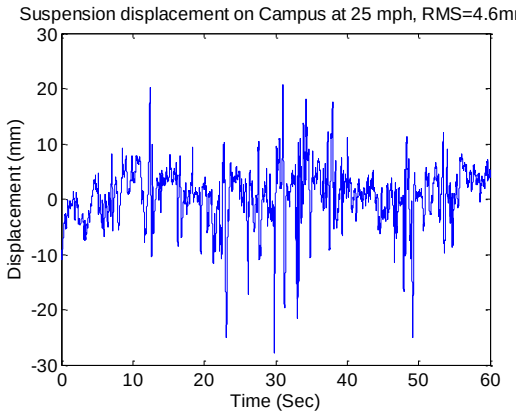

FIGURE 2.19 MEASURED SHOCK DISPLACEMENT PROFILE ON CAMPUS ROAD AT 25MPH

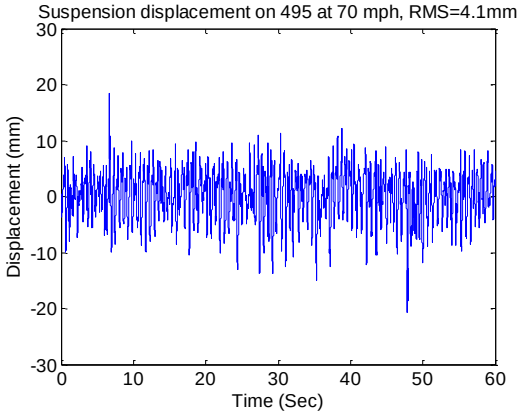

FIGURE 2.20 MEASURED SHOCK DISPLACEMENT PROFILE ON LIE AT 70MPH

The power spectrum density (PSD) of vehicle shock displacement is plotted in Figure 2.21 and Figure 2.22. The black line represents the ideal PSD from ground velocity input of white noise. Results indicate the ground excitation is dominating from 1 Hz to 30 Hz which is in between the first and second natural frequency of the vehicle and noise shows up at high frequency. Large difference shown at low frequency, possible reason is the centrifuge force excitation dominates due to road curvature for low speed tests and impulse input from dividers for highway tests.

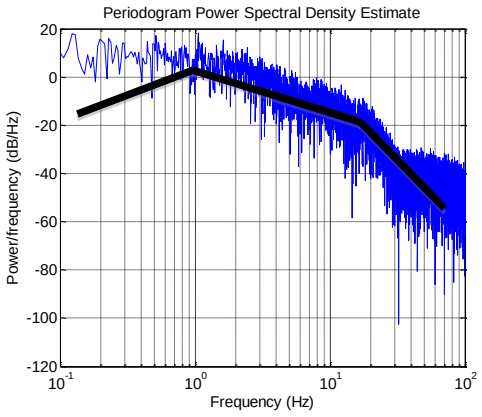

FIGURE 2.21 PSD OF SHOCK ABSORBER DISPLACEMENT ON CAMPUS AT 25 MPH

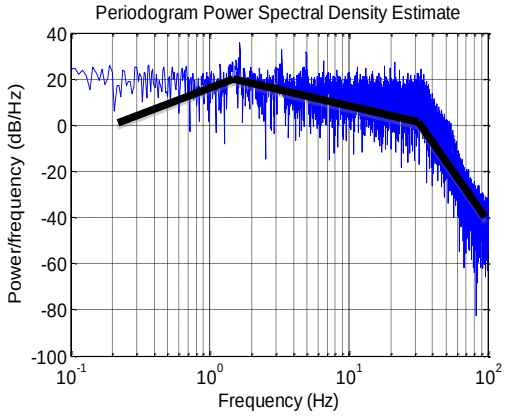

FIGURE 2.22 PSD OF SHOCK ABSORBER DISPLACEMENT ON LIE AT 70 MPH

2.5.3. SUSPENSION VELOCITY AND POWER

The data attained by the sensor is in displacement profile. In order to understand the shock dissipated power, velocity profile should be considered by taking derivation. Noises are added to the system when shifting to velocity profile. More importantly, regenerative shock is inactive with high frequency. Therefore, a filter is used to filter out both low frequency and high frequency as illustrated in Figure 2.23.

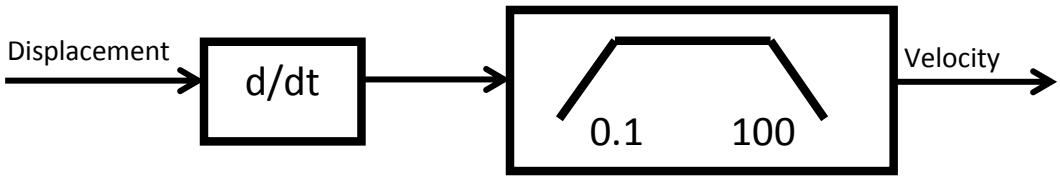

FIGURE 2.23 DATA PROCESSING BLOCK DIAGRAM

The velocity profiles after filter are plotted in Figure 2.24 and Figure 2.25 corresponding to displacement profiles. The root mean square values of velocity profiles are 0.085 m/s and 0.1 m/sec respectively. Note, the rms value of displacement profile for campus road is higher than for highway, but the rms value of velocity profile is lower than for highway. This is because campus road is much rougher than highway and is illustrated in velocity curves too. Hence the mean powers are obtained as 14.57 W for campus road due to low suspension velocity and 40 W for highway condition.

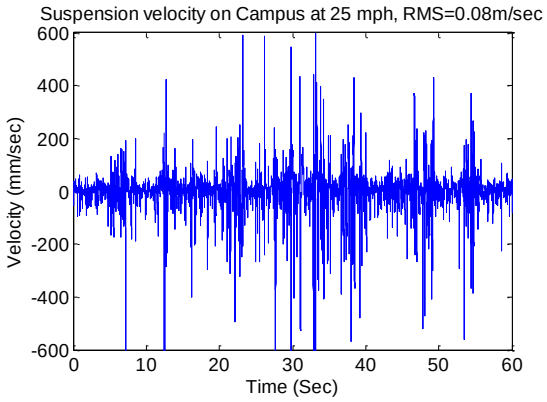

FIGURE 2.24 SHOCK VELOCITY PROFILE ON CAMPUS ROAD AT 25 MPH

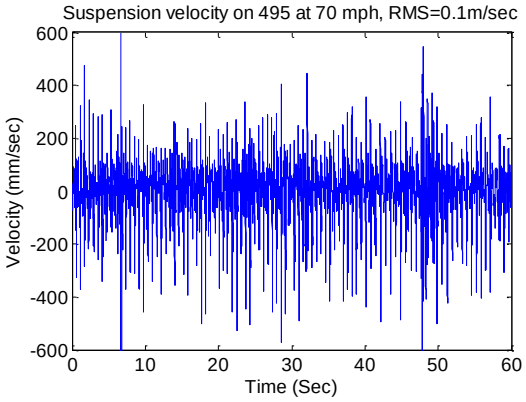

FIGURE 2.25 SHOCK VELOCITY PROFILE ON LIE AT 70 MPH

Some researchers may question about the actual energy can be harvested by regenerative shock absorbers. The results may show significant high frequencies of vibration but vehicle suspension system acts as a low pass filter. The probability density graphs of velocity profiles are plotted in Figure 2.26 and Figure 2.27. Most of the velocity falls in between ±100 mm/s. Further analysis is studied in frequency domain as shown in Figure 2.28 and Figure 2.29. Frequency response graphs indicate the dominating frequency is from 0 to 20 Hz for both low-speed and high-speed profiles.

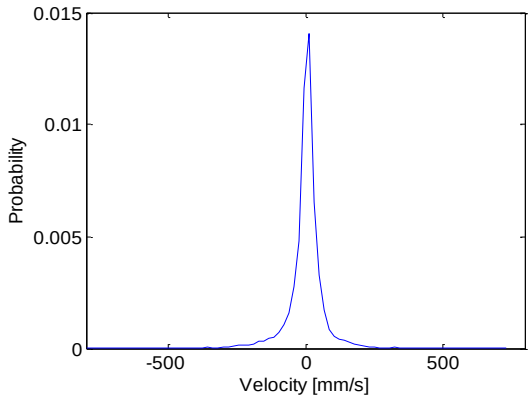

FIGURE 2.26 PROBABILITY DENSITY DISTRIBUTION ON CAMPUS ROAD AT 25MPH

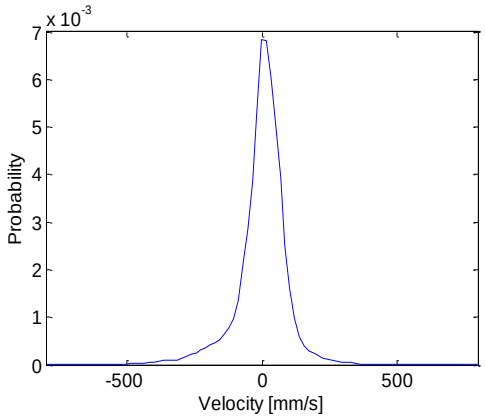

FIGURE 2.27 PROBABILITY DENSITY DISTRIBUTION ON LIE AT 70 MPH

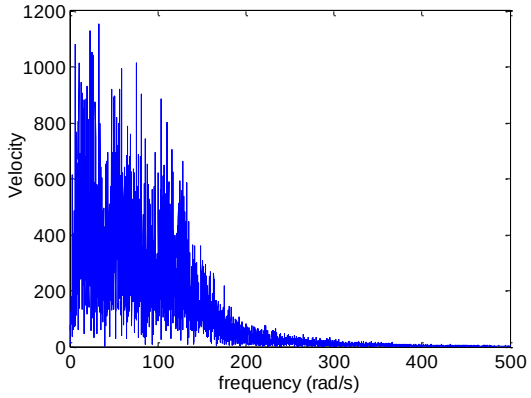

FIGURE 2.28 FREQUENCY RESPONSE OF VELOCITY ON CAMPUS ROAD AT 25 MPH

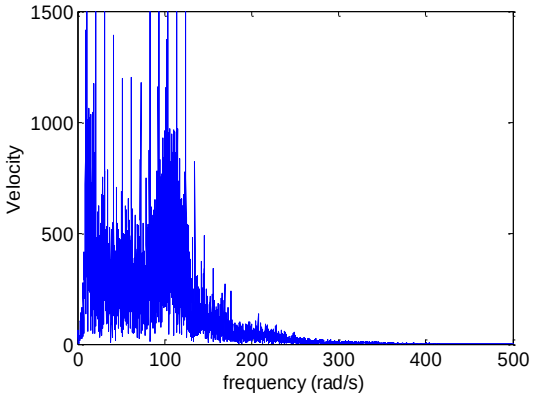

FIGURE 2.29 FREQUENCY RESPONSE OF VELOCITY ON LIE AT 70 MPH

As mentioned, power is proportional to shock velocity square, $P = C(\dot{x}_2 - \dot{x}_1)^2$. Since shock velocity is a statistical data, power will vary with time as well. Therefore, mean value of dissipated power is evaluated as

$$\bar{P} = \frac{1}{T}\oint_0^T [C(\dot{x}_2 - \dot{x}_1)^2]\, dt \tag{2.13}$$

Impressively, instant peak power is on the order of kW at peak velocity as shown in Figure 2.30 and Figure 2.31. Highway and campus road are categorized as Class B and Class C road roughness separately. Peak displacement, velocity, and power happened when the vehicle went over the sewer cover. This implies significant amount of energy on rougher road, especially for military vehicle traveling on no road conditions.

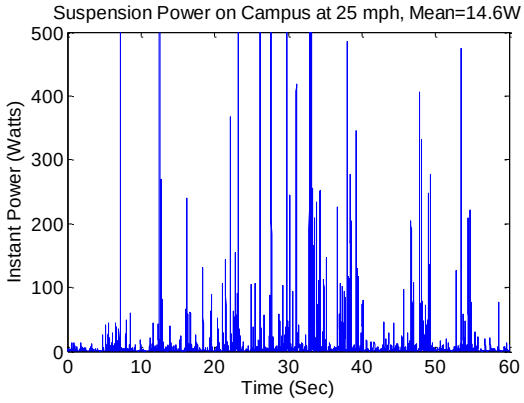

FIGURE 2.30 INSTANT DISSIPATIVE POWER PROFILE FROM SHOCK ABSORBER ON CAMPUS AT 25 MPH

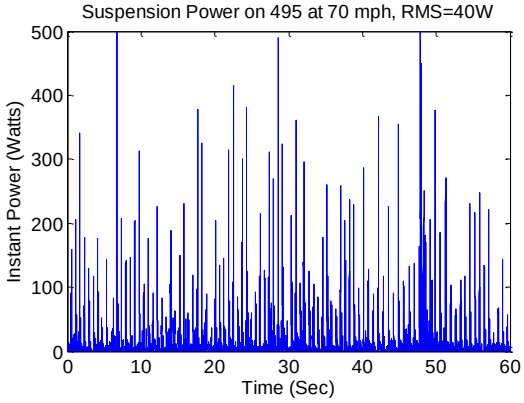

FIGURE 2.31 INSTANT DISSIPATIVE POWER PROFILE FROM SHOCK ABSORBER ON LIE AT 70 MPH

Similar studies are conducted for shock dissipative power profiles. The normalized probability curves in Figure 2.32 and Figure 2.33 show most power is concentrated below 50 watts. Results of frequency response confirm the dissipative power falling in low frequency range which is between 0 to 25 Hz as illustrated in Figure 2.34 and Figure 2.35. Most of the shock powers are dissipated at low frequency. The results also validate the dynamics of vehicle suspension system as a low pass filter. High frequency powers do not contribute major effects on total power generation.

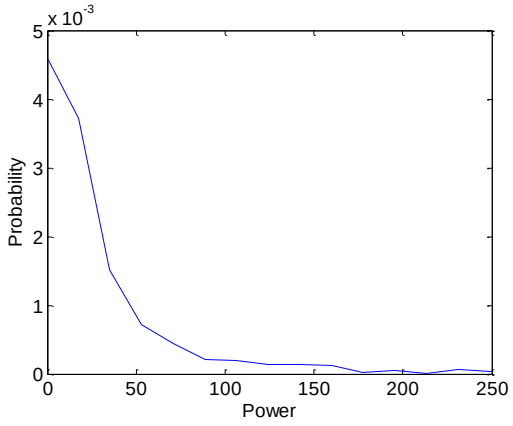

FIGURE 2.32 NORMALIZED PROBABILITY DISTRIBUTION OF POWER AT 25 MPH

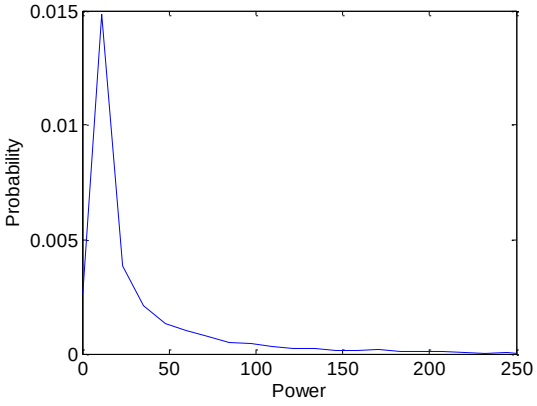

FIGURE 2.33 NORMALIZED PROBABILITY DISTRIBUTION OF POWER AT 70 MPH

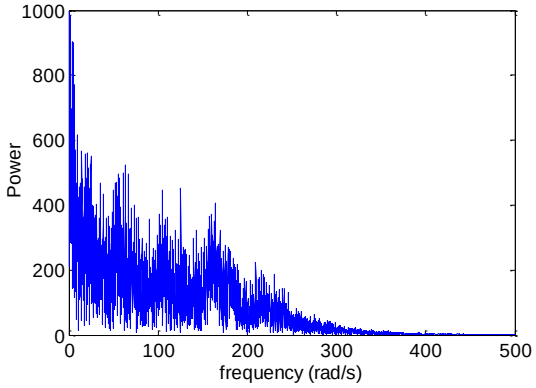

FIGURE 2.34 FREQUENCY RESPONSE OF POWER AT 25 MPH

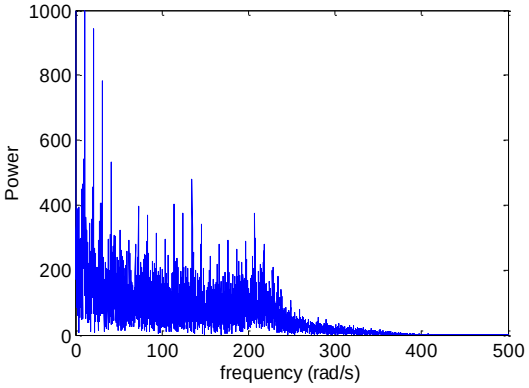

FIGURE 2.35 FREQUENCY RESPONSE OF POWER AT 70 MPH

In addition to the experimental results, only shock displacement, velocity and dissipated power are evaluated. The actual shock mounting is not perpendicular to super compact electrical car body. As a result, the vehicle vertical displacement, velocity and power are difference from experimental results. In the experiment situation, the damper is mounted at an angle θ along vertical axis. The vertical vehicle body displacement is the result of suspension displacement and suspension rotation. Therefore, the vehicle vertical displacement profile is found to be

$$Disp_{vertical} = \frac{Disp_{shock}}{\cos(\theta)} \tag{2.14}$$

In the experiment setup for electrical car, θ is about 30 degree. Thus, vehicle vertical displacement is 1.15 times of shock displacement. Hence, vehicle vertical velocity is increased by 15.47%. Since power is proportional to velocity square, as a result, the damping increases by a factor of 1.33 to maintain the same damping force for super compact electrical car. θ is zero for BMW X5 testing which means shock absorber is vertically mounted. Therefore, suspension power remains as experimentally obtained.

2.5.4. INFLUENCE OF VEHICLE SPEED

The above resulting figures show the performance of shock absorber and vehicle dynamics on campus road at 25 mph and on LIE at 70 mph. Further data were taken at 5 to 25 mph with speed increment of 5 mph for electrical car and relationship between shock displacement, shock velocity, and dissipated power to vehicle speed is plotted in Figure 2.36, 2.37, 2.38. Blue and red lines represent average and good condition roads respectively. Green dots are average results of experiments after two sets of data are acquired from on road experiments back and forth from campus road testing. All suspension displacement, velocity and power increases as vehicle speed increases which verify predicted trajectories. At higher vehicle velocity, the larger suspension displacement, velocity and power achieved.

The experiments are conducted with super compact electrical vehicle, while the numerical results are based on a middle size passenger car. In order to remain the same natural frequency, larger curb mass middle sized vehicles with stiffer tire will result in more power regeneration when compare to super compact vehicles which is shown in purple dots. Resulting figures show that campus road falls between average and good road conditions. The slopes of actual experimental results are sharper than predicted values. Moreover, the predicted power curves are quasi-linear to vehicle speed and experiment result shows a greater power at higher vehicle speed. The power dissipation will be over 80 Watts of harvestable energy from one shock absorber on campus road at 65 mph using super compact electrical car.

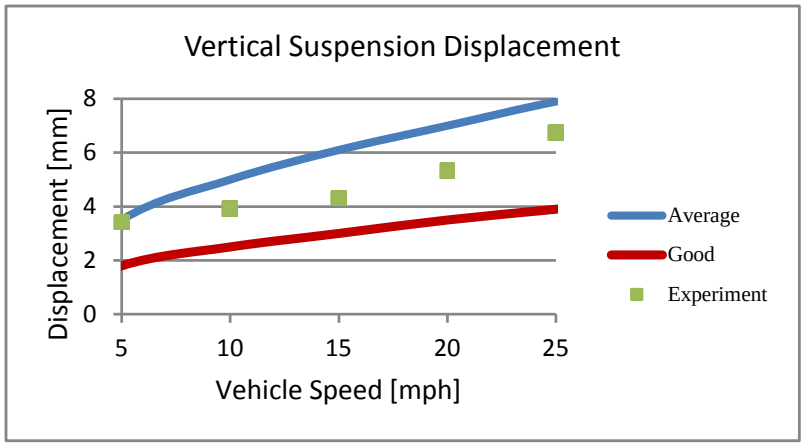

FIGURE 2.36 THEORETICAL AND EXPERIMENTAL VEHICLE VERTICAL DISPLACEMENT

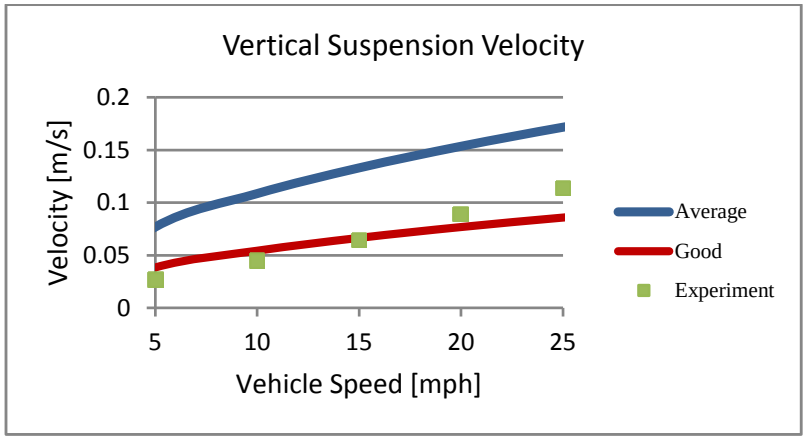

FIGURE 2.37 THEORETICAL AND EXPERIMENTAL VERTICAL SUSPENSION VELOCITY

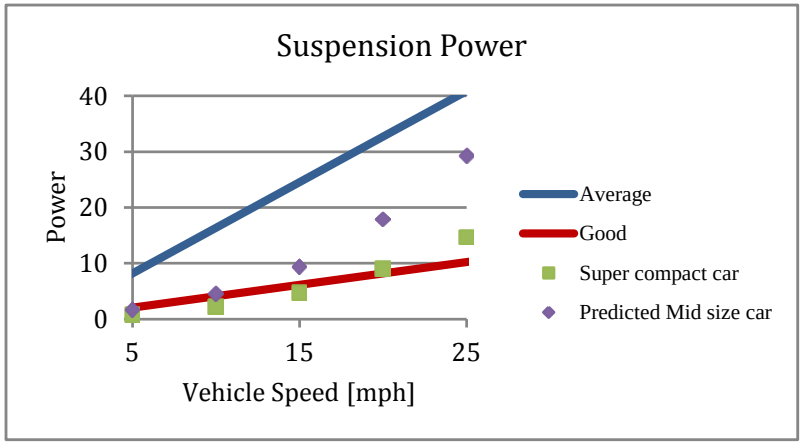

FIGURE 2.38 THEORETICAL AND EXPERIMENTAL VERTICAL SUSPENSION POWER

Similar results are obtained for high speed tests on LIE. Different vehicle speeds are tested from 45 mph to 70 mph with an increment of 5 mph. Results show more power can be dissipated from shock absorber at higher speed. However, the high speed test on Long Island Expressway does not show 80 Watts of dissipative power. This is because the LIE is smoother than campus road and the vehicle parameters of BMW X5 are different from the super compact electrical car.

2.6. CONCLUSION

This chapter has investigated the evaluation on existing power induced by road irregularity numerically. From automobile engineer's point of view, ride comfort and safety are well considered when achieving higher power output. The relationship between power, weighted acceleration, suspension velocity, suspension displacement, and tire position corresponding to vehicle speed is studied and plotted. The higher vehicle speed will achieve higher dissipative power and at the same time causing uncomfortable ride and safety issue. Furthermore, sensitivity studies of vehicle performances on system parameters are illustrated graphically based on numeric calculation. Results show the power generation has significant proportionality with tire stiffness, while lower sprung mass will cost ride comfort and safety issue. So does suspension damping. The optimal ride comfort happens to conflict optimal ride safety. The tradeoff between power and ride comfort and safety is worth a thought. Moreover, the drawbacks of increasing tire stiffness can be solved by tuning other parameters such as wheel mass, suspension spring rate, and sprung mass.

More importantly, more than 400 watts of energy can be harvested from all four shock absorbers on regular highway driving at 60 mph based on numerical results. To validate the numeric prediction of road energy, on-road data acquisition is adopted and processed by mounting a laser displacement sensor on the shock absorber of an electrical car and driving on campus road. Results show a greater similarity between predicted curves and actual experimental curves. In addition, the experimental power curves act even better than predicted power curves. More than 600 watts of energy is harvestable from all four shock absorbers when the mid-size vehicle is traveling at 60 mph on

campus road condition when further prediction is made based on experimental power curve. Aside from low vehicle speed data, we also conducted high vehicle speed testing on Long Island Expressway from Exit 62 to Exit 65 using BMW X5. The results are similar to low speed experiments. However, there are some dividers on the concrete expressway which makes the experiments no typical. Interestingly, when the vehicle goes over a bump or a hole, instant energy dissipated by shock absorber is remarkable and it is on kW order.

The road energy is evaluated in both numerical and experimental methods. Results indicate a great potential of energy harvesting from vehicle shock absorber. In general, researchers only take energy harvesting into account to study the feasibility of active control using regenerated energy. Only laboratory experiments are conducted to validate their numerical predictions. However, this chapter takes a further step forward. The actual on road shock displacement profile is measured with different vehicles on different roads. Moreover, not only power generation is considered, but also vehicle performances such as ride comfort and ride safety are also taking into account. The conflictions between power generation and comfort or safety are investigated numerically; the tradeoffs between vehicle's performances are well studied; the effects on vehicle hardware parameters on performance are also compared. These real time experiments and analysis make this chapter more significant and remarkable.

CHAPTER 3 ELECTROMAGNETIC HARVESTER DESIGN

3. ELECTROMAGNETIC HARVESTER DESIGN

According to Faraday's law of induction, regenerated voltage is proportional to flux density and the crossing velocity of the conducting wire. Therefore, two approaches are proposed to increase the power generation. This chapter will introduce harvester designs for both approaches: linear electromagnetic harvester design on flux increment; rotational electromagnetic harvester designs on motion magnification.

3.1. LINEAR HARVESTER DESIGN

As previously discussed, linear electromagnetic regenerative shock absorbers were first used as dampers in late 1970s. The flexibility on tuning damping by changing shunt resistance caught many researchers' attentions. Variable damping coefficients are favored for better control strategies thus better vibration reduction. On the other hand, a number of theoretical studies have been conducted on the feasibility of energy harvesting using linear electromagnetic motor while providing damping for vibration migration. Simulations are done for possible energy output. Prototypes were made and evaluated for power output. However, energy density [watts/cubic meters] is these designs are not enough. In this section, we study different magnets configurations. Electromagnetic finite element is used to analyze and optimize to achieve higher energy density. Power estimation of the optimal design will be studied. Finally, the new designs are compared with previous ones.

3.1.1. DESIGN PARAMETERS

From design perspective, the linear electromagnetic regenerative shock absorbers should be retrofitted to replace the conventional viscous dampers. The limited space to provide enough damping force raises the concern. The performance of the linear regenerative shock absorber is investigated from design and material perceptions. The individual parameter is evaluated for optimal design, and favorable materials will be

selected to achieve higher energy density as well as better damping control. Shock absorber is integrated in vehicle suspension system compactly. The linear regenerative shock absorber is designed to have similar dimensions as conventional shock absorber.

3.1.1.1. CENTER ROD DESIGN

With the limited size, space and material, output power can be increased by increasing the magnetic flux density. Since magnetic flux has to travel in a guided loop, the electrical and magnetic properties of the materials are important. Zuo et al [14] built a half scaled linear electromagnetic harvester with single layer magnets with output power of 8 Watts after modifying the materials. He concluded that the aluminum center rod and steel outside cylinder will have significant effects on guiding magnetic flux to intersect with wire coil, thus more regenerative power can be achieved. The relative magnetic permeability for steel is 100 which can act as a good guide on magnetic flux; while the relative magnetic permeability for aluminum is the same as air which is only 1, thus the magnetic flux loops are pulled by steel cylinder. As a result the magnetic flux density on the intersection increases and more power can be generated. In order to study the characteristics and behaviors of magnetic flux, the 2 D flux plot of linear electromagnetic harvester is studied on ANSYS. Figure 3.1 compares the configurations with aluminum and steel center rods. With aluminum rod, the flux lines are evenly distributed inside the aluminum bad air gap. However, when switching to steel rod, most flux lines are forced to travel inside the steel rod due to the high permeability of steel which left only a few flux lines inside the air gap. Therefore, picking the rod material with lower magnetic permeability will have significant effects on flux density inside the air gap. In this case, aluminum rod is preferred for our design.

Some researchers may be worrying about the fatigue issue of using aluminum rod. The concern is worth to think but not to worry. The weight of the car body is supported by suspension springs and the dampers are majorly under influence of tensile and compressive forces which will be countered by damping force of the actuator. Moreover, aluminum alloys are much stronger than pure aluminum nowadays and the steel cylinders also ensure the damper quality.

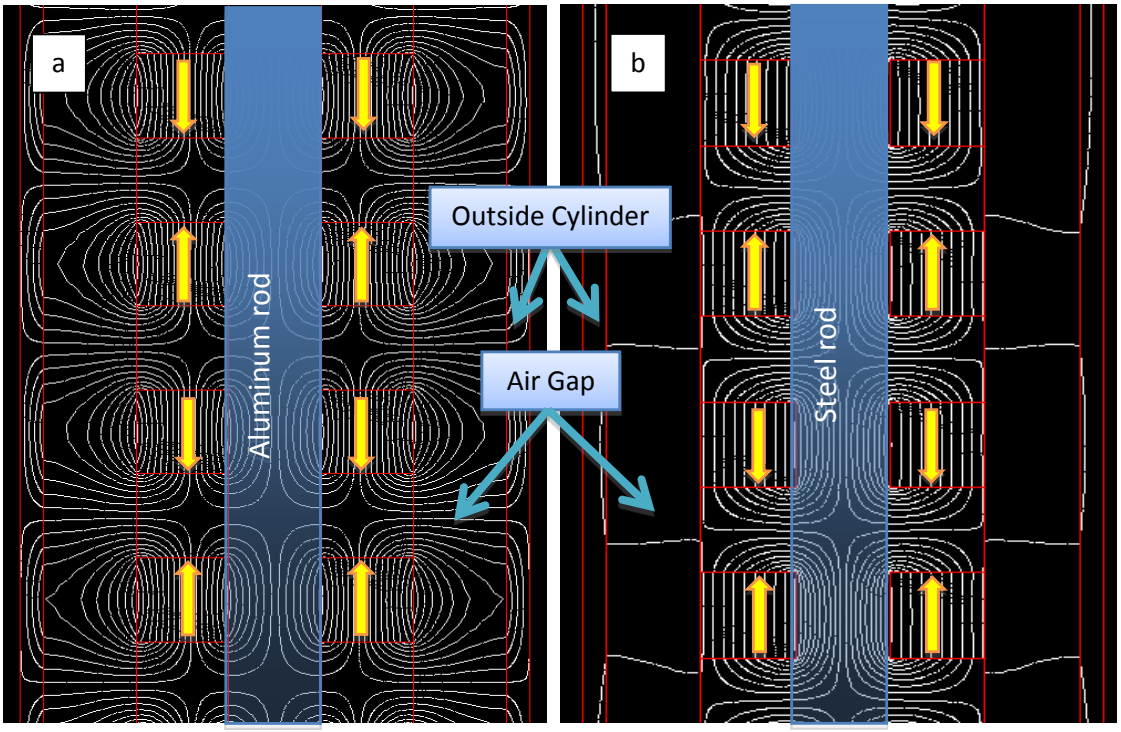

FIGURE 3.1 2D FLUX PROFILE: A) ALUMINUM CENTER ROD, B) STEEL CENTER ROD

3.1.1.2. OUTSIDE CYLINDER DESIGN

Different materials have different capability of guiding magnetic flux. The study of selecting center rod is shown previously for pushing most flux the air gap by using aluminum rod with relative permeability of 1. The following section will introduce the selection of outside cylinder material for both single layer design and double layer design of linear electromagnetic harvester. We believe outside cylinder material selection will make different result on single and double layer designs.

3.1.1.3. SINGLE LAYER OUTSIDE CYLINDER DESIGN

The configuration of single layer cases design is illustrated in Figure 3.2. Without the steel cylinder, magnetic flux acts freely on the plane, and the loop size is larger in diameter, which reduces the flux density. The purpose of steel case will guide more flux passing through the steel cylinder; therefore more horizontal flux lines formed in the air gap which corresponding to more energy generation. The peak flux density along the centerline of air gap increases from 0.25 T to 0.28 T.

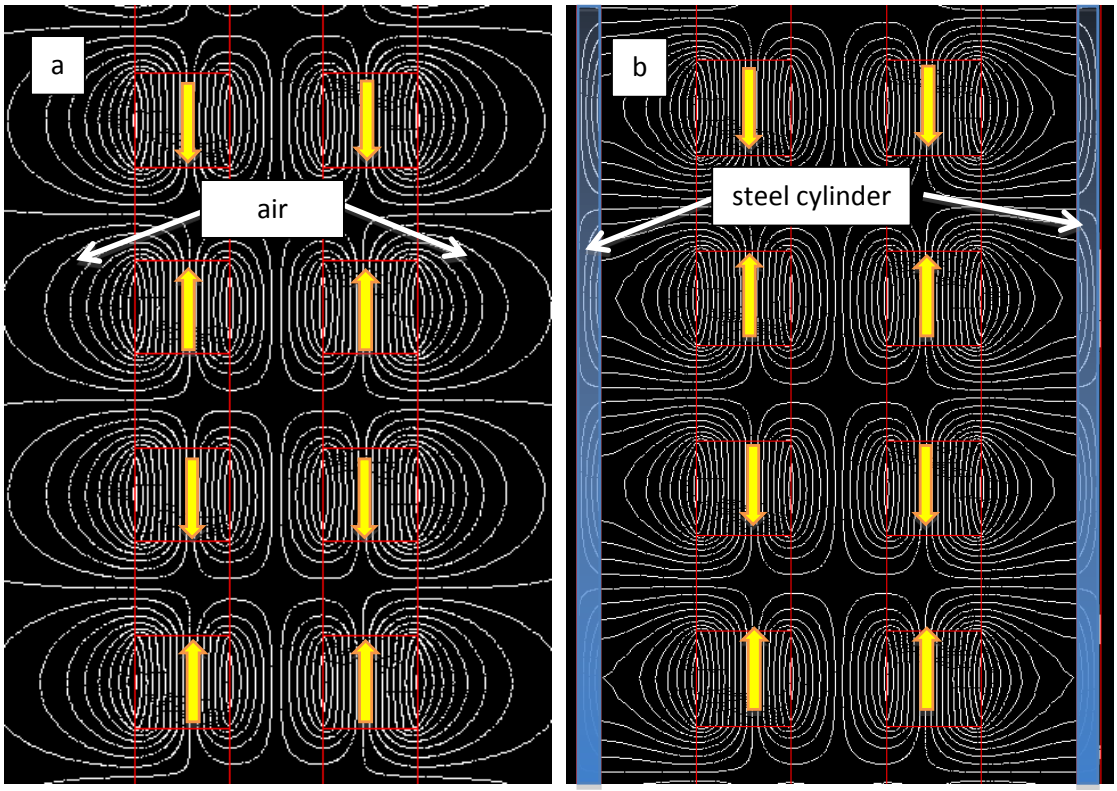

FIGURE 3.2 SINGLE LAYER SHOCK OUTSIDE CYLINDER DESIGN; A) WITHOUT CYLINDER, B) WITH STEEL CYLINDER

3.1.1.4. DOUBLE LAYER OUTSIDE CYLINDER DESIGN

For single layer, a steel case with high relative permeability is applied to guide flux thus increase the flux density inside the air gap. Initially, the magnetic flux is guide with the application of two layers of magnets in a loop for double layer design. It is significant to study the case material selection of double layer design. Different from single layer design, the wire coils are traveling between two layers of magnets. Therefore, flux will be majorly guided by the configuration of magnets. However, it is worth to understand the cylinder effects of magnetic flux through FE analysis.

The magnetic flux lines for double layer design are shown in Figure 3.3, left figure shows magnetic flux plot using steel cylinder and right flux plot is the result of applying aluminum cylinder. The permeability for steel is 100 times more than the permeability of aluminum and air. Most flux is pulled to pass through the steel case instead of the air gap. Therefore, flux density is higher inside the air gap by using aluminum case.

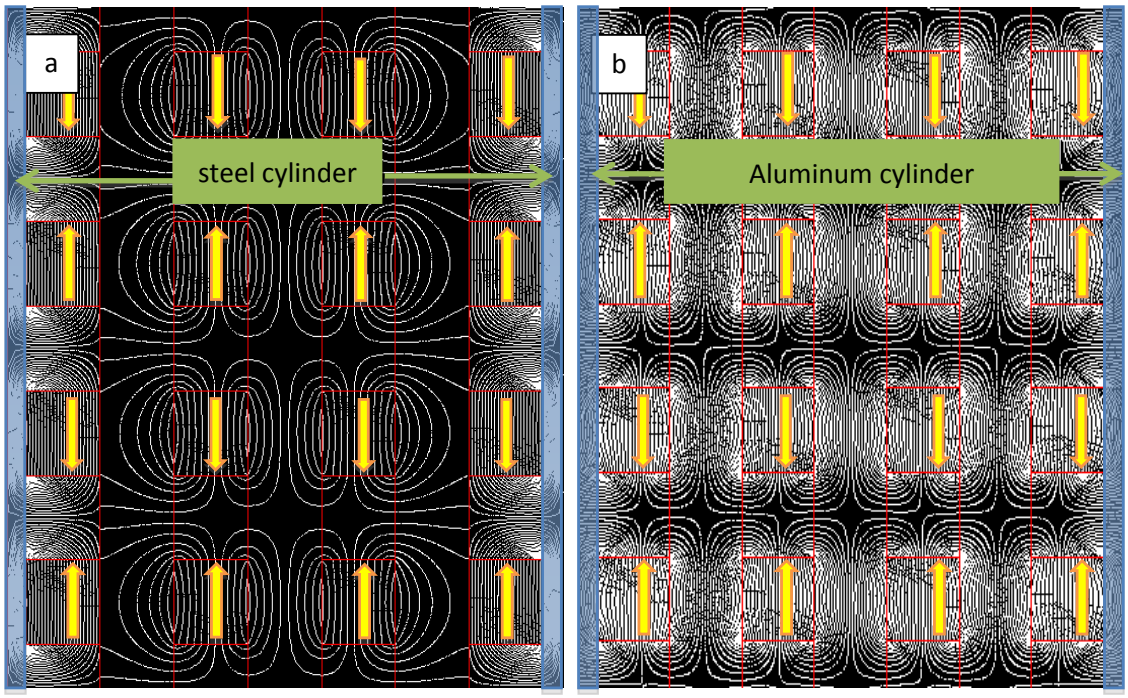

FIGURE 3.3 DOUBLE LAYER CYLINDER DESIGN; A) STEEL CYLINDER, B) ALUMINUM CYLINDER

3.1.1.5. EXTREME CONDITION DESIGN

People may question on why only aluminum and steel is chosen for constructing the linear electromagnetic harvester. If the material with even lower permeability than aluminum or higher permeability than steel applied to the design, will it make significant changes or difference? Will magnetic flux density increase greatly if all the flux is pushed to the air gap where wire coil is by using superconductor as center rod and electrical steel to guide the flux? To this question further, the magnetic flux figure is plotted with electrical steel case and superconductor rod as shown in Figure 3.4. Here, superconductor with zero relative magnetic permeability and electrical steel with 40 times stronger magnetic permeability than steel is compared. The figure on the left shows the flux with superconductor center rod and electrical steel cylinder; flux graph is plotted with aluminum center and electrical steel shown in the middle; and right figure is using aluminum center rod and steel cylinder.

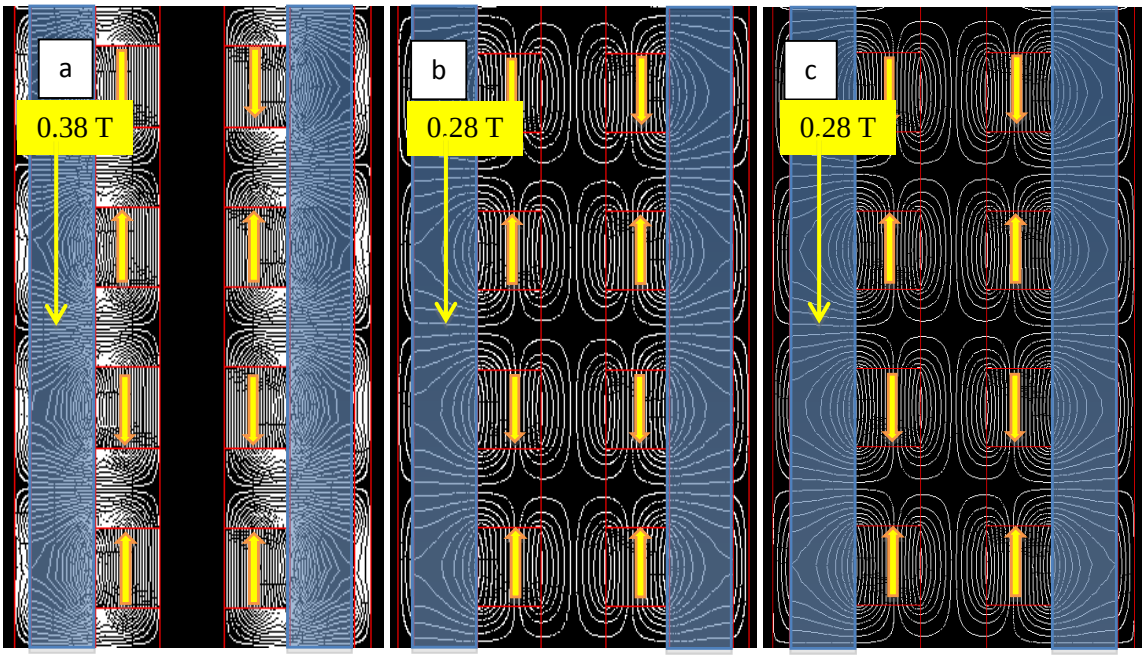

a. Superconductor rod with electrical steel case

b. Aluminum rod with electrical steel cylinder

c. Aluminum rod with steel cylinder

FIGURE 3.4 EXTREME CONDITION STUDY OF CENTER ROD AND CYLINDER DESIGN

The result indicates a positive effect of the extreme condition. ANSYS flux plot shows much more magnetic flux is passing through the air gap and the implementation of superconductor does significant contribute pushing flux to the air gap. This is because no flux can travel through the superconductor thus all flux lines are force to go the other direction. The high magnetic permeability of electrical steel acts as an excellent guidance to pull flux lines passing through the electrical steel. As a result, the peak flux density inside the air gap increases from 0.28 Tesla to 0.38 Tesla.

The magnetic flux always goes in a loop and it can be directed by selective materials which can result more magnetic flux density in air gap. The peak flux density along the centerline of the air gap can be boosted up 30 % when extreme conductions are applied. Material selection is just one way to increase the flux density inside the air gap, the other way to increase the field density in the air gap is to manipulate the configurations of magnets arrangement and will be investigated and discussed in the following section

3.1.2. SINGLE LAYER CONFIGURATIONS

Difference magnets configuration or arrangement will have different effects on the flux passing through air gap. Traditionally, only axial magnets are used for electromagnetic harvester and the ways of arrangement are very limited. Babak Ebrahimi [22] introduced some design of eddy current damper using the radial magnets, where the flux goes from inner ring to outer ring or the other way. He proposed the higher eddy current damping can be achieved with axial and radial magnets combination. Figure 3.5 shows the characteristics of axial and radial magnets where blue color and red color corresponding to south and north poles respectively.

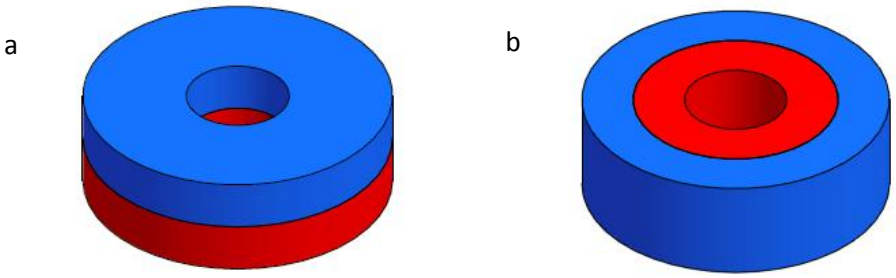

FIGURE 3.5 AXIAL AND RADIAL MAGNETS CONFIGURATION; A) AXIAL, B) RADIAL

Using two types of magnets more arrangements can be designed and compared. Four different selected arrangements of single layer harvester design are shown in Figure 3.6.

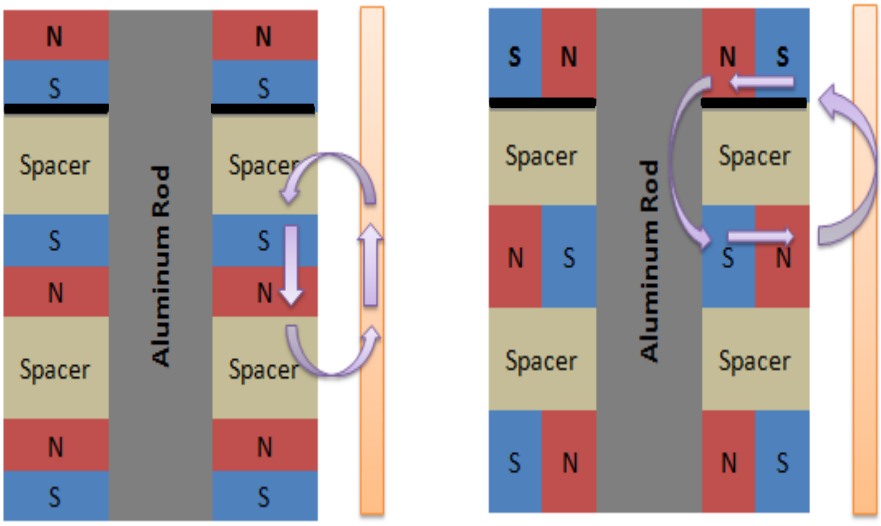

a. Axial magnets with spacers

b. Radial magnets with spacers

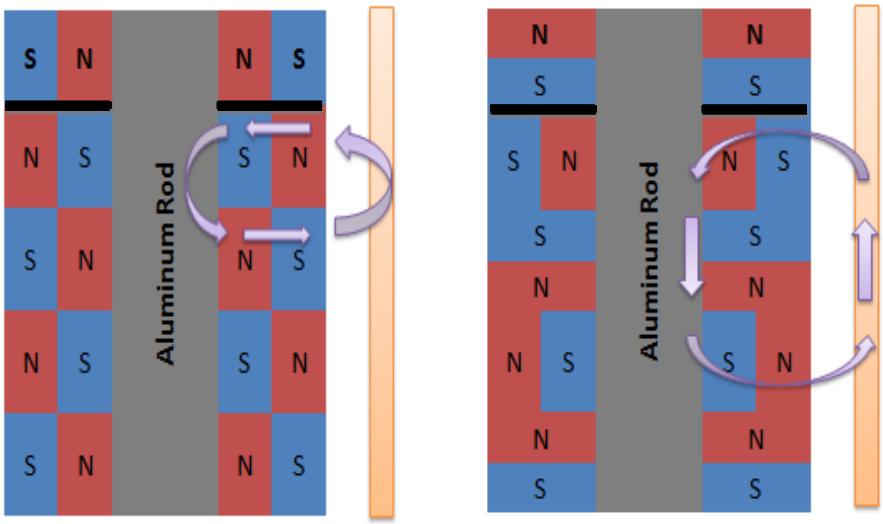

d. Radial magnets alternative

c. Axial and radial magnets

FIGURE 3.6 SINGLE LAYER MAGNETS ARRANGEMENTS

First arrangement is only composed of axial magnets with iron spacers in between. The same pole facing each other will push the flux to sides, and then steel cylinder with aluminum rod will guide most flux passing through the air gap. Moreover, this is the configuration Zuo [14] built for conducting experiments. The second arrangement to the right only applied radial magnets with iron spacer in between. The flux loops are clearly revealed with this arrangement. The lower left arrangement is studied for the purpose of spacer's application. Only radial magnets are applied which might result in short loops. Lastly, the combination of axial and radial magnets configuration is shown in the lower right corner. The axial and radial magnets are arranged alternately; so does the orientations.

3.1.3. DOUBLE LAYER CONFIGURATIONS

For the single layer configurations, we can only push more flux to the air gap where wire coil cuts. In order to have a better guiding on magnetic flux, a double layer configuration concept is introduced as shown in Figure 3.7. Two different sizes of magnetic rings are used to accomplish this job. Here, only radial magnets are used in this sample configuration.

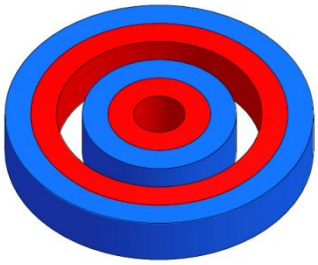

FIGURE 3.7 DOUBLE LAYER DESIGN OF MAGNETS LAYOUT

Instead of cutting the flux outside the magnets using single layer, the wire coils are used to cut the flux in between the two layers of magnets. We expect more flux density will exist for double layer magnets configuration. With two layers of magnets configuration, more arrangements can be made for further study. Figure 3.8 illustrates four selected arrangements of magnets of double layer electromagnetic harvester. The expected loop is also shown in arrows.

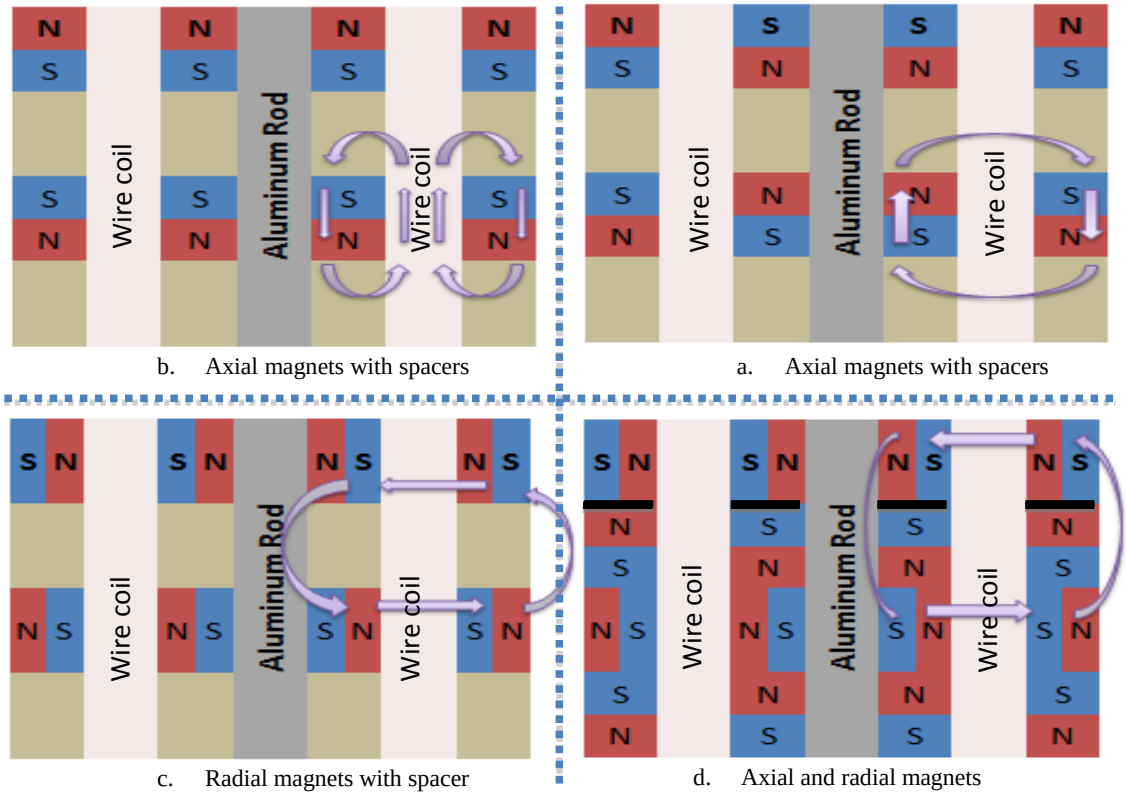

FIGURE 3.8 FOUR ARRANGEMENTS OF MAGNETS FOR DOUBLE LAYER DESIGN

Arrangements *a, b, and c* use single type of magnets; either axial or radial magnets with spacers. The difference between first and second arrangement is the 180 degree phase shift. The fourth arrangements combine both axial and radial magnets to guide magnetic flux. Higher flux density inside the air gap is expected in fourth arrangement.

3.1.4. RESULT AND DISCUSSION

Both single layer and double layer arrangements are plotted and studied by using ANSYS. This section will have a detailed discussion on selecting right configuration and right arrangement. Through FE analysis, the flux projection of different arrangements are revealed and studied graphically.

3.1.4.1. SINGLE LAYER

Figure 3.9 shows the flux lines inside the air gap of each arrangement in highlighted areas. Arrangement *a* and *d* shows the most flux lines in the air gap by analyzing the plots graphically. Instead of pushing magnetic flux to the air gap shown in arrangement *a*, most of the flux of arrangement *d* are guided by the axial permanent magnets, thus less flux lines are shown inside the center rod. The combination of axial and radial magnets forms flux loops mostly passing through the air gap, while flux loops are evenly distributed in both air gap and center rod when only axial magnets are applied.

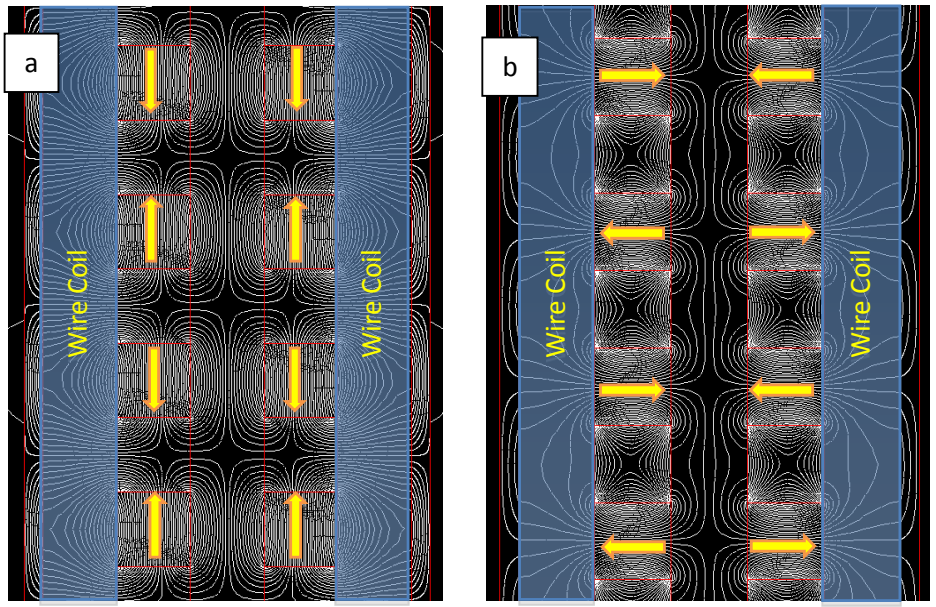

a. Axial magnets with spacers b. Radial magnets with spacers

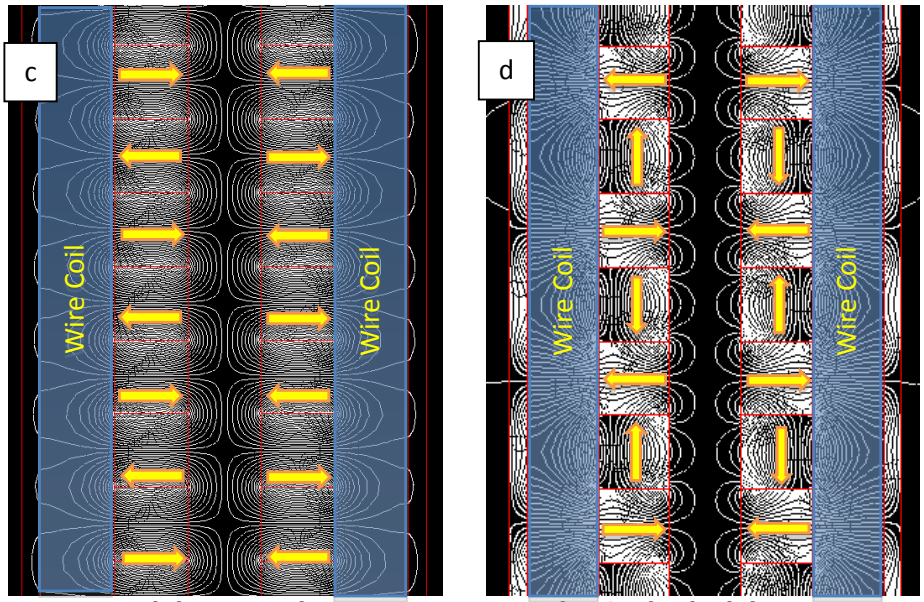

c. Radial magnets only d. Axial and radial magnets

FIGURE 3.9 2-D FLUX PLOTS OF SINGLE LAYER CONFIGURATIONS

To further study the best arrangement, the flux density figures are illustrated in Figure 3.10. According to the flux density plot, arrangement *a* is made of 1/4 of 0.7 tesla and 5/8 of 0.4 tesla and 1/8 of 0.1 tesla while arrangement *d* is made of ½ of 0.7 tesla, 3/8 of 0.4 tesla and 1/8 of 0.1 tesla. Therefore, the average flux density of arrangement *a* is 0.4375 tesla approximately and the average flux density for arrangement *d* is about 0.5125 tesla. As the result arrangement *d* has the highest flux density in the air gap. The calculations are based on the average flux density inside the air gap graphically since it is filled with wire coil entirely.

Undoubtedly, arrangement d won the highest flux density award for single layer design. This is because the radial magnets in alternate arrangement compose better loops to guide magnetic flux. Arrangement *b* and *c* are simply short looped, where flux travels back to south poles straightly without passing through the air gap.

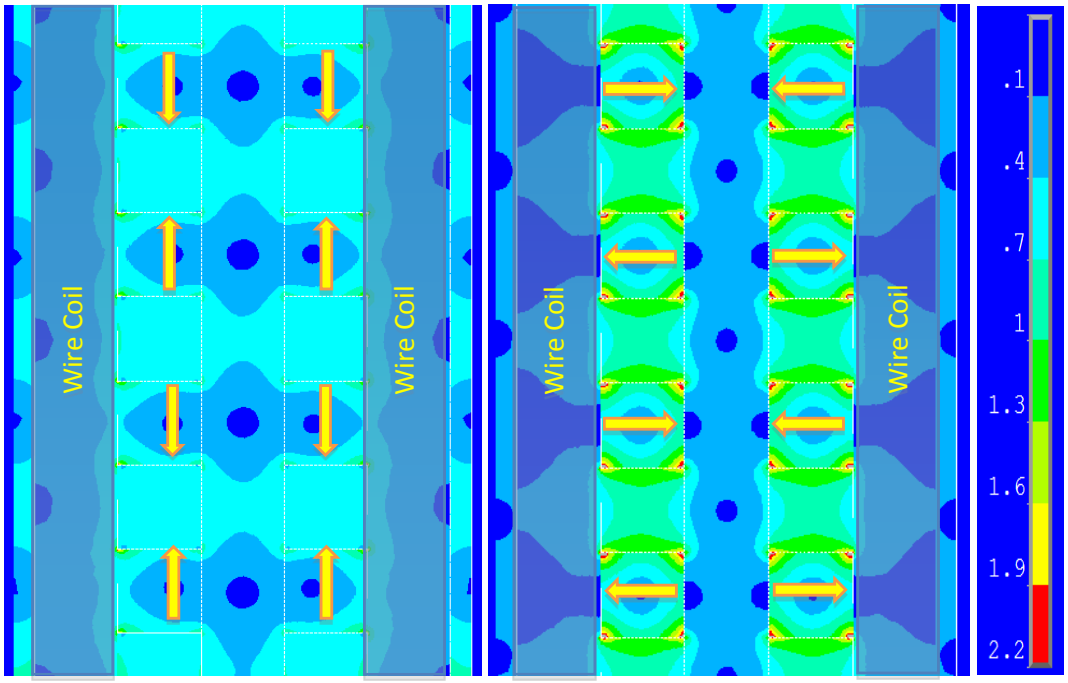

a. Axial magnets with spacers b. Radial magnets with spacers

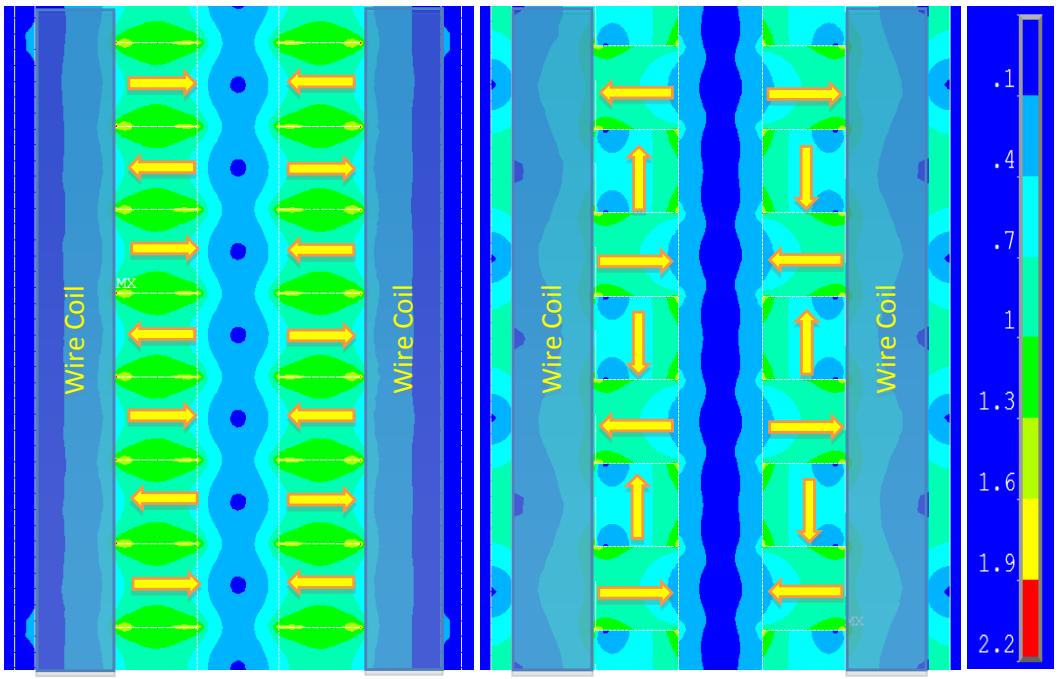

c. Radial magnets only d. Axial and radial magnets

FIGURE 3.10 FLUX DENSITY PLOT OF FOUR ARRANGEMENTS WITH SINGLE LAYER CONFIGURATION

3.1.4.2. DOUBLE LAYER

There will be larger magnetic flux density in the air gap using double layer magnets according to the hypothesis we made. This section is going to study or verify the advantages of double layer configuration. The 2D flux lines are plotted in Figure 3.11 for all four arrangements.

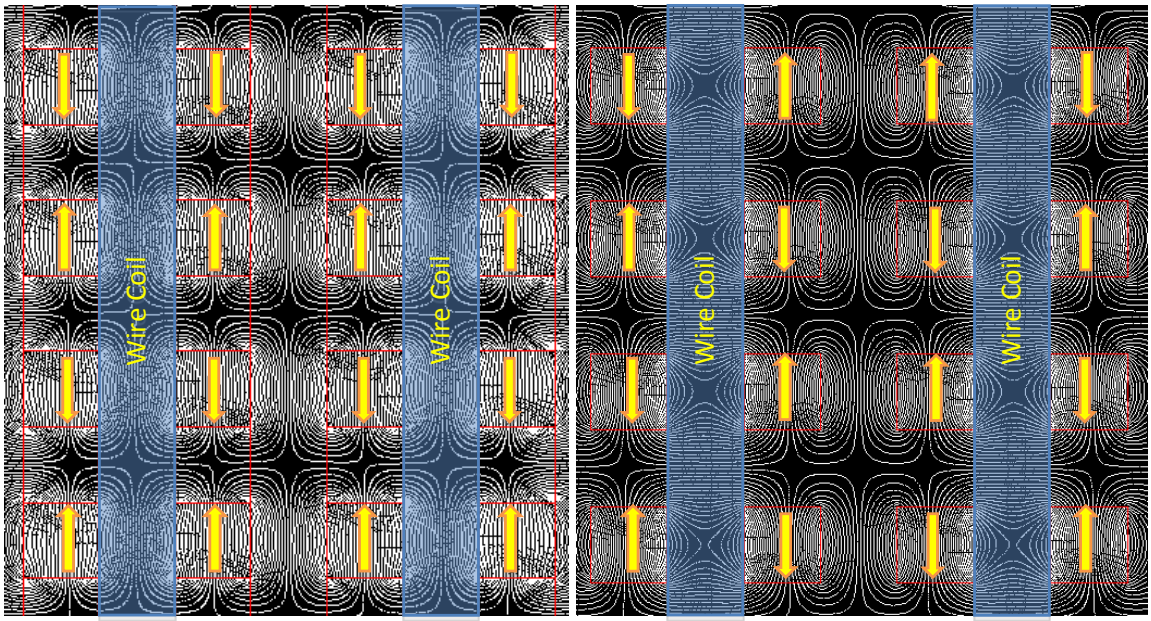

a. Axial magnets with spacers

b. Axial magnets with spacers

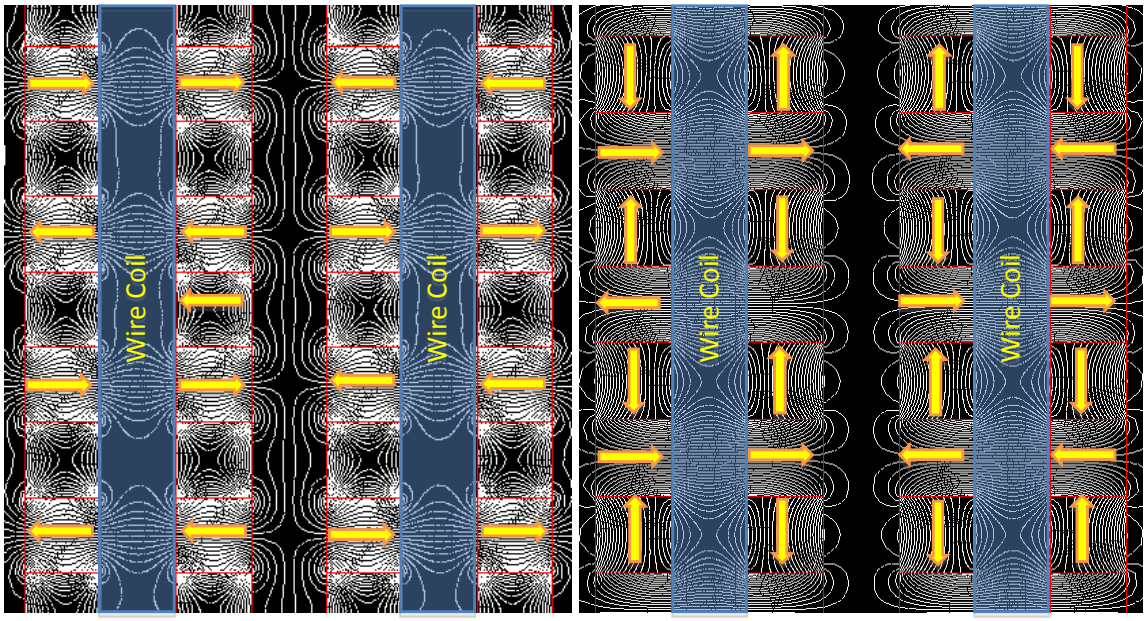

c. Radial magnets with spacers

d. Axial and radial magnets

FIGURE 3.11 2-D FLUX LINES FOR ALL FOUR ARRANGEMENTS WITH DOUBLE LAYER CONFIGURATION

The trajectories of flux loops are revealed clearly. Arrangement *a*, *b*, and *d* have the most flux lines in the air gap. Note that the maximum energy generation occurs are the wire cuts the magnetic field perpendicularly. Therefore, arrangement *a* is not favorable for energy generation. Flux lines illustrate the magnetic trajectory, but they do not show the flux density inside the air gap. Further studies are inspected to understand the best arrangement to provide maximum output power. The flux density plots are shown in Figure 3.12.

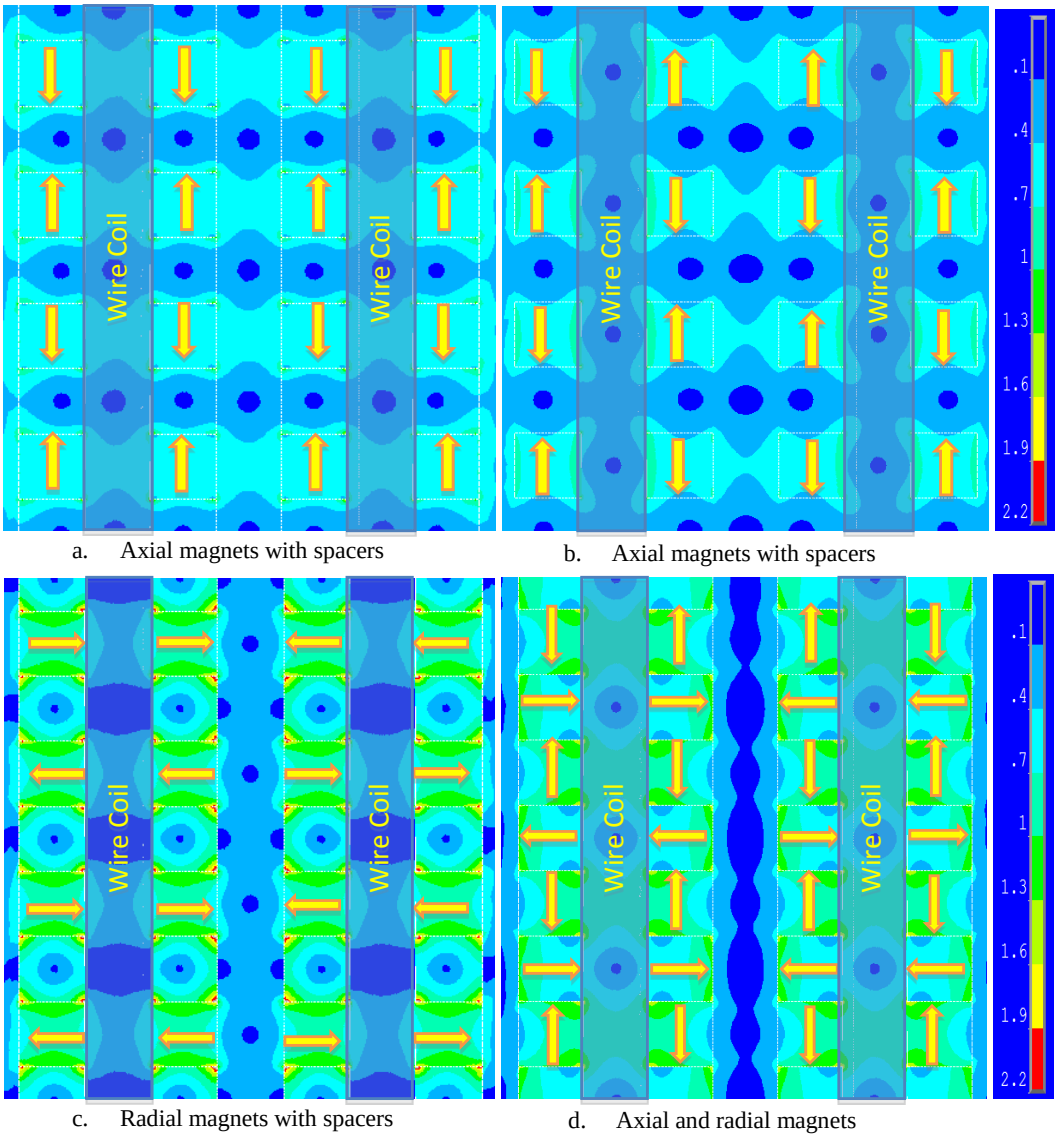

a. Axial magnets with spacers

b. Axial magnets with spacers

c. Radial magnets with spacers

d. Axial and radial magnets

FIGURE 3.12 FLUX DENSITY PLOTS FOR ALL FOUR ARRANGEMENTS WITH DOUBLE LAYER CONFIGURATION

Results indicate similar flux density for arrangement *b* and *c*, which is about 0.35 tesla in average inside of the air gaps. The two best arrangements are arrangement *a* and arrangement *d*. However, most flux for arrangement *a* is vertical direction which will be parallel to wire coil and result in few power generation. The average flux density for arrangement *d* is calculated to be 0.84 tesla by adding 10% of 1.3 tesla, 45 % of 1 tesla, 25 % of 0.7 tesla, 20% of 0.4 tesla and 5 % of 0.1 tesla. Results also show the great opportunity on the space outside the outer magnets. There is significant amount of flux outside the outer layer. If the wire coil is made of double layer too, more energy can be harvested.

After studying both single layer and double layer configurations with eight different arrangements in total, peak magnetic flux density in horizontal direction along the center line of air gap are filled in Table 3.1 referring to Figure 3.10 and Figure 3.12. The best arrangement is *d* for double layer with both axial and radial magnets where peak flux density is shown as 0.8 T. The second best arrangement is *d* for single layer also with both axial and radial magnets and the peak flux density is 0.45 T. Radial magnets contribute the significant function on guiding magnetic flux in loops. Arrangement *a* for single layer configuration was used in our initial research prototype and it shows 0.28 T as the peak flux density along the center line of air gap.

For single layer only, implementation of radial magnets can increase the peak flux density by 160.7%. Therefore, the regenerated power will increase 2.56 times. So does the energy density since they are the same size design. When another layer of magnets with both axial and radial magnets are added to the configuration, the peak flux density increased 285.71% compare to original design. The increment of flux density inside the wire coil significantly increases the power generation by a factor of 8. Since energy density is mostly considered for design, the energy density of double layer design increases 5 times. This is because the volume of double layer design increases 1.6 times.

TABLE 3.1 PEAK FLUX DENSITY ALONG CENTER LINE OF AIR GAP

Single Layer	Peak Flux	Double Layer	Peak Flux
Arrangement *a*	**0.28 (Initial)**	Arrangement *a*	0.015
Arrangement *b*	0.17	Arrangement *b*	0.37
Arrangement *c*	0.14	Arrangement *c*	0.35
Arrangement *d*	**0.45 (Improved)**	Arrangement *d*	**0.80(Optimal)**

3.1.5. POWER GENERATION

When a conductor of length *l* crossing a magnetic field B [T] at a constant velocity *v*, the EMF voltage *V* is expressed as

$$V = vl \text{ X } B = vl * B \sin(\theta) \tag{3.1}$$

In linear harvester, the wire coils are perpendicular to the magnetic field. Therefore, the EMF voltage is also read as

$$V = vl * B \sin\left(\frac{\pi}{2}\right) = Bvl \tag{3.2}$$

The maximum current *I* (A) is generated by shunt the circuit, and is calculated as

$$I = \frac{V}{R} = \sigma B v A_w \tag{3.3}$$

where σ is the electrical conductivity and A_w is the cross sectional area of the conducting wire. Therefore, the peak power is the product peak voltage and peak current.

$$P = VI = B^2 v^2 l \sigma A_w \tag{3.4}$$

Power is proportional to both flux density square and velocity square. Therefore, two approaches on increasing generated power. One way is by redesigning the linear harvester using both axial and radial magnets in double layer configuration to increases the magnetic flux density inside the air gap which is discussed in this chapter; the other way is to magnify the velocity to increase the generated power and is going to be discussed in rack & pinion and ball screw designs.

3.1.5.1. FLUX PROFILE

The magnetic flux density profiles are plotted and discussed above. The flux density is not evenly distributed inside the air gap. Instead, it shifts from positive to negative alternatively due to the flux direction. In general case, the center line magnetic flux density profile is taken to consider and is plotted in Figure 3.13 for arrangement *d* in double layer configuration. Marker (*) is horizontal direction flux density read from flux density figures. The colored lines represent fitting sin curves and they match the picked points very well. Thus the flux density can be modeled as the sine curves.

$$B = B_0 \, sin\left(\frac{x\pi}{2h}\right) \tag{3.5}$$

Where, B_0 is the peak flux density which happens to be 0.8 T, *x* is the axial position of magnets, and *h* is the thickness of axial and radial magnets.

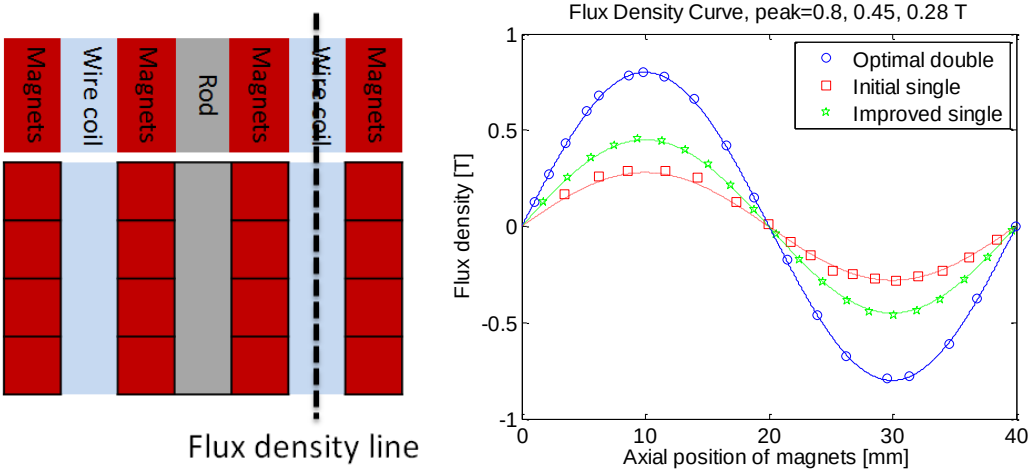

FIGURE 3.13 MAGNETIC FLUX DENSITY ALONG THE CENTER LINE OF AIR GAP

3.1.5.2. COIL PROFILE

Inside the air gap, several wire coils are used to generate electricity by crossing magnetic fields. The wire coils consist of wire loops and windings. The length of a single wire coil is found to be

$$l = ND_a\pi \tag{3.6}$$

where, D_a is the average loop diameter and N is number loops which is determined

$$N = \frac{\pi}{2\sqrt{3}}\frac{A_c}{A_w} \tag{3.7}$$

Here, A_c and A_w are the cross sectional areas of wire coil and wire. By substituting the wire length into the generated voltage and power equations we obtain the peak voltage and power as

$$V = \frac{\pi^2 B v D_a A_c A_w}{2\sqrt{3}} \tag{3.8}$$

$$P = \frac{B^2 v^2 \pi^2 \sigma D_a A_c}{2\sqrt{3}} \tag{3.9}$$

3.1.5.3. PHASE PROFILE

The thickness of the wire coil determines the amount of output energy from vibration. This is because the flux inside the air gap varies and shifts signs refer to Figure 3.13. If the thickness of the wire coil equal to the magnetic flux cycle length which is 40 mm, there will be no electricity generated at all. There will be same amount of positive charges generated as the negative charges. A typical 2-phase design motor is shown in Figure 3.14. Two wire coils are used to harvester the generate electricity. Assume the initial stage is shown as in figures, the maximum voltage in both coils happen concurrently at 0 and 180 degrees. There is no electricity generated when the phase are 90 and 270 degree because the positive flux average out with the negative flux.

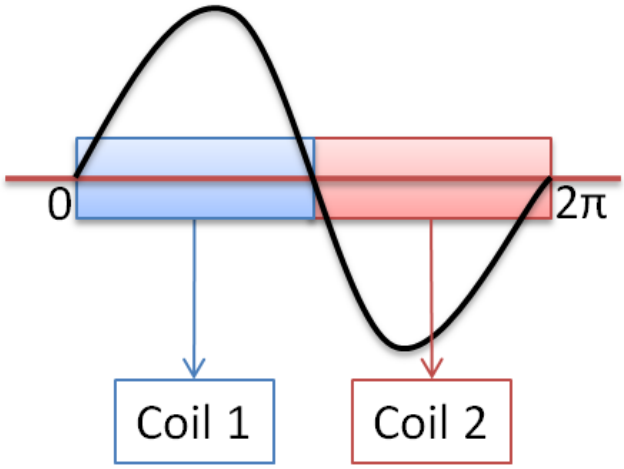

FIGURE 3.14 TWO PHASE DESIGN

Generally speaking, three phase motor design will have more power generated than two phase design. Instead on have two coils fitting the flux cycle, three wire coils are installed for power generation and is illustrated in Figure 3.15.

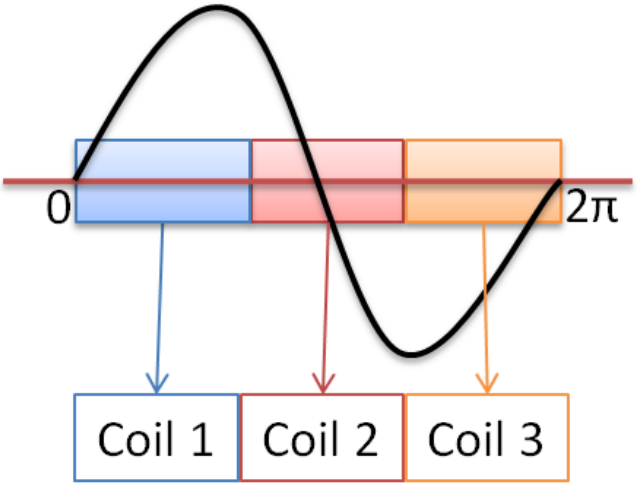

FIGURE 3.15 THREE PHASE DESIGN

Each coil width is one third of the cycle length which is 13.3 mm. At the initial stage, second coil generates no electrical. As the winding moves to the right, voltage in coil 1 increases to its maximum at 30 degrees. Inversely, voltage in coil 3 decreases to it minimum at 60 degrees. When the coils move to 90 degrees, maximum voltage achieved at coil 2. Coil 3 experiences maximum load at 150 degrees.

Zuo designed a four-phase motor which the width of wire coil is the same as the thickness of the magnets. The four-phase motor design is illustrated in Figure 3.16 bellow. Each coil occupies a phase 90 degree of the flux cycle. Eight peaks can be achieved in a cycle. They are 45 & 225 degrees for both coil 1 & coil 3 and 135 & 315 degrees for both coil 2 & coil 4. Here, coil 1 and coil3 are moving out of phase. So does coil 2 and coil 4.

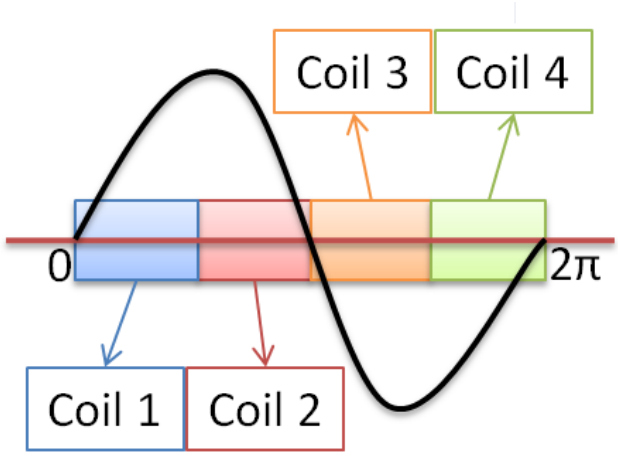

FIGURE 3.16 FOUR PHASE DESIGN

Table 3.2 gives the overall performance of both two-phase, three-phase, and four phase motor. The number peaks corresponding to the number of phases. Therefore, four-phase motor will have the most power output than both three-phase and two-phase motors.

TABLE 3.2 OVERALL PERFORMANCE OF 2-PHASE, 3-PHASE, AND FOUR-PHASE MOTOR

Two Phase Motor	Minimum	Maximum
Coil 1	90 & 270	0 & 180
Coil 2	90 & 270	0 & 180
Three Phase Motor		
Coil 1	120 & 300	30 & 210
Coil 2	0 & 180	90 & 270
Coil 3	60 & 240	150 & 330
Four Phase Motor		
Coil 1	135 & 315	45 & 225
Coil 2	45 & 225	135 & 315
Coil 3	135 & 315	45 & 225
Coil 4	45 & 225	135 & 315

3.1.5.4. POWER CALCULATION

Recall from the flux density curve in Figure 3.13, the flux is not evenly distributed. Therefore, average flux density is applied to calculate the voltage generation. As a result, voltages generated in three wire coils are expressed as below

$$V_i = \bar{B}_i v l \tag{3.10}$$

The maximum power generated using the linear generator for one coil is then express as

$$P_i = \frac{\bar{B}_i^2 v^2 l^2}{R} \tag{3.11}$$

The circuit is shunt with internal resistance R. Therefore, the total power generated by the linear harvester is

$$P_{total} = N \sum_i P_i \tag{3.12}$$

Here, N is the number of flux cycles and *i* is equivalent to 1, 2, and 3.

The power estimation is adopted to evaluate the performance of the linear motor using all three designs. AWG 30 cooper wire is used and assumptions are made for the approximation. Related linear harvester specifications and certain parameters are presented in Table 3.3.

TABLE 3.3 HARVESTER PARAMETERS FOR POWER ESTIMATION

	2-phase	**3-phase**	**4-phase**
Air gap width	1 mm	1 mm	1 mm
Winding width	1 mm	1 mm	1 mm
Coil inner diameter	17 mm	17 mm	17 mm
Coil outer diameter	24 mm	24 mm	24 mm
Coil height	20 mm	13.3 mm	10 mm
Average loop diameter	41 mm	41 mm	41 mm
Wire diameter	0.254 mm	0.254 mm	0.254 mm
Coil length	322.75 meter	215.17 meter	161.38 meter
Coil velocity	0.25 m/s	0.25 m/s	0.25 m/s
Coil resistance	109.24 Ohm	72.8 Ohm	54.62 Ohm

All two-phase, three-phase and four-phase voltage curves are generated after plotting all parameters as shown in Figure 3.17, Figure 3.18, and Figure 3.19 respectively. The graphs represent a complete cycle (360 degrees, 40mm) motion of each wire coil. Voltage generated using two-phase motor is slightly higher than both three-phase motor and four-phase motor because the wire length of two-phase motor is the longest. More importantly, the generated voltage using double layer configuration is much higher than single layer harvester design done my Zuo. Peak voltages are estimated as 41 volts, 35 volts and 29 volts for two-phase, three-phase, and four-phase motors respectively.

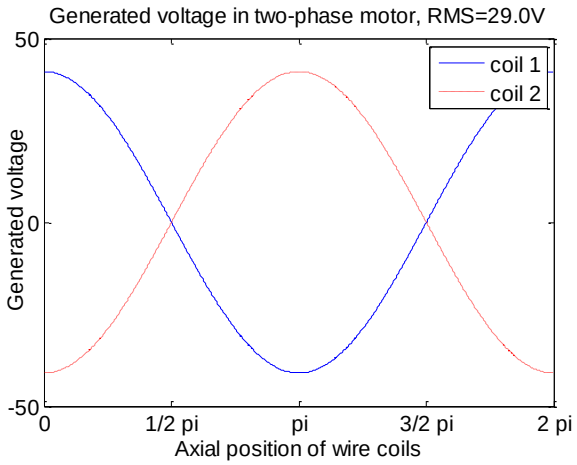

FIGURE 3.17 GENERATED VOLTAGE CURVES FOR TWO-PHASE MOTOR DESIGN

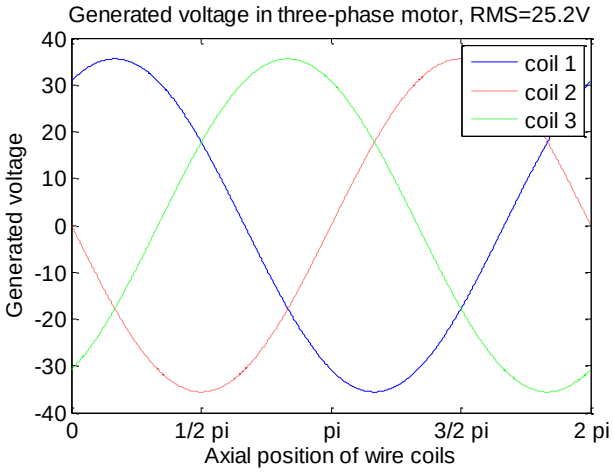

FIGURE 3.18 GENERATED VOLTAGE CURVES FOR THREE-PHASE MOTOR DESIGN

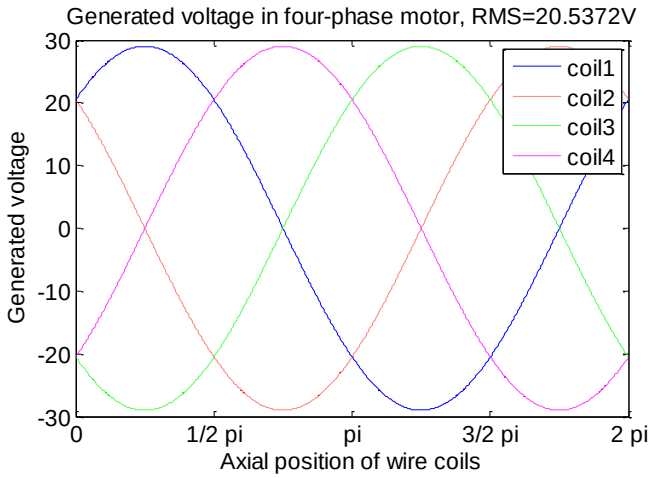

FIGURE 3.19 GENERATED VOLTAGE CURVES FOR FOUR-PHASE MOTOR DESIGN

Maximum power is achieve by short the circuit. The generated powers for all two-phase, three-phase, and four-phase motors are plotted in Figure 3.20, Figure 3.21, and Figure 3.22 accordingly. For two-phase motor, power curves overlap with each other although coils move out of phase. This is because power is the calculated as the square of voltage over the internal resistance. Peak power happens at 15.5 watts, with mean power of 7.7 watts for each coil. For three phase-motor, generated powers are in different phases. Peak power is found higher than two-phase motor which is about 17.5 watts. So does the mean power value and is shown to be 8.7 watts for each wire coil in three-phase motor. For four-phase motor, only two phases of power curves are revealed. This is because coil 1 is paired with coil 3 and coil 2 is paired with coil 4. Interestingly, wire coils inside two-phase and four-phase motors experience the same peak power which is 15.5 watts thus the mean power is also the same. This is because the average flux for four-phase coils is two times stronger than the average flux for two-phase coils. It evens the gap created by wire length and wire resistor.

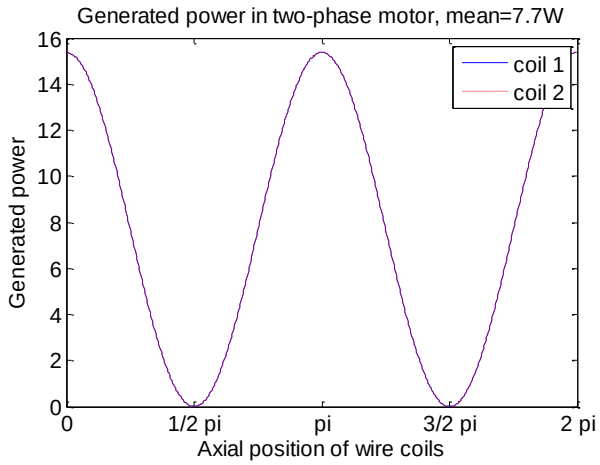

FIGURE 3.20 GENERATED POWER CURVES IN TWO-PHASE MOTOR

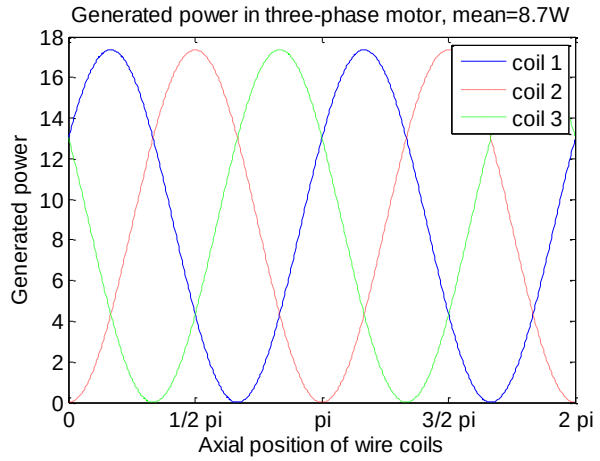

FIGURE 3.21 GENERATED POWER CURVES IN THREE-PHASE MOTOR

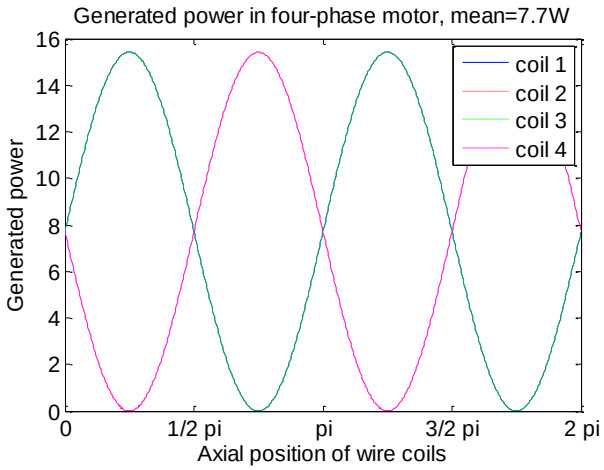

FIGURE 3.22 GENERATED POWER CURVES IN FOUR-PHASE MOTOR

The performances of all three phase designs are illustrated graphically above. Four-phase motor shows the most power generation. The overall comparison of phase design is filled in Table 3.4 below. The total generated power can exceed 100 watts using both three-phase and four-phase motor design when 4 cycles of magnets are applied. Three-phase motor can generate 43 watts more power than two-phase motor design which is equivalent to 169.5 % increment. More importantly, four-phase motor design doubled the power generation compare to two-phase design.

TABLE 3.4 EVALUATION ON PHASE SELECTION AT 0.25 M/S

Performance (one	**Two-phase motor**	**Three-phase motor**	**Four-phase**
NO. of coils in a cycle	2	3	4
Number of cycles	4	4	4
Peak value voltage	41 volts	35 volts	29 volts
RMS value voltage	29.02 volts	25.16 volts	20.54 volts
Peak value power	15.5 watts	17.5 watts	15.5 watts
Mean value power	7.7 watts	8.7 watts	7.7 watts
Total power generated	61.6 watts	104.4 watts	123.2watts

3.1.5.5. OPTIMAL PHASE DESIGN

With the same cycle length, the number phases increase will result in shorter wire length. Therefore, the generate voltages and wire resistances decrease exponentially as shown in Figure 3.23 and Figure 3.24. However, there is no voltage shown at 1-phase design.

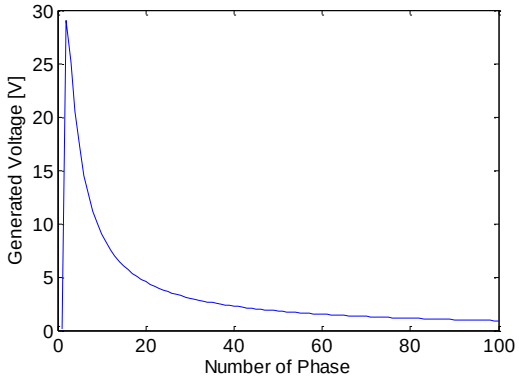

FIGURE 3.23 GENERATED VOLTAGES WITH DIFFERENT PHASE DESIGN

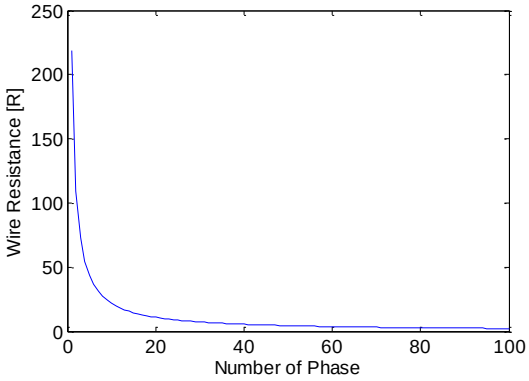

FIGURE 3.24 WIRE COIL RESISTANCES AT DIFFERENT PHASE DESIGN

Table 3.4 shows a direct relationship between total power generation and number of phase design. Is more phases contributing more power generation? Is there an optimal phase design for maximum power generation? To answer this question, regenerated power at 100 phase designs are studied in Figure 3.25.

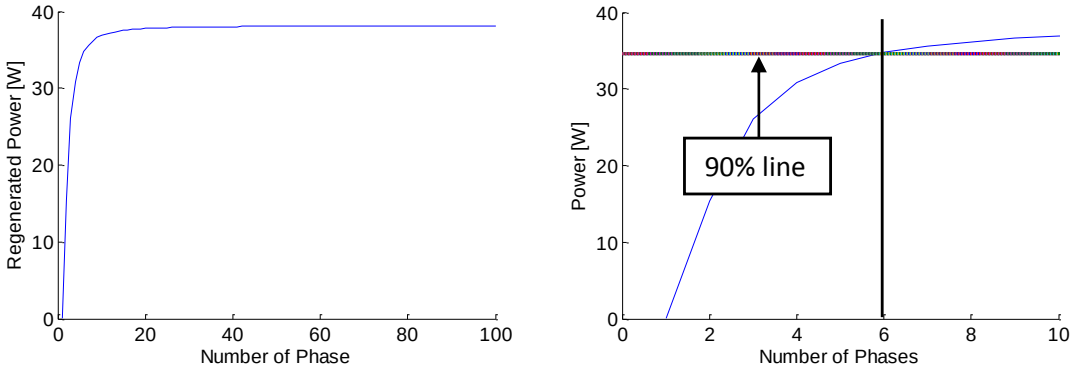

FIGURE 3.25 OPTIMAL PHASE DESIGN

Generated power is increasing with number of phases. However, there is a limit for maximum power generation which is 38.5 Watts for one cycle when number of phases approaches to infinity. The generated power increases significantly with number of phases before 10-phase design. 90% of maximum power can be achieved with 6-phase motor design as shown in dot-line.

3.1.6. LINEAR HARVESTER CONCLUSION

Both single layer and double layers of magnets configurations are studied in this chapter. Material selection on center rod and case design are investigated and studied. Eight different arrangements in total are studied and analyzed using finite element method by ANSYS. The flux lines and flux densities are evaluated and compared graphically. Result shows the double layer configuration with arrangement *e* contributes the highest energy density where 0.8 tesla of flux density exists in the center line of air gap. The new configuration of using two layers of magnets along with guiding loop arrangement has significant improvement on power generation

Improving the flux density inside the air gap is one way to increase power generation. Result of using both radial and axial magnets shows significant improvement. The peak flux density inside the air gap increases by 285.71% compare to the original design. As a result, the energy generated by the new design can harvest more than 5 times energy than the prototype built by Zuo's research. Moreover, a four phase motor is designed to harvest more energy. The generated power is increasing with number of phase design. 90% of maximum power can be achieved with 6-phase design. Total power generation is estimated to be over 100 watts for the new design. It shows the significant improvement in power generation.

In this thesis, different configuration and arrangements are studied by finite element method and evaluated using ANSYS graphically. Best configuration with arrangement is selected with most energy density. The next step is to build an actual prototype to verify the improvement of theoretical results.

3.2. ROTATIONAL HARVESTER

The method of increasing power generation by optimize flux density inside the air gap is shown in linear electromagnetic harvester previously. As mentioned, other way to increase power generation is to magnify the motion which will be thoroughly discussed in the following section. There are two mechanisms will be explored to study the advantage of motion magnification, they are rack & pinion harvester and ball screw harvester.

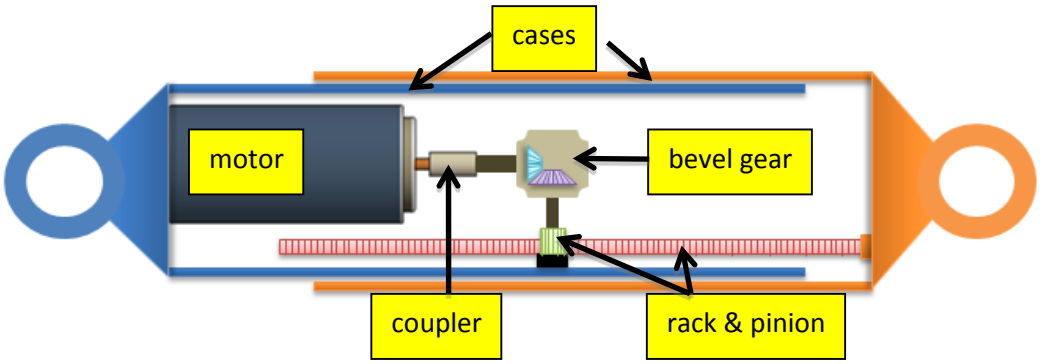

FIGURE 3.26 RACK AND PINION DESIGN OVERVIEW

The basic idea of rack & pinion harvesters is shown in Figure 3.24, where the linear motion of shock absorber is changed to rotational motion through rack and pinion mechanism. A 90 degree bevel gear is applied to change to rotational plane, thus the motor can be vertically placed inside the shock absorber for the purpose of size reduction.

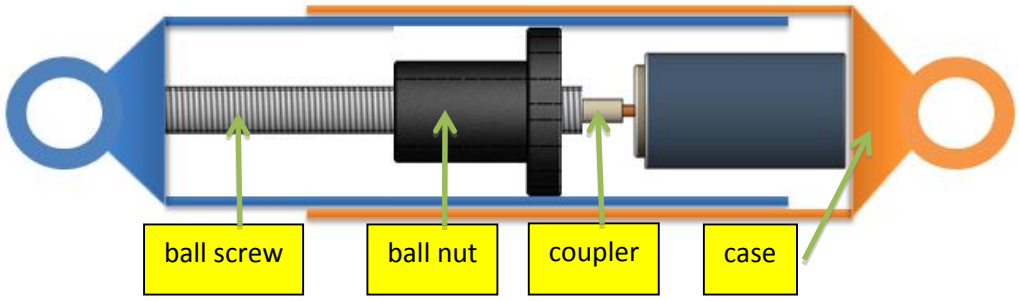

FIGURE 3.27 BALL SCREW HARVESTER DESIGN OVERVIEW

The design overview for the ball screw harvester is illustrated in figure 3.25. Rotational motion can be achieved by integrating ball screw mechanism. When ball nut is constrained to move linearly in one direction, the ball screw will be forced to rotation to accomplish linear motion of ball nut. A coupler is used to connect ball screw to motor shaft, thus to rotation motor for power generation.

3.2.1. MOTOR CHARACTERISTICS

Both rack & pinion harvester and ball screw harvester uses geared motor for power generation, it is very important to understand the motor characteristics. The rotational speed ω of the motor has the direct result on output power. The relationship between vertical velocities to rpm is expressed as

$$\omega = \frac{V}{2\pi r} \tag{3.13}$$

where V is suspension velocity and r is the pinion radius. In geared motor case, the rpm of motor is multiple of gear ration which lead to

$$\omega_m = R_G \omega \tag{3.14}$$

here, R_G is the gear ratio. After intensive research, the maximum shock velocity is found to 0.6 m/s and root mean square value of 0.3 m/s. Therefore, the root mean square value of motor input speed is 358 rpm.

The geared motor is considered for this design is because of simplicity and efficiency. The alignments and precisions can be done in a more professional way from geared motor manufacture. The mechanical power of the motor is expressed the product of torque and angular velocity

$$P_{mechanical} = T\omega \tag{3.15}$$

In general, the angular velocity is presented in rpm which needs to be converted into rad/s to calculate rotational power.

$$\omega_{rad/sec} = \omega_{rpm}\left(\frac{2\pi}{60}\right) \tag{3.16}$$

When considering linear force input for the shock absorber, the mechanical input power is then modified as

$$P_{mechanical} = Fv \tag{3.17}$$

here, F represent the force applied to the shock absorber and v is the induced shock velocity. The electrical power of the generator is then measured from the loaded object – resistor

$$P_{electrical} = \frac{V^2}{R} \tag{3.18}$$

here, V is the voltage generated and R is the shunt resistance. The generator also carries internal resistance. The maximum power output of the generator is calculated when load resistance is equal to generator internal resistance.

$$P_{maximum} = I^2 R_{total} = \left(\frac{V}{R_{total}}\right)^2 R = \frac{V^2}{\frac{R_m^2}{R} + 2R_m + R} \tag{3.19}$$

Differentiate the power equation, maximum power is found at $R_m = R$, where R_m is motor internal resistance.

The efficiency of the motor is expressed as the ratio between electrical power to mechanical power.

$$\eta = \frac{P_{electrical}}{P_{mechanical}} \tag{3.20}$$

Consider the basic function of shock absorber, damping force provide by shock absorber is evaluate based on power damping relation

$$P = CV^2 \rightarrow C = \frac{P_{electrical}/\eta}{V^2} \tag{3.21}$$

where C is the damping P is motor power, and V is shock velocity. Consider harvestable power from road roughness, actual damping for shock absorber and the motor's nominal rpm, a 117 watts geared motor from EBM-Papst is used for the rack and pinion design. The basic specifications are shown in Figure 3.26 and Table 3.5.

FIGURE 3.28 GEARED MOTOR FROM EBM-PAPST

The gear ratio is chosen to magnify the rotational speed by a factor of 9. Therefore, the input angular speed is reduced to 367 rpm at suspension speed of 0.3 m/s.

TABLE 3.5 EBM GEARED MOTOR SPECIFICATION

Manufacture	*EBM-Papst*	Gear Type	*Planetary*
Model	*BCI 63.55 PX 63-9*	Nominal Torque	*2.2 [Nm]*
Power Output	*117 [W]*	Nominal Speed	*367[Rpm]*
Gear Ratio	*9:1*	Nominal Current	*4.9 [A]*

3.2.1.1. MOTOR PERFORMANCE

The performance of the motor/generator is tested on lay machine with different rpms and shunt resistances. The results of power shunt resistance relationship are illustrated in Figure 3.27. Higher power output is presented with lower shunt resistance. The power can be reached to 100 watts at 2900 motor rpm with shunt resistance 0.8 ohm.

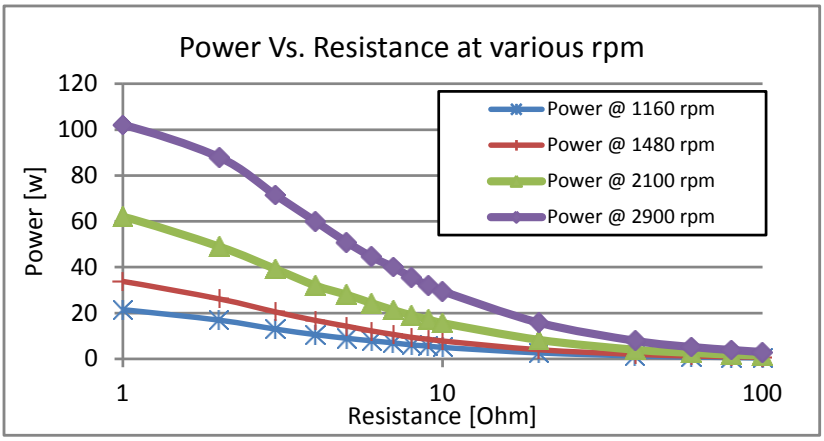

FIGURE 3.29 POWER OUTPUT TO EXTERNAL ELECTRICAL LOADS OF VARIOUS RESISTANCES

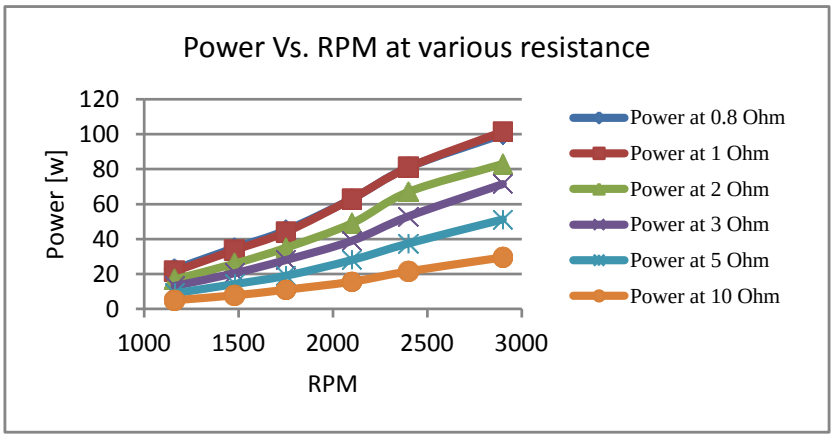

FIGURE 3.30 OUTPUT POWER ON THE EXTERNAL LOAD AT DIFFERENT MOTOR SPEED

The relationship between generated powers with rpm is plotted in Figure 3.28. Graph shows the higher speed implies higher power output a constant shunt resistance. For instant, the motor generates 63 Watts of power at 2100 RPM with 1 Ohm shunt resistance; it generates 81 Watts when the speed is boosted to 2400 RPM. The RPM is increased by 114% while the generated power is increased by 128% which is equivalent to square of velocity increment. Therefore, motion magnification will have significant effect on boosting power generation. Furthermore, the internal resistance of the motor is revealed to be 0.8 ohm which is also measured using a multimeter.

The motor is heavily loaded internally when shunted resistance is approaching to internal resistance. The internal load energy is dissipated as heat. The motor malfunctions when it is overheated. Since the vehicle is under vibration throughout the whole driving interval, the sustainability of motor is concerned. Although, we can achieve maximum power output with shunt resistance equal to motor internal resistance, heat caused by the same amount of energy consumed by motor will result problem. Here, choose 3 ohm shunt resistance as an example, the average power output at average suspension velocity of 0.3 m/s is 80 watts respect to Figure 3.28.

3.2.2. RACK & PINION HARVESTER

As previously discussed in this chapter, regenerated voltage is proportional to flux density, conductor velocity and conductor length. Hence, power is directly proportional to the conductor velocity square and flux density square. Due to space constraints and internal resistance, conductor length is not favored to magnify the voltage. In this chapter, the rack and pinion electromagnetic regenerative shock absorber will be further discussed. Based on the concepts on electricity generation, linear harvester was designed and simulated. The result of first prototype of single layer linear harvester does not show enough energy generation. Further simulation was done on different magnets configurations which shows much higher power density due to increase in flux density. Another way to increase the power generation is to magnify the motion. Magnify linear motion will create uncomfortable situations to riders or imply safety hazards, thus, rack and pinion mechanism is applied to change linear motion into rotational motion, and

gearbox is used to increase rpm to generate higher power. Suda [15] show the capability of self-powered vibration control using rack and pinion design. However, the experiments were conducted using a so called rack and pinion harvester and it does not has the characteristics of shock absorber. Therefore, an actual rack and pinion shock absorber prototype is built and evaluated in this section.

3.2.2.1. RACK & PINION

Rack and pinion is important on transmitting linear motion into rotational motion precisely. The backlash and friction should be well concern on the efficient transmission. More importantly, the safety issue should be included in the design. Force and stress analysis will be investigated for material selection and dimension determination. Starting from the generator's side, the force transmitted from generator is

$$T = F * r \rightarrow F = \frac{T}{r} \tag{3.22}$$

where T is the torque, F is the tangential force and r is the pinion radius. To further dig to stress level analysis, we need the area of the gear tooth which is expressed as the product of the face width and tooth thickness

$$A = W * t = W * \frac{p}{2} = W * \pi * \frac{d}{2N} \tag{3.23}$$

Here, *W* denotes as the face width, *t* is the tooth thickness, *p* is the circular pitch, *N* is number of pitches, and d represents pitch diameter. By knowing the force corresponding to assert area, the shear stress the rack and pinion experience will be known as

$$\tau = \frac{F}{A} \tag{3.24}$$

Hence, the safety factor of the transmission design is yield stress of the selected material over stress assert on rack and pinion.

$$SF = \frac{\Sigma}{\tau} \tag{3.25}$$

where, $\boldsymbol{\Sigma}$ denotes as yield stress. Understanding the shear stress is not the only stress acting on the rack and pinion, normal force acting during the transmission is also evaluated. As shown in Figure 3.29, the pressure point is where the pitch circle of the pinion and the pitch line of the rack meet at position *P*. The normal force transmitted from pinion to rack is calculated based on shear force and pressure angle Φ.

$$F_A = F_B * \cos(\Phi) \tag{3.26}$$

and the normal stress is given as the ration between normal force to contact area

$$\sigma = \frac{F_A}{A} \tag{3.27}$$

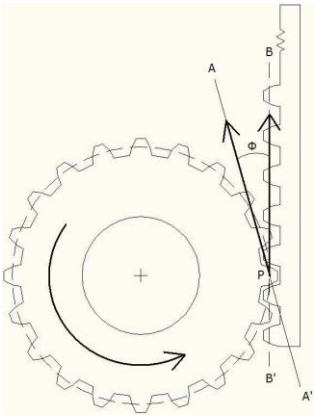

FIGURE 3.31 RACK AND PINION

Rack and pinion from SDP/SI, part number, A1X12MYK05300 and S10T05M032S0308 respectively are selection according to calculations for the design of rack and pinion prototype. Considering the compact size of shock design, with a safety factor of 2, rack and pinion with pinion face width of 3 mm and pitch diameter of 16 mm in stainless steel is employed.

3.2.2.2. SYSTEM LEVEL EXPERIMENTS

After studying the feasibility design of rack and pinion, a prototype is built to validate the harvestable energy as shown in Figure 3.30. The first prototype is manufacture to study the regenerative energy from suspension system, thus it is larger in diameter and further refine works will be applied on the retrofitted design.

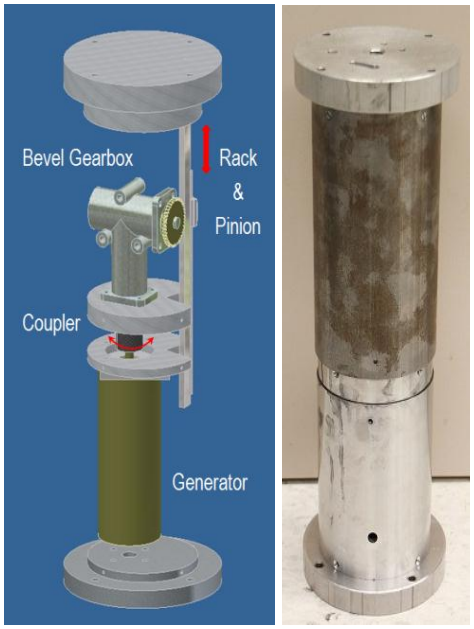

FIGURE 3.32 RACK AND PINION ELECTROMAGNETIC HARVESTER DESIGN AND PROTOTYPE

The whole system is integrated in the cylindrical shells with flat ends. Unlike traditional damper with end ring mounting, flat ends with flange are specially design for experimental examination. Since rack and pinion will have to match precisely, the rotational motion was constraint by employ a slat on lower layer and a pin on upper layer. The basic dimension is shown in Table 3.6.

TABLE 3.6 RACK & PINION ELECTROMAGNETIC SHOCK ABSORBER SPECIFICATION

Parameters	Specification
Upper Case Diameter	4 Inches
Lower Case Diameter	3.75 Inches
Compressed Length	12 Inches
Extended Length	18 Inches
Weight	20 lbs.
Upper Case Material	Stainless Steel
Lower Case Material	Aluminum
End Mounting	Aluminum in circular shape

The experiment set up was shown in Figure 3.31. ILD 1401 Laser displacement sensor from Micro Epsilon is used to acquire shock displacement at sample rate of 1000 points per second. A constant voltage of 15 volts is applied to power the sensor by EZ

Digital. The force of mechanical input is measure by piezoelectric based force sensor from PCB. All the displacement, force, and voltage output data are acquired and displayed on dynamic signal analyzer graphically from Hewlett Packard (HP 35670A). Due to the limitation of lab equipment, the vibration shaker in our lab cannot provide large force at high displacement. Therefore, human power is applied to give relative motion to the shock absorber. The data of displacement, force and voltage output are recorded.

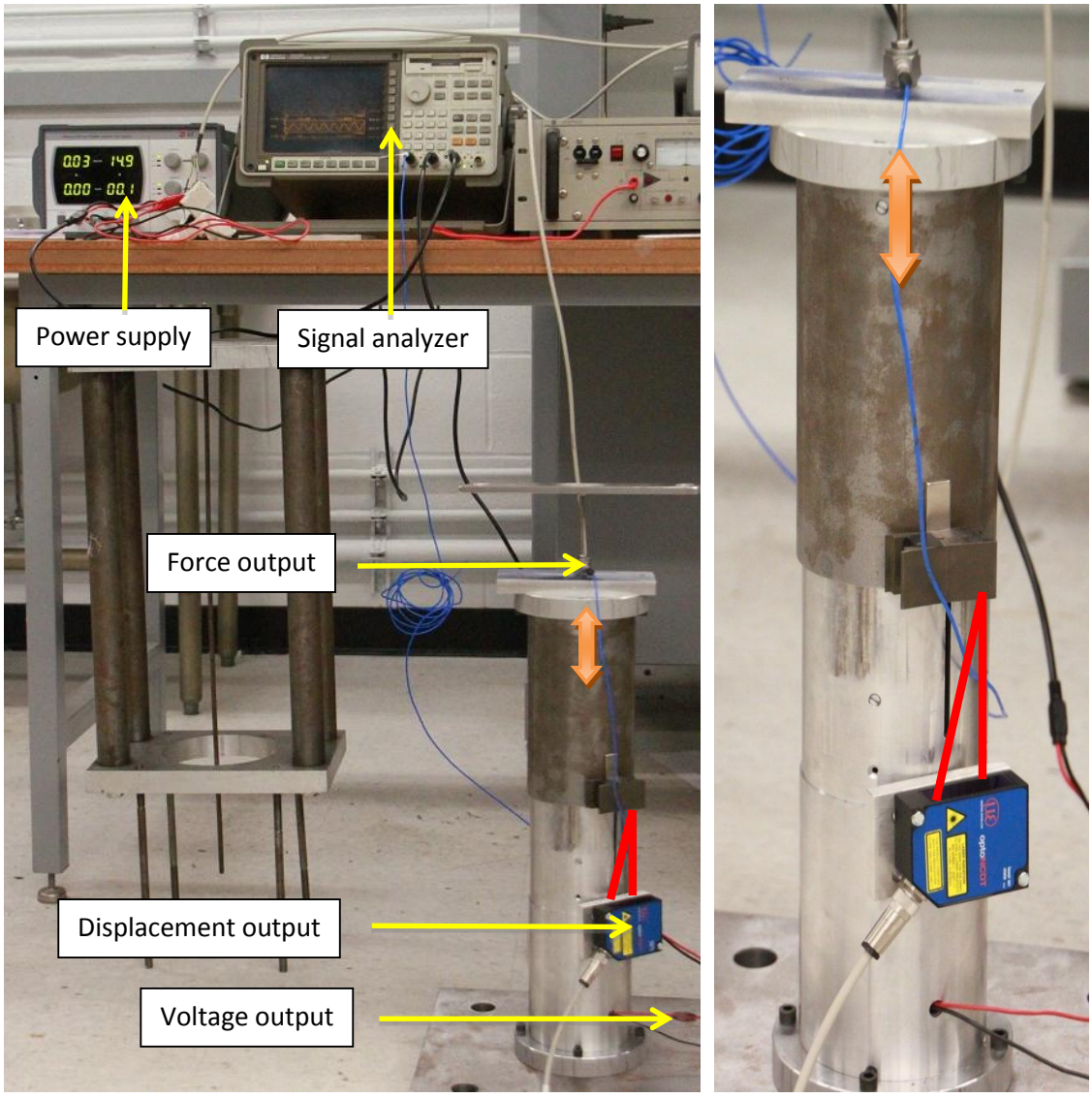

FIGURE 3.33 SYSTEMATIC VIEW OF EXPERIMENT SETUP

3.2.2.3. RESULTS

According to the experimental setup, there are three outputs measured. They are, shock displacement from laser displacement sensor; applied force using piezoelectric force sensor; and voltage output of the installed motor. All the data is acquired by the dynamic signal analyzer in time domain, and will be used to evaluate the performance of the shock absorber. Different shunt resistances of 3.3 Ohm, 4.7 Ohm, and 10 Ohm are applied to measure the output power of the harvester. Furthermore, open circuit is also studied in this section.

3.2.2.3.1. SHOCK DISPLACEMENT AND VELOCITY

The vertical displacements of the harvester are recorded and plotted. Figure 3.32 below shows the displacement curve in time domain with shunt resistance of 3.3 Ohm. According to the graph, the frequency of displacement curve response to force input is about 0.64 Hz and the excitation is nearly sine function. The root mean square value of shock displacement is 19.74 mm and the peak to peak displacement is 60 mm in average which lies within the typical shock strokes.

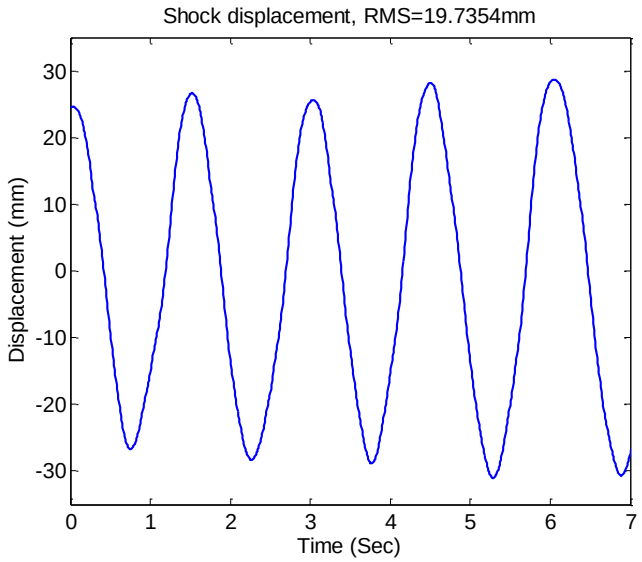

FIGURE 3.34 SHOCK DISPLACEMENT CURVE WITH 3.3 OHM RESISTOR SHUNT

The shock vertical velocity is calculated by taking direct difference respect to time variance. The filter is applied to eliminate both above 100 Hz high frequency and below 0.1 Hz low frequency noises. The velocity curve is plotted in Figure 3.33. The root mean square value of shock velocity over the measured time interval is 0.081 m/s and the peak velocity happens at 0.13 m/s by analyzing the figure graphically. Recall from the theoretical work and experimental results from Chapter 2. *This result is close to the super compact electrical car traveling at 25 mph on campus road*. However, in real life situation, the frequency of shock velocity curve is higher.

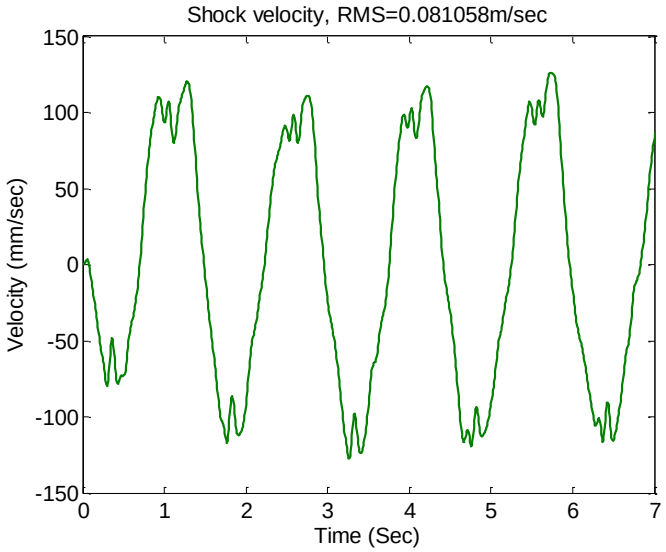

FIGURE 3.35 SHOCK VELOCITY PROFILE WITH 3.3 OHM RESISTOR SHUNT

3.2.2.3.2. FORCE AND MECHANICAL POWER

The shock vertical displacement and velocity profiles respect to force input are measured and studied in previous section. The input forces in time domain are also measured and processed. Figure 3.34 shows the input force in time domain during the force excitation. The root mean square value of input force is found to be 263.83 Newton with shunt resistance of 3.3 Ohm. However, the instant peak force can reach as high as 500 Newton.

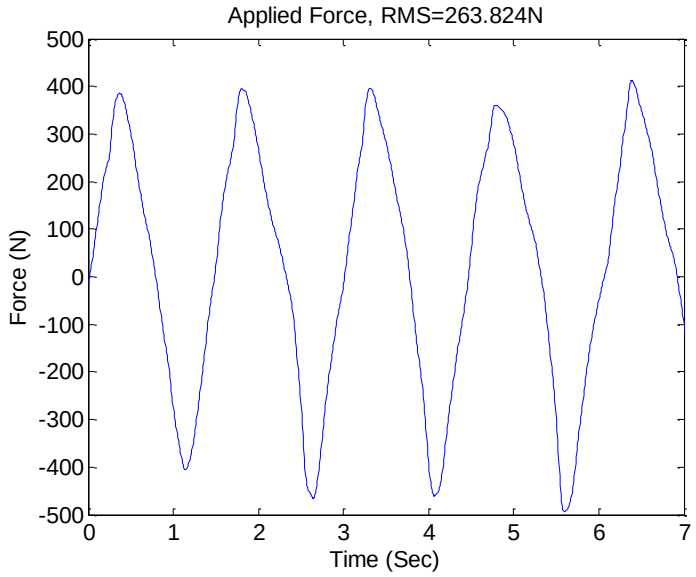

FIGURE 3.36 FORCE EXERT ON THE SHOCK WITH 3.3 OHM RESISTOR SHUNT

To study the efficiency of the harvester, force measurement is significant. Force input corresponding to mechanical power input to achieve the shock displacement at resultant velocity. The input mechanical power is simply calculated as the product of Force respect to velocity.

$$P_{mechanical} = FV \tag{3.28}$$

here, F represents the input force and V is the corresponding velocity profile. The input mechanical power is expressed in Figure 3.35. Similar to force and velocity profiles, input mechanical power profile is also statistic values in time domain and they are calculated as the absolute values so the frequency is doubled. Moreover, the mean value of input mechanical power is calculated. Here, it is shown as 20.17 Watts with 3.3 Ohm resistor shunt. More importantly, the peak power is more than 50 Watts

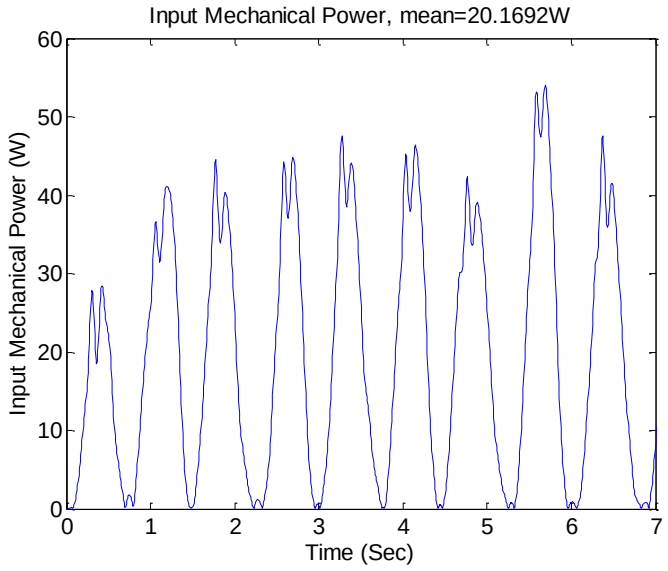

FIGURE 3.37 INPUT MECHANICAL POWER PROFILE WITH 3.3 OHM RESISTOR SHUNT

3.2.2.3.3. VOLTAGE AND ELECTRICAL POWER

Output power is one of the most important elements of this research project. In the lab setup, electrical power is dissipated by the power resistors. Voltage load across the resistor are recorded and studied for electrical power generation. Figure 3.36 illustrates the voltage curve happens at 3.3 Ohm shunt resistor.

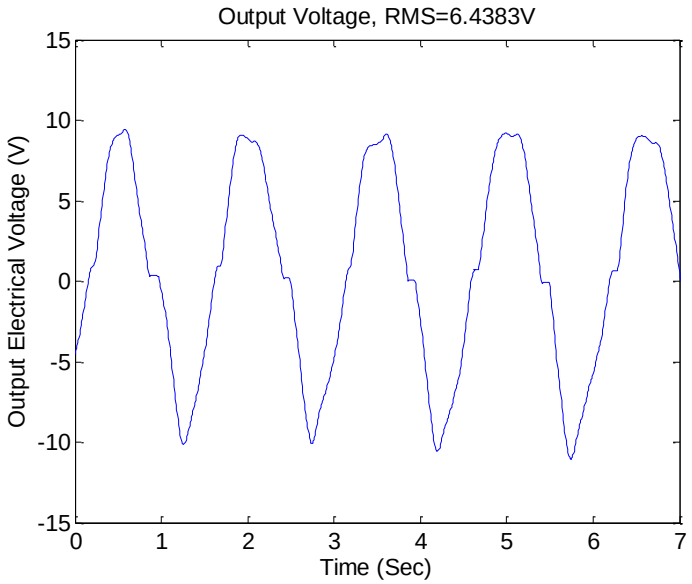

FIGURE 3.38 OUTPUT VOLTAGE PROFILE WITH 3.3 OHM RESISTOR SHUNT

The root mean square value of voltage output from the harvester is 6.44 volts and the peak voltage is around 10 volts. From the graph, curve is not smooth when approaching zero volts. This is because of the 180 degree motion shits of the harvester. Backlash plays an important role at switching signs.

Once the voltage curve is acquired and plotted, the electrical output power curve can be generated with the known shunt resistance. The Figure 3.37 shows the output electrical power curve with 3.3 Ohm resistor shunt.

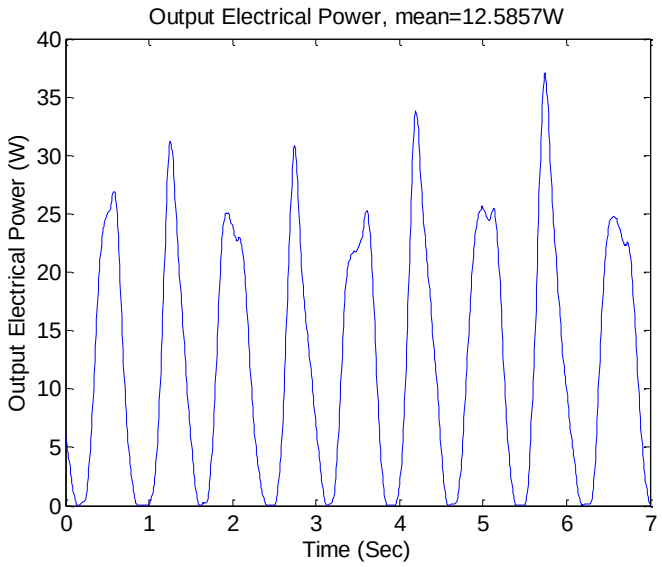

FIGURE 3.39 OUTPUT ELECTRICAL POWER WITH 3.3 OHM RESISTOR SHUNT

The mean power is also calculated by taking absolute values of the electric power which is 12.59 Watts. The peak electrical power output is about 38 Watts. The difference of mechanical power input and electrical power output is because of the friction in the system, the internal resistance of the motor coils, and the backlash of rack and pinion.

Referring to the experimental result from the electrical car, the suspension dissipative power is 14.57 Watts in mean value at shock velocity of 0.081 m/s root mean square value. This harvester can harvest 12.59 Watts of electrical power under 20.17 Watts mechanical power input at the same shock velocity with shunt resistance of 3.3 Ohm. Comparing to the theoretical work on power estimation, the mechanical power of 20.17 Watts is more than predicted dissipative power at the same shock velocity, which means

the damping provided by this regenerative shock absorber is larger than what need in the vehicle traveling at 25 mph on campus road. So we can increase the external resistor to achieve the ideal damping.

3.2.2.3.4. SYSTEM EFFICIENCY

This section evaluates the quality of power transmission from mechanical power input to electrical power output. Efficiency of transformation is implied and defined as input power divide by output power.

$$\eta = \frac{P_{mechanical}}{P_{electrical}} \tag{3.29}$$

Here, the efficiency of the rack and pinion system with shunt resistance of 3.3 Ohm is found to be 62.5%. With 20.17 Watts of mechanical power input, only 12.59 Watts of electrical power can be generated. There is a loss of 7.58 Watts energy during transmission and internal coil resistance.

3.2.2.3.5. FORCE DISPLACEMENT RELATION

Further studies are made on the characteristics of the rack and pinion harvester by plotting the input force and displacement output relation curve. Figure 3.38 illustrates the relationship between force input and displacement output with at 3.3 Ohm.

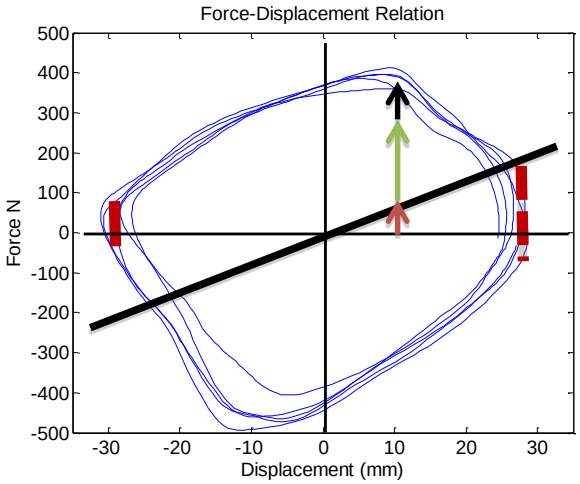

FIGURE 3.40 FORCE AND DISPLACEMENT RELATION WITH 3.3 OHM RESISTOR SHUNT

Under pure damping force, the relationship should be an ellipse. However, the graph shows a tilted ellipse. Result indicates the rack and pinion harvester does not only experience the viscous damping force, but give a stiffness force and frictional force as well. Therefore, the force is a function of stiffness, friction and damping system as shown in Figure 3.39. The constant force is shown at maximum displacement where no damping force exists due to zero shock velocity shown in dashed lines. Frictional force contributes certain amount to the total force. For instant, the force combination is revealed by three arrows in Figure 3.39, where red, green and black arrows represent stiffness, damping and frictional forces respectively. To understand the system better, modeling is necessary. However, there is no good understanding on harvester modeling so far.

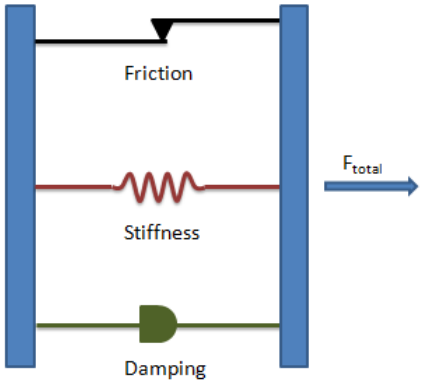

FIGURE 3.41 TOTAL FORCES EXPERIENCED BY THE EM HARVESTER

The total force experienced on the system is expressed as

$$F = kx + c\dot{x} + F_r \tag{3.30}$$

For harmonic motion of frequency ω and amplitude X,

$$x(t) = X\ sin\ \omega t \tag{3.31}$$

Therefore, the force equation becomes

$$F(t) = kX\ sin\omega t + cX\omega\ cos\omega t + F_r = kx \pm c\omega\sqrt{X^2 - x^2} + F_r \tag{3.32}$$

Here, the stiffness of the system is the slope of the ellipse's orientation as illustrated in black line.

$$k = \frac{\Delta F}{\Delta x} \tag{3.33}$$

The total energy dissipated by the damper is the area of the loop

$$\Delta W = \oint F dx \tag{3.34}$$

In the case of the 3.3Ohm resistor shunt, the stiffness of the harvester is estimated at $1.1x10^4$ N/m (typical suspension stiffness is about $2x10^4$ N/m). The total dissipative energy is estimated by adding all the areas which is about 28 N-m. ω is the frequency of the harmonic motion and it is 0.643 Hz or 4 rad/s. X is the shown as 0.03m. Therefore the damping is calculated as

$$c = \frac{\Delta W}{\pi \omega X^2} = \frac{28}{4\pi * 0.03^2} = 2475 \frac{Ns}{m} \tag{3.35}$$

In addition, the equivalent hysteresis damping constant is given as

$$h = c\omega = 9900 \frac{N}{m} \tag{3.36}$$

or a lost factor h/k = 0.9.

3.2.2.4. DISCUSSION

The performance of rack & pinion harvester with shunt resistance of 3.3 0hm is discussed and illustrated graphically in previous section. The experiments are also conducted with open loop and different closed loop resistances to study the effect of resistances on system performance of the harvester. Table 3.7 shows the overall experiment results for both open circuit and closed circuit at different resistances. The effects of shunt resistances on efficiency, power output and damping force are revealed in the table. Larger shunt resistance results in smaller the damping force. Please note that due to inconsistent of human power input, the motion amplitudes of the four cases are not the same.

TABLE 3.7 EXPERIMENT RESULTS OF DIFFERENT SHUNT RESISTANCES

Shunt Resistance	**3.3 Ohm**	**4.7 Ohm**	**10 Ohm**	**Infinity**
Displacement [mm]	19.74	23.32	26.37	26.01
Force [N]	263.82	278.60	265.81	149.90
Shock Velocity [m/s]	0.08	0.12	0.16	0.15
Motor Speed [RPM]	900	1287	1764	1656
Voltage [v]	6.44	8.91	12.53	12.54
Mechanical Power [W]	20.17	30.19	36.50	17.24
Electrical Power [W]	12.59	16.91	15.71	0
Efficiency [%]	62.4	56	43	0
Total Damping [Ns/m]	2475	1200	1364	591
Hysteresis Damping	9900	6193	7958	3183
Stiffness [N/m]	$1.1x10^4$	$2x10^4$	$1x10^4$	5000

The input force for 3.3 Ohm and 10 Ohm shunt system is about the same, but the shock velocity increased from 0.08m/s to 0.16 m/s, hence, the output voltage doubled from 3.3 Ohm to 10 Ohm. Increase in harvester's velocity results in increase in input mechanical power, but does not have significant effect on output electrical power. Thus, the efficiency of the system with increasing shunt resistance decreases. It is 62.4 % efficient for 3.3 Ohm resistor shunt, and it goes down to 43% for 10 Ohm resistor shunt. Another observation made is the damping force provided by the harvester: the lower shunt resistance the higher damping force. The damping force decreases from 2475 Ns/m with 3.3 Ohm resistor shunt to 591 Ns/m at open circuit. The 591 Ns/m damping is the contribution of friction, motor eddy current, etc.

Some people may question the influence of combination of damping, stiffness and frictional force on ride comfort. As mentioned previously, human are only sensitive to absolute acceleration. Moreover, there are also frictional and stiffness forces existing in traditional viscous dampers in reality. The dampers were initially design based on dry frictions and the air chambers inside the single-tube & twin-tube viscous dampers nowadays will have stiffness effects as well. Therefore, the existence of stiffness and frictional force in our current design will not cause uncomfortable situations for occupiers.

3.2.2.5. RACK & PINION HARVESTER CONCLUSION

Some researchers studied the feasibility of using rack and pinion mechanism for regenerative control, but haven't shown any possible design or efficiency of rack & pinion harvester. This is because the nature of hardware design makes difficulties to integrate rack and pinion mechanism into conventional shock size. This thesis focuses on the compact design of rack and pinion harvester and at the same time the energy transmission efficiency is discussed. A 90 degree bevel gear transmission is implemented to change the plane to rotation for geared motor. Therefore, the geared motor can be installed vertically to reduce the shock size. The performances of the harvester are investigated at different shunt resistance. The experimental results validate the capability of rack and pinion mechanism on energy recovering. Motion magnification shows a significant contribution in power generation. It is able to harvest most of the dissipated energy from vehicle shock absorbers. The shock dissipated energy at 25 mph on campus road is slightly higher than the harvested electrical energy from the rack and pinion harvester prototype at shunt resistance of 3.3 Ohm when all other parameters are matched. The result implies the high efficiency of the energy transformation by using rack and pinion harvester. However, the harvester's efficiency is at an acceptable range and it decrease with increasing shunt resistance when testing the harvester alone. The efficiency of the harvester goes from 62.4 % at 3.3 Ohm shunt resistor to 43 % at 10 Ohm shunt resistor. Moreover, with higher closed loop resistor load, the damping force provided by the harvester decrease. Therefore, by tuning the shunt resistance, varies damping forces can be achieved, thus more comfortable ride quality will be.

Although the rack and pinion design has good performance on energy harvesting, it has some drawbacks and need to be improved later. First, the size and weight of the harvester is unexpected. The diameter and weight of the harvester almost doubled when comparing with traditional viscous shock absorbers. This is due to the size of the bevel gear and motor. Smaller sustainable bevel gear may be applied with smaller generator to narrow down the size of the harvester. Another method is to change the design configuration by getting rid of bevel gear by placing the motor perpendicular to the rack. Secondly, the efficiency of the mechanism needs to be improved. The harvester prototype

experiences a significant amount of friction force due to rack and pinion transmission. One of the reasons is the imprecise and misalignment during design and machining process since the parts are not made continuously. Third, comprehensive modeling work is required to understand the effect of friction, motion transmission, inertia mass, motor constant, and elasticity on the harvesting performance as well as the vehicle dynamics. Model-based optimization should further be conducted. Last but not least, the testing equipment needs to be capable for conducting experiments, such as shaker. Pure human power is applied for powering the system due to insufficient lab equipment.

3.2.3. BALL SCREW HARVESTER

Due to the size constraint, rack and pinion design needs more precise improvements. Another mechanism of transmitting linear motion into rotational motion is by ball screw actuator. Some researchers show great interests in ball screw harvester. Not only ball screw is capable to energy generation, but also it is sufficient to provide enough force to migrate vibration. Suda [16] studied the energy generation and vibration control using ball screw harvester who claimed the sufficient forces can be achieved for active vibration control. Kawamoto, Suda, Inoue, and Kondo [23] modeled active suspension control using ball screw actuator. The experimental results validate the ability of vibration migration using ball screw actuator. In this section, the design of ball screw harvester is studied and the experiments on energy harvesting using ball screw harvester is conducted and analyzed.

3.2.3.1. HARVESTER DESIGN

There is significant advantage of ball screw design over screw. Balls within a ball nut are applied to reduce the contact force area thus to reduce frictional force. More importantly, balls are able to rotate as they travel on the ball screw. The rolling motions of balls have meaningful reduction on friction. Therefore, ball screw mechanism is applied for this test.

As mentioned in previous section on rack and pinion design, the nominal motor rotational speed is about 3000 rpm since we are using the same motor due to the

advantages of the motor, compact and efficient. The gear ratio of the geared motor we chose is 9:1. Therefore, the input shaft speed is 333 rpm according to equation below.

$$Shaft\ speed = \frac{Motor\ nominal\ speed}{Gear\ Ratio} \tag{3.37}$$

The input shaft speed is achieved by ball screw mechanism. The average shock velocity is said to be 0.3m/s shown in Chapter 2. In order to bring the shaft speed to about 333 rpm, ball screw pitch of 54mm is needed for the system as carried out by

$$Pitch = \frac{RPM_{input}}{Velocity_{shock} * 60s/m} \tag{3.38}$$

However, under the regular driving condition when test, the average shock velocity is about 0.15 m/s. Therefore, the pitch size can be half of original prediction. As a result, a ball screw with ball diameter and pitch of one inch is picked from Roton for our prototype purpose. The main components of ball screw harvester is determined and selected. In order to verify the performance of ball screw harvester, a prototype of ball screw harvester shown in Figure 3.40 is manufactured to run the experiments.

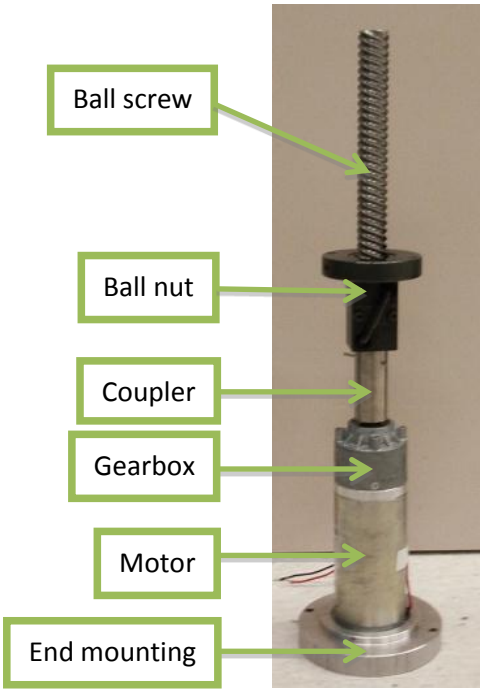

FIGURE 3.42 BALL SCREW PROTOTYPE

The prototype is only for conducting experiments, thus the outer cases for ball screw harvester is not designed. The motor is mounted on an aluminum disk which will be screwed on the ground. A coupler is applied to connect the ball screw and motor shaft together. On one end, the motor shaft is inserted in coupler and fixed with a set screw; on the other end, the ball screw is machined to insert in the other end of coupler and fixed by a pin. Therefore, the ball screw is coupled with motor shaft steadily.

3.2.3.2. SYSTEM OVERVIEW

The ball screw prototype is ready for conducting experiments. The systematic view of testing bed is shown in Figure 3.41. The harvester prototype is fixed on a two-mass-system integrated with linear guiding system. This is to prevent rotational motion of ball nut and achieve better accuracy and precision. As show, the coupled motor and ball screw is fixed on the lower plate with a disk and screws. The ball nut is fixed on the upper plate indirectly and it is driven by the motion of upper plate. As mentioned, the motion of the two plates are fixed to single axis motion, thus ball nut is only experiencing linear motion.

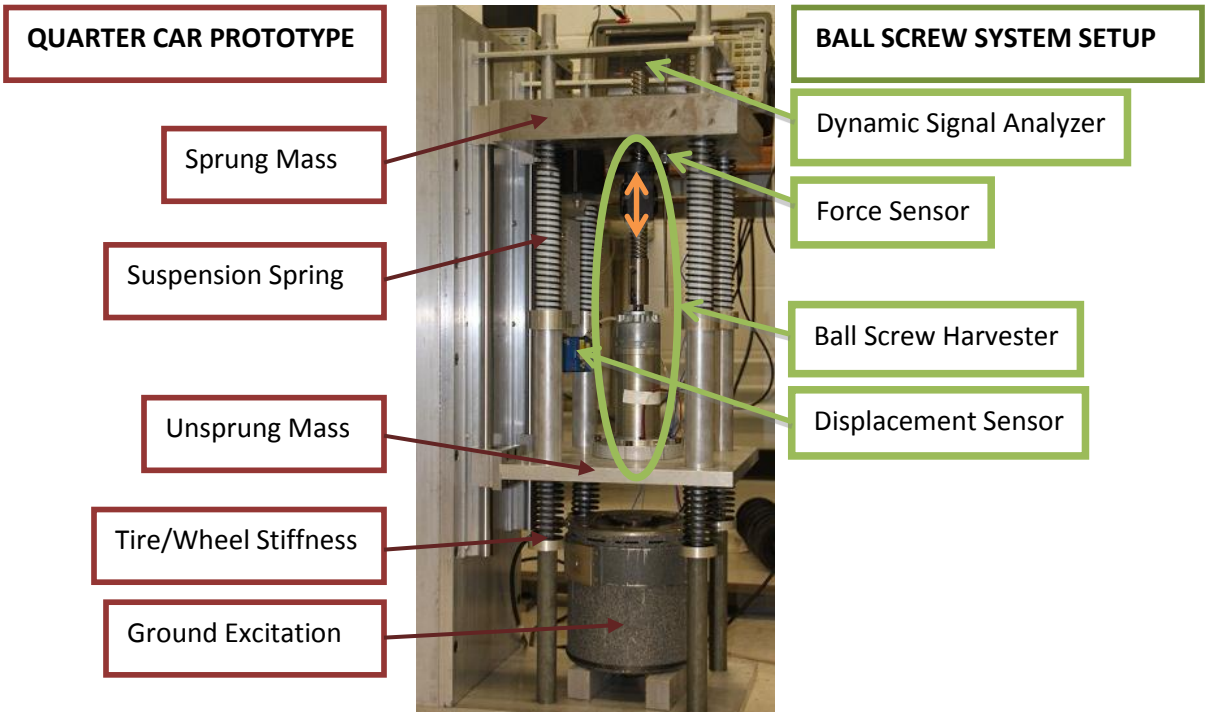

FIGURE 3.43 EXPERIMENT SETUP FOR BALL SCREW HARVESTER

In between ball nut and upper plate there is a pressure sensor shown in Figure 3.42. The purpose of pressure sensor is to measure the tensile and compressive forces experienced by the ball screw harvester. It is also used to verify the efficiency of the ball screw prototype by comparing mechanical work input to electrical work output which will be discussed later in this section.

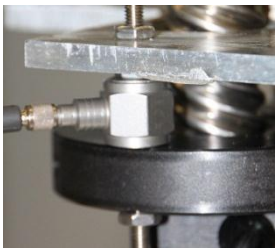

FIGURE 3.44 PRESSURE SENSOR MOUNTING

The shock displacement is measured by laser displacement sensor from Micro-Epsilon, the same displacement sensor used on the rack and pinion experiments. It is attached to the upper plate by strong permanent magnets and it takes relative motion of upper and lower plates which is also equivalent of linear motion of ball nut.

The output of displacement, force and voltage generated by motor is displayed with dynamic signal analyzer from HP. Figure 3.43 shows a set of data acquisition displayed in time domain. First window measures the force sensor dynamics; second window shows the voltage generated by the motor; the displacement value is plotted in the third window. Note that all the values are in voltage, a gage factor is applied to convert the acquired value to Newton, Watts, and millimeters respectively.

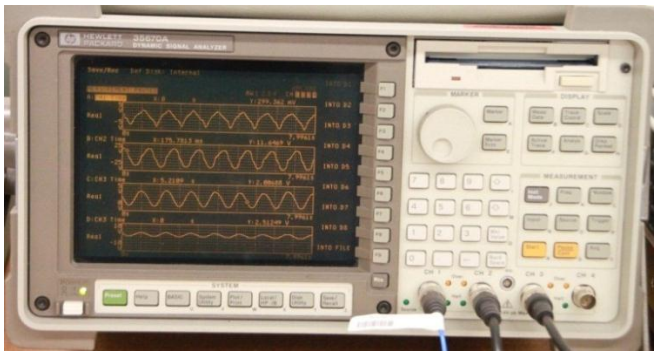

FIGURE 3.45 DYNAMIC SIGNAL ANALYZER

3.2.3.3. RESULT

There are three outputs of the testing system which are the vertical force experienced by the shock absorber, the voltage generation and relative shock displacement. They are measured to evaluate the performance of the shock absorber. The prototype is tested with open circuit, 10 Ohm, 4.7 Ohm, and 3.3 Ohm resistors shunt to understand the behavior of ball screw regenerative shock absorber.

3.2.3.3.1. DISPLACEMENT AND VELOCITY

Suspension displacement is the output response to force input. The relative harvester displacement in time domain with 10 Ohm shunt resistor is shown in Figure 3.44. The root mean square value of shock displacement is 14.01 mm.

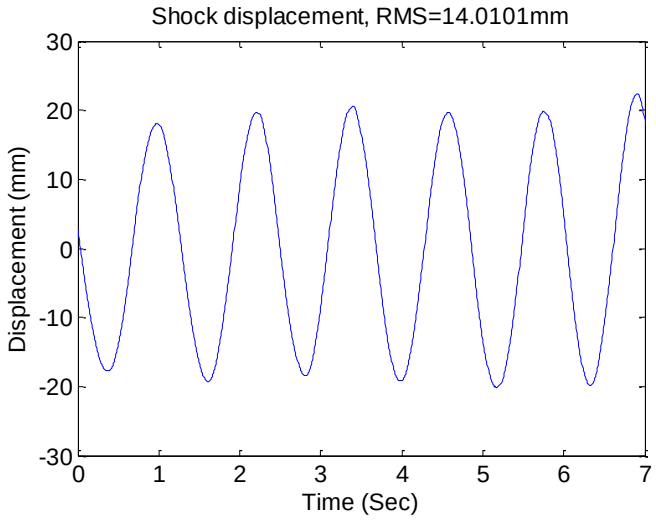

FIGURE 3.46 SHOCK DISPLACEMENT WITH 3.3 OHM RESISTOR SHUNT

The vehicle suspension velocity profile in time domain calculated by take the direct difference of displacement respect to time variance. The curve of velocity profile is plotted in Figure 3.45. Peak velocity of the experiment happens to be 0.1 m/s and the root mean square value of harvester velocity is only 0.073 m/s. Since power dissipated by shock absorber is proportional to shock velocity square, the low velocity response to low shock energy dissipation. In another words, low power dissipation also corresponding to

low power generation since the output power of the motor is directly related to rotational speed.

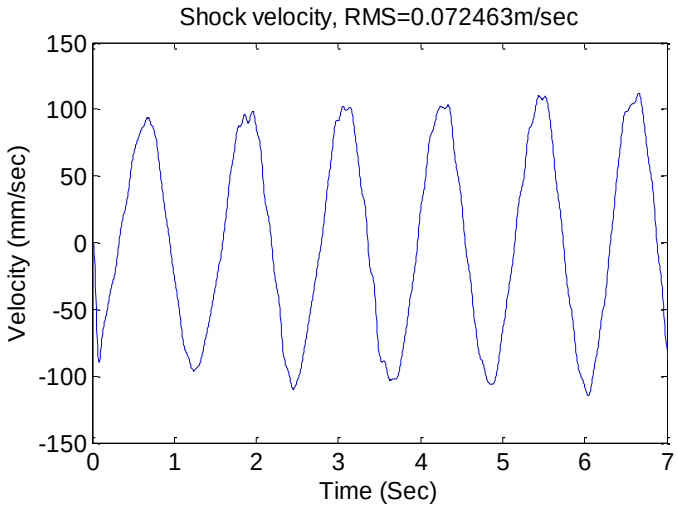

FIGURE 3.47 SHOCK VELOCITY PROFILE WITH 3.3 OHM RESISTOR SHUNT

3.2.3.3.2. FORCE AND MECHANICAL POWER

From road modeling chapter, road irregularity acts as ground displacement input and drives vehicle suspension to be displaced. Since the displacement input is the same as force input.

$$F = kx_0 \tag{3.39}$$

Here, k is the spring rate, and x_0 is the relative displacement. Force sensor is placed to measure the amount of force consumed during power generation. It is used to determine the mechanical power input for power generation. Otherwise, it is also applied to illustrate the electrical power generated while maintaining certain amount of mechanical force to migrate vibration. It is used to tune the damping force to improve vehicle isolation and handling.

Figure 3.46 shows the force curve of the ball screw harvester with 10 Ohm resistor shunt. High frequency is filtered out by the same filter in Chapter 2. The root mean square value of force exert on the ball screw harvester is 267.59 Newton with excitation frequency of 0.85 Hz. One observation from the force curve is the unevenness.

The tensile and compression force is different. More compression force is needed than tensile force to provide the same performance which implies the similarity to actual damper.

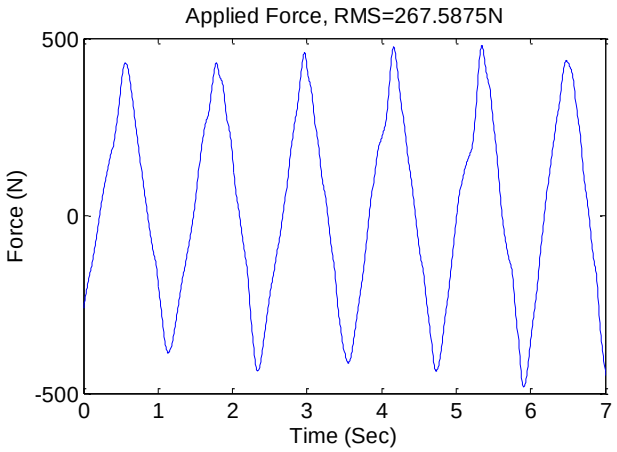

FIGURE 3.48 FORCE PROFILE EXERTED ON SHOCK WITH 3.3 OHM RESISTOR SHUNT

The mechanical power input is the product of force input respect to velocity.

$$P_{mechanical} = FV \tag{3.40}$$

Here, F is the force applied to the shock absorber and V is the shock velocity. The mechanical input power is plotted in Figure 3.47 below. To achieve 0.1 m/s of shock velocity, the peak mechanical power input is as high as 45 Watts at that instant. The mean power input is about 16.92 Watts to drive the shock at 0.073m/s root mean square.

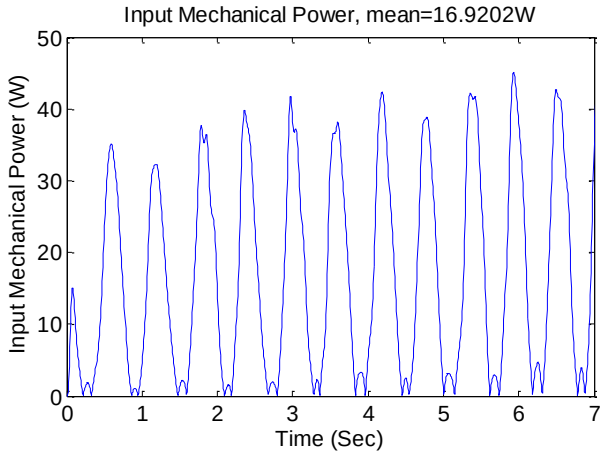

FIGURE 3.49 INPUT MECHANICAL POWER PROFILE WITH 3.3 OHM RESISTOR SHUNT

3.2.3.3.3. VOLTAGE AND ELECTRICAL POWER

Power is one of the most important factors we are considering and measuring. Regenerative shock absorber is meant to harvester the hundreds watts of dissipated energy from shock. A resistor is used to shunt the circuit. The voltage curve with shunt resistance of 10 Ohm is shown in Figure 3.47. The peak to peak voltage from the shock absorber is 30 volts and the root mean square value of the voltage is about 11.47 volts

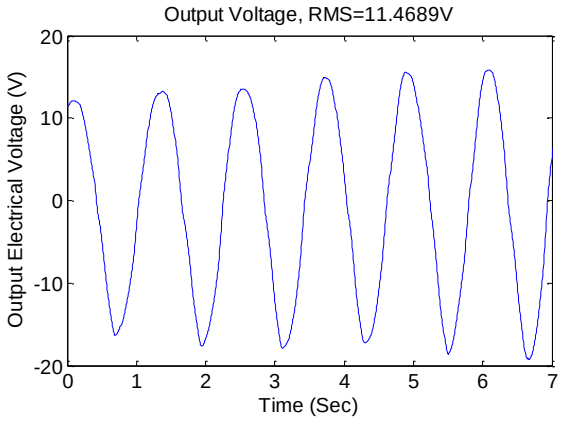

FIGURE 3.50 GENERATED VOLTAGE PROFILE WITH 3.3 OHM RESISTOR SHUNT

Power generated by the motor is calculated directly from the equation of electrical power generation and the power curve is illustrated in Figure 3.48.

$$P_{electrical} = \frac{Voltage^2}{Resistance} \tag{3.41}$$

Since power is a statistic value over time. Mean value of power is calculated to evaluate the performance of the regeneration. With the 10 Ohm resistance shunt at root mean square value of 0.073 m/s shock velocity, we are able to generate 13 watts of energy. Velocity has significant effects on power generation as discussed in previous chapter. 0.073 m/s is much lower than the actual situation. If at least 0.15 m/s shock velocity is achieved, more than 80 Watts of electrical power can be generated which is also verified from the motor power curve in previous section.

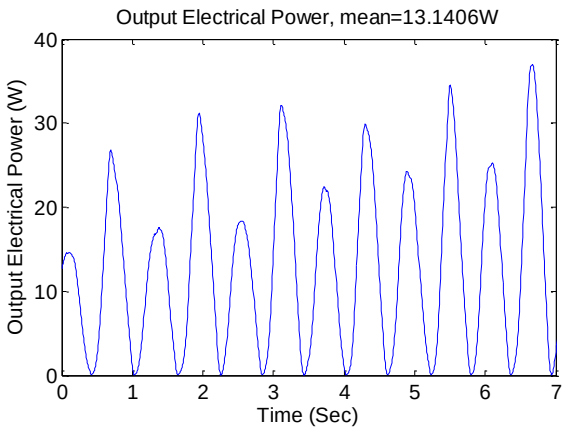

FIGURE 3.51 GENERATED POWER PROFILE WITH 3.3 OHM RESISTOR SHUNT

3.2.3.3.4. SYSTEM EFFICIENCY

As previously mentioned, the efficiency of transmission from mechanical power input to electrical power output is defined as

$$\eta = \frac{P_{mechanical}}{P_{electrical}} \tag{3.42}$$

Therefore, the efficiency of the system at shunt resistance of 10 Ohm is more than 77%. The result indicates the high efficiency of ball screw transmission. Most energy is transferred from mechanical input to electrical output. Rolling balls inside the ball nut have the significant contribution on friction reduction.

3.2.3.3.5. FORCE DISPLACEMENT RELATION

The damping characteristics of the electromagnetic harvester can be revealed as force displacement relation. Figure 3.51 shows the experimental result of the force and displacement relation. The result shows an ellipse shape, however, it is not horizontally placed. This indicates the damping is not the only force acting on the system. The stiffness of the harvester is also contributing some amount of force to the total residual force which is shown as the slope the of ellipse orientation. Therefore, the system can be viewed as hysteresis damping system where total force is equivalent to combination of stiffness force and damping force as illustrated in Figure 3.50.

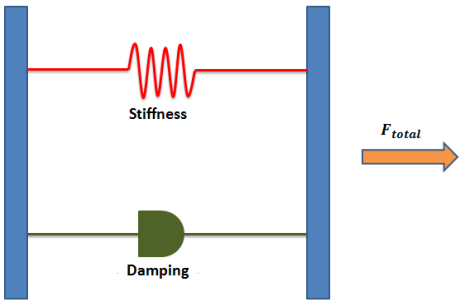

FIGURE 3.52 HYSTERESIS DAMPING MODELING

Total force is expressed as

$$F = kx + c\dot{x} \tag{3.43}$$

For harmonic motion of frequency ω and amplitude X,

$$x(t) = X\ sin\ \omega t \tag{3.44}$$

Therefore, the force equation becomes

$$F(t) = kX\ sin\omega t + cX\omega\ cos\omega t = kx \pm c\omega\sqrt{X^2 - x^2} \tag{3.45}$$

Here, the stiffness of the system is the slope of the ellipse's orientation

$$k = \frac{\Delta F}{\Delta x} \tag{3.46}$$

The total energy dissipated by the damper is the area of the loop

$$\Delta W = \oint F dx = \int_0^{2\pi/\omega} (kX\ sin\omega t + cX\omega\ cos\omega t)(\omega X\ cos\omega t) dt = \pi\omega c X^2 \tag{3.47}$$

The damping of the system is calculated as

$$c = \frac{\Delta W}{\pi\omega X^2} \tag{3.48}$$

The total stiffness of the harvester is found approximately to be 16 kN/m at 10 Ohm. The stiffness is partially contributed by springs of the two-mass system. Furthermore, modeling is required to understand the mechanism and to give more physical insights.

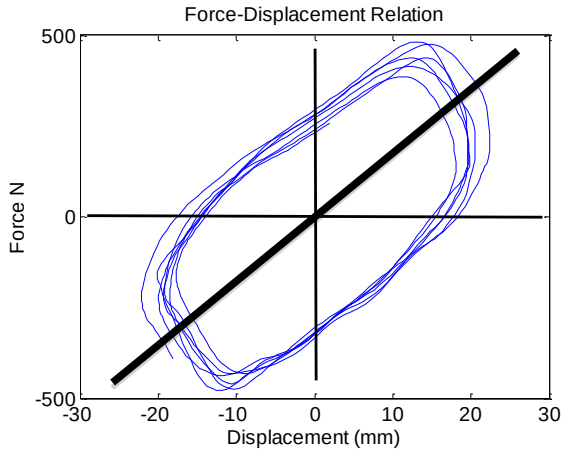

FIGURE 3.53 FORCE AND DISPLACEMENT RELATION CURVE

The damping provided by the harvester is also calculated using the formula mentioned in previous section. Result shows the high damping force can be achieved with 10 Ohm resistor shunt which is about 2080 Ns/m in total.

3.2.3.4. DISCUSSION

The experiments are conducted with different resistor shunts which are 3.3 Ohm, 4.7 Ohm, 10 Ohm, and Infinity (open circuit). This section will explore the difference when using different shunt resistors.

Table 3.8 shows the test result with all resistors shunt and open circuit. Less force is required to provide the same electrical power output when resistor load is larger. With 3.3 Ohm resistor shunt, it required 370 N (rms) to get 13.12 Watts of electrical power, while only 267 N (rms) of force is required to achieve same amount of electrical power output. This is because of internal power consumption is relative smaller at higher resistance load, thus less back EMF is produce to encounter the motion.

TABLE 3.8 EXPERIMENT RESULTS AT DIFFERENT SHUNT RESISTANCES

Shunt Resistance	3.3 Ohm	4.7 Ohm	10 Ohm	Open
Displacement [mm]	11.3	12.2978	14.01	15.6
Force [N]	370	368	267	230
Shock Velocity [m/s]	0.04	0.05	0.07	0.09
Motor Speed [RPM]	862	1143	1541	1936
Voltage [v]	6.58	8.23	11.47	14.72
Mechanical Power [W]	14.44	19.27	16.92	14.98
Electrical Power [W]	13.12	14.48	13.14	0
Efficiency [%]	90.9	75.16	77.66	0
Stiffness [N/m]	$2x10^4$	$2.2x10^4$	$1.6x10^4$	$1.3x10^4$
Damping [Ns/m]	7661	5501	2080	1015
Hysteresis Damping Constant	27508	24689	9337	5919

Another observation is that the shock velocity varies at the same work required. With the same mechanical power input of 14.5 Watts, the rms values of shock velocity is only 0.04 m/s at 3.3 Ohm resistor, and it increase to 0.09 m/s when change to open circuit (infinity resistor). The increased velocity results in increasing output voltage.

Furthermore, harvester's efficiency decreases when load resistance increase. With increase of load resistance, less electrical power is dissipated from resistor. At the same force input, efficiency of 3.3 Ohm resistor shunt is over 90 %. However, it decreases to 75 % when shunt resistance increases to 4.7 Ohm. Last but not least, the damping force can be tuned by changing shunt resistance. When the shunt resistance increases from 3.3 Ohm to 10 Ohm, the damping force provided by the harvester decreases from 7661 Ns/m to 2080 Ns/m which is about the same damping as mid-sized car.

3.2.3.5. BALL SCREW HARVESTER CONCLUSION

Following the idea of ball screw designs explored by previous researchers; a ball screw prototype is manufactured with integrated gearbox for motion magnification. Different from other researchers' studies on ball screw harvester, this thesis approaches and emphasizes on the energy harvesting and efficiency aspects based on feasibility studies made by other researchers. The gearbox implementation has significant influence on power generation.

In this section, a ball screw electromagnetic harvester is examined and studied. The experimental results show the potential of ball screw harvester. The point contact with ball rolling has great influence on friction reduction. Therefore, a higher efficiency is achieved. The shock velocities from the experiments are relatively smaller than desired velocity. This is due to in sufficient lab equipment. The excitation is purely human powered. As a result, none uniform sign wave excitation is applied and excitation frequency is not uniform as well. Over 80 Watts of electricity can be produced with shock absorber velocity of 0.15 m/s. Further studies are made to show the effect of changing resistance values. The results show reduction in force when load resistance increases. Less force is required to produce same electrical power output and at the same time achieve higher shock velocity. Vice versa, soft damper is tuned when load resistance increases. Further work needs to be done to acquire better solution. Shaker excitation should be included in future work to assure the uniform in excitation inputs. Modeling work needs to be implemented to understand the behavior of the system.

3.3. CONCLUSION

The designs of electromagnetic harvesters are discussed based on optimizing power generation in this chapter. Linear harvester design is introduced to increase power generation by increasing magnetic flux density. Both radial and axial magnets are used to guide magnetic flux in loops. Moreover, double layer design is explored for power optimization. Electromagnetic finite element results show a great improvement of the new linear electromagnetic harvester comparing our initial prototype. The generated power is eight times and the power density increases by a factor of 5. Rotational harvesters are further discussed on behalf of motion magnification. Both rack & pinion harvester and ball screw harvester designs are disclosed in this chapter. Geared motors are applied to increase the rotation motion by a factor of 9 thus generators are running at optimal states primarily. Experimental results show more than 100 watts of electrical power can be generated using rotational motor with motion magnification. However, there are significant frictional and stiffness forces existing on our first prototypes. Therefore, modeling works are preferred to acquire better understanding of rotational

harvester dynamics. Both linear and rotational harvesters have shown great interest in power generation. The comparison of all three harvesters will be discussed in the following chapter.

4. HARVESTER EVALUATION

Traditional shock absorbers are designed to dissipate vibration energy induced by road unevenness. Regenerative shock absorbers are introduced to replace the traditional ones because they can achieve better vibration isolation by tuning damping coefficient and at the same time harvest vibration energy and stored it in forms of electricity to reduce car engine's load. Three electromagnetic harvesters are designed and their performances are studied, they are linear electromagnetic harvester, rack & pinion electromagnetic harvester, and ball screw electromagnetic harvester.

4.1. DESIGN PERSPECTIVE

Since shock absorbers are integrated in vehicle suspension system and there is limited space available for installation, the size of regenerative shock absorber is one of the biggest concerns. According to the table of harvester specifications below, linear harvester takes the advantage of being most compact regenerative harvester. Although ball screw harvester has the same outer diameter as linear harvester, the initial and extended lengths of ball screw harvester is not expected.

TABLE 4.1 DESIGN SPECIFICATIONS OF ELECTROMAGNETIC HARVESTERS

Design	**Linear harvester**	**Rack & pinion**	**Ball screw**
Outer Diameter	*2.76 inches*	*4 inches*	*3 inches*
Compressed	*11 inches*	*15 inches*	*18 inches*
Extended length	*20 inches*	*22 inches*	*27 inches*

On the other hand, the drawback of rack and pinion harvester design is the outer diameter. The diameters of conventional shock absorbers used in most vehicles nowadays are between 2 to 2.5 inches. 4 inches in diameter might be too big to install in suspension system.

4.2. ENERGY HARVESTING PERSPECTIVE

Undoubtedly, power generation is also one of the most considerable parameters to evaluation the harvesters. Regenerative shock absorbers are meant to harvester vibration energy to power car electronics, thus to increase fuel efficiency. The amount of energy can be regenerated by all three shock absorbers are contributes a major factor of harvester evaluation. According to the table of power regeneration below, all three harvesters shows great potential of power regeneration. Ball screw harvester shows the most power regeneration if the same shock velocity achieved at 0.25 m/s. The power regeneration is 167.6 Watts. Rack & pinion harvester is predicted to generate 123 Watts, but the damping force is relatively higher than the other two harvesters. Linear harvester shows 104 Watts of total power with reasonable damping force. The drawback is the large coil internal resistance of the harvester, most power is consumed internally. Therefore, ball screw harvester is favored.

TABLE 4.2 POWER REGENERATION

Power Regeneration	**Linear harvester**	**Rack & pinion harvester**	**Ball screw harvester**	**Viscous shock**
Tested electrical power	N/A	12.6 Watts At 0.08 m/s	13.14 Watts At 0.07 m/s	NA
Predicted electrical power	52.2 & 66.6 Watts	110 Watts At 0.25 m/s	120 Watts At 0.25 m/s	NA
Total power at 0.25 m/s RMS	104.4 & 123.2 Watts	123.05 Watts 62.5% efficient	167.6 Watts 77.7% efficient	94 Watts
Equivalent damping [Ns/m]	1664 & 1964	2475	2080	1500

4.3. SAFETY PERSPECTIVE

From users' perspective, safety often ranks NO. 1 when weight the overall performances. According to sensitivity discussion in Chapter 2, damper not only is used for vibration migration, but also to achieve a safer ride. It has direct influence on vehicle vertical acceleration and tire-ground contact force which are corresponding to ride

comfort and ride safety respectively. Failure of regenerative shock absorber will cause serious problems. Recall from the design of all three harvesters, rack and pinion harvester shows a more reliable design. The winding for wire coil in linear harvester is made of plastic for eddy current reduction. There is no linear guiding or pin nut to constraint the motion. Small bending of shock absorber will cause failure. Moreover, the design of radial magnets is by combining four arc radial magnets, thus strong repel force inside the radial magnets become a potential hazard. For ball screw harvester, the torsional force of ball nut respect to ball screw is inevitable and the tensile force on the coupler experiences a limit. Ejection of coupler due to high tensile force will result damage of harvester. Rack and pinion harvester is constraint with single axial motion only and it does not experience high torsional force between two cylindrical cases because of bevel gear transmission. From safety perception, rack and pinion is chosen.

4.4. OVERALL RATING

All three harvesters show great potential of regenerative harvesters. From design's point of view, linear harvester shows the best interest of having similar dimensions as conventional shock absorber. Rack & pinion harvester also shows potential on size reduction. From energy harvesting perspective, all three harvesters are able to generate over hundred Watts of power and provide reasonable damping. Ball screw harvester is the best while considering both energy and damping; on the side of safety aspect, rack and pinion is favored. Depending on how people weight each performance, the best design varies. Rack & pinion harvester is bigger in diameter; there is still space for size reduction. The first rack & pinion prototype was not made precisely; some hardware parts can be resized to be smaller. The linear harvester is yet to be designed and manufactured. Therefore, some design specifications are not determined. However, in order to constrain the single axial motion, the outer diameter of the linear harvester will definitely increase. More importantly, the repel force existing in the radial magnets might create failure. Ball screw harvester shows great power generation due to motion magnification. However, torsional force and tensile force create a problem and the size of ball screw harvester is also considerable to redesign.

CHAPTER 5 SUMMARY AND FUTURE WORKS

5. CLOSURE

The primary function of vehicle suspension system is to reduce the vibration transmitted from ground due to road irregularity. Conventionally, the vibration energy is dissipated to the environment as heat through shock absorber. The existing energy brought us attention to start a new type of shock absorber, the regenerative generation. Different from conventional shock absorber, regenerative shock absorber can utilize the relative motion of shock absorber, and convert it into electricity and store the energy to battery for later use by using electromagnetic mechanism. By applying regenerative shock absorber, we are able to input less heat waste into environment, and at the same time improve vehicles' fuel efficiency by 10% theoretically according to Figure 1.1.

5.1. SUMMARY

The study of regenerative shock absorber consists of understanding the amount of harvestable energy on shock absorbers and the performance of EM harvesters and the vibration performance. To understand the vibration energy induced by road irregularity, a vehicle-ground model including road roughness, vehicle parameters, traveling speed was created then ride comfort, road safety, and power are analyzed. Theoretical results show hundred watts of energy are available in suspension system. The sensitivity of the power, ride comfort, and ride safety to different vehicle parameters was further analyzed. Experiments were conducted to estimate the power by measuring the relative strokes of shock absorber on both campus and highway. Numerical results show that regenerated power is only sensitive to tire stiffness. The higher tire stiffness contributes the larger amount of harvestable vibration energy from suspension. However, higher tire stiffness also contributes worse ride comfort and less safe ride. Suspension damping has major influence on ride comfort and safety. Optimal damping for ride safety conflicts with ride comfort. Therefore, compromised parameters need to be determined. Experimental

results show the potential of vibration energy induced by road irregularity. Hundreds Watts of power can be recycled from shock absorbers on classed C road at 65 mph.

On the side of harvester design, the first prototype gives us a taste of sweetness. However, 16 watts of energy is not what our project aims for. As mentioned, our goal is to harvest hundreds watts of energy from all four shock absorbers. Therefore we moved forward to redesign. In order to generate more energy, we have to increase the flux density, conductor length or to magnify the conductor velocity. Increase in conductor length will result in larger volume and internal resistance which is not favored for designing compact regenerative shock absorber and will not be discussed. Therefore, the two approaches on flux increment and motion magnification are adopted.

Different from the first single layer prototype, the proposed design has two layers of magnets with implementation of radial magnets to guide the flux inside the air gap. Finite element analysis using ANSYS is adopted to understand the improvement of using radial magnets and double layer design and different arrangements are studied. Result shows the significant improvement in flux density. The new proposed design will have five times more energy density then the initial design. The peak flux density in the wire coils increases from 0.28 to 0.8 Tesla which mean the regenerated power from double layer design is able 8 times than initial design. The prototype is waiting to be manufactured and assembled to test the power output. The improvement of the new design of shock absorber brings us the tradeoff on price. The redial magnets are rare on market which shoots the price higher compare with passive shock absorbers.

We also apply rack & pinion and ball screw mechanism to change the linear motion into rotational motion and a gearbox is used to magnify the rotational motion to harvest more energy. As tested with the rack and pinion design and ball screw design, we are able to generate hundreds watts of energy each shock absorber. The improvement from the previous design shifts the energy harvesting idea to hundred watts. The results are more impressive; however, the drawbacks are also very considerable. The main concern about the regenerative shock absorber is the friction lost on motion transmission. The current design of regenerative shock absorber experiences significant amount of frictional force.

This is because of some false dimension of design. Other drawbacks are the size and weight of the shock absorber. The second phase prototype is expecting to be redesigned and modified. Ball screw harvester also show great potential in energy harvesting perspective, however it is too long for real time implementation and the tensile & torsional force might also cause problems.

Before the shock absorber can be installed on the real car or bus, it needs to be tested on the experimental model. In order to design better energy regenerative shock absorber, we moved forward to build a quarter car models to test the shock absorber. The quarter car model is simply modeled as spring-mass-damping system. The design parameters have the same ratio of a typical passenger car. All designs of the shock absorbers will be tested on the experimental model and modify accordingly before it can installed to the actual passenger vehicle.

The research of regenerative suspension system receives a lot of attention and support. First of all, this project is supported by New York State Energy Research and Development Authority (NYSERDA). Since there are more than 270 million vehicles moving on the U.S. territory, the success of regenerative shock absorber will have great influence on energy efficient vehicle industry and save millions gallons of fuel consumption annually. With the support from NYSERDA and the University, we have built the first half scaled prototype of regenerative shock absorber in year 2008, which is able to generate 16 Watts of energy for the full scaled shock absorber. The results impressed us validate the feasibility of energy harvesting from vehicle suspension. The design received first place on that year senior design competition (URECA). Besides, the idea of energy harvesting from vehicle suspension received a lot more attention from media such MIT press, Physic.org, New York Times etc. Furthermore, the university took a step forward to support our project by offering us a small electrical vehicle and university bus to examine the actual size shock absorber.

From the day the idea of regenerative shock absorber was explored to the progress we have received today, we are enthusiastic to convey our energy to make the regenerative shock absorber more practical to be marketable. Not only have we improved the design to

harvest more energy, but also seeking to have a better and more reliable shock absorber. We believe we will have the regenerative shock absorber installed on the passenger cars and benefit both the users and environment in short future.

5.2. FUTURE WORK AND DIRECTION

The feasibility and potential of rack & pinion, ball screw, and linear harvesters are studied and analyzed theoretically and experimentally. Result shows great interest of power output using motion magnification. The next steps are to model the rack & pinion and ball screw harvesters, to design an electrical circuit to stored energy and to conduct vibration control. So far, only a few researches are done on ball screw and rack and pinion harvester modeling, and only simple circuit designs using AC-DC converter and DC-DC booster are investigated for energy harvesting. It is significant to study the physical force and inertia of the system for safety investigation. It is also important for circuit design because it has direct effects on harvesting efficiency. Different duty cycle will contribute great difference. From the vibration control aspect, passive damping with constant shunt resistor will no longer satisfy our requirements. To achieve better vibration migration, semi-active or active suspension control using feedback controls are worthy to invest further.

5.2.1. HARVESTER MODELING

Mathematically model the harvester system is an important skill to analyze and characterize the system. Karnopp [24] model the generated force, mechanical time constant and electrical time constant mathematically to study the feasibility of linear electrodynamic variable shock absorber. In this thesis, rotational harvesters are evaluated by considering both mechanical and electrical power of the overall system. There is no actual model of the transmission of rack and pinion or ball screw design. In fact, it is important to understand the limit of rotational harvester by considering inertia, backlash, torsion, motor parameters, frictions and transmission. Kawamoto, Suda, Inoue, and Kondo [23] have done a simple modeling on ball screw transmission by taking only inertia and torque into account.

5.2.2. CIRCUIT DESIGN

After studying the harvestable energy existing from regenerative shock absorber, the next step is to build an electrical circuit to store the electricity. The study of circuit design is also very important because it has direct effects of charging efficiency. The power generated by the shock absorber is in AC power, and it needs to be converted into DC to charge the battery. Sometimes, the regenerated voltage is not enough to charge the battery, thus a DC to DC booster is required to meet the charging barrier by shunt the circuit. Different duty cycle length contributes different charging efficiency. The basic circuit design is also illustrated by Nakano, Suda, and Nakadai [13]. A battery is charged after going through AC-DC converter and DC-DC booster. Lallart and Guyomar [25] investigate the optimal switching circuit for low output voltage based on Synchronized Switch Harvesting on Inductor (SSHI). Yet there is still a blank space to explore the optimal circuit design to have maximum power stored at high efficiency.

5.2.3. CONCURRENT VIBRATION CONTROL AND SELF-POWER SUSPENSION CONTROL

Back to the basic function of shock absorbers, the vibration isolation is considered. Since electromagnetic harvester provides a shortcut for semi-active or active control by tuning load resistance, the vibration migration of vehicle suspension system is favored by many researchers. Different control methods are developed to achieve better vibration isolation. Traditionally, PID controls are favored. As the level of satisfaction increases, researchers start to combine different control method together to achieve better control strategy such as PI controller with anti-windup [26] and PI sliding control [27]. Another commonly used control method is using feedback control. Displacement, velocity, acceleration and force can act as feedback parameters to apply proper actuating force to counter the vibration [26, 28, 29, 30]. Aside with feedback control, feed forward control is also explored by some researchers [31]. Moreover, skyhook control is popular due to the excellence in isolation performance [9, 32, 33] and adaptive control combining with other control methods are well developed for vehicle suspension isolation [34, 35, 36, 37]. Nowadays, the H_2, $H_{infinity}$, LQG, and LQR control are used in modern days [30, 38, 39].

REFERENCE

[1] News Archive, Press Release, U.S. Department of Energy 2010
www.energy.gov/news/archives
[2]Motor Vehicle Fuel Consumption and Travel in the U.S., Department of Transportation, 2007
www.dot.gov
[3] Advance Technologies and Energy Efficiency, Fueleconomy.gov 2010
http://www.fueleconomy.gov/FEG/atv.shtml
[4] Transportation Statistics Annual Report, the US Bureau of Transit Statistics, 2010
http://www.rita.dot.gov/
[5] Bose Suspension System, Bose 1997 - 2010
http://www.bose.com/controller?url=/automotive/bose_suspension/index.jsp
[6] Michelin Active Wheel, Michelin 2010
http://www.michelin.com/corporate/actualites/en/actu_affich.jsp?id=13730&codeRubrique=58&lang=EN
[7] D. Karnopp 'Power Requirement for Vehicle Suspension Systems', Vehicle System Dynamics 21: 1, 65 – 71

[8] N. Hammad 'Electric Utilization of Vehicle Damper Dissipated Energy' Electronics Research Institute, AEIC 2003

[9] Suda, Nakano (1998) 'Hybrid Suspension System with Skyhook Control and Energy Regeneration' Vehicle System Dynamics, 29:1, 619-634

[10] Fodor Graduate Research Assistant, M.G. and Redfield, R (1993) 'The Variable Linear Transmission for Regenerative Damping in Vehicle Suspension Control', Vehicle System Dynamics, 22:1, 1-20

[11]James A. Stansbury, 'Regenerative Suspension with Accumulator System and Methods', Patentdocs,
http://www.faqs.org/patents/app/20090229902
[12] Okada, Harada, and Suzuki 'Active and Regenerative Control of an Electrodynamic-Type Suspension', JSME International Journal, C:40 – 2, 1997

[13] Nakano, Suda, and Nakadai, 'Self-powered active vibration control using a single electric actuator', Journal of Sound and Vibration, 260 (2003) 213 – 235

[14] Lei Zuo, Scully, Shestani, and Zhou, 'Design and characterization of an electromagnetic energy harvester for vehicle suspensions', Smart Material and Structure, 19 (2010)

[15] Suda, Yoshihiro and Shiiba, Taichi (1996) 'A New Hybrid Suspension System with Active Control and Energy Regeneration', Vehicle System Dynamics, 25:1, 641 – 654

[16] Nakano, Kimihiko (2004) 'Combined Type Self-Powered Active Vibration Control of Truck Cabins', Vehicle System Dynamics, 41:6, 449-473

[17] Ping Hsu 'Power Recovery Property of Electrical Active Suspension Syetems' San Jose State University, IEEE

[18] Velinsky, Steven A. and White, Robert A. (1980) 'Vehicle Energy Dissipation Due to Road Roughness', Vehicle System Dynamics, 9: 6, 359 – 384

[19] Lei Zuo, Samir A. Nayfeh (2003) 'Structured H2 Optimization of Vehicle Suspensions Based on Multi-Wheel Models' Vehicle System Dynamics 40: 5, 351 – 371

[20] Hamid D. Taghirad, E. Esmailzadeh (1997) 'Automobile Passenger Comfort Assured Through LOG/LQR Active Suspension' Journal of Vibration and Control

[21] L.Zuo, S.A. Nayfeh (2003) 'Low Order Continuous-time Filters For Approximation of the ISO 2631-1 Human Vibration Sensitivity Weightings', Journal of Sound and Vibration 459-465

[22] Babak Ebrahimi (2009) 'Development of Hybrid Electromagnetic Dampers for Vehicle Suspension Systems', A Ph.D Thesis, University of Waterloo

[23] Kawamoto, Suda, Inoue, and Kondo (2007) 'Modeling of Electromagnetic Damper for Automobile Suspension' Journal of System Design and Dynamics, Vol. 1, No. 3

[24] Karnopp, Dean (1989) ' Permanent Magnet Linear Motors Used as Variable Mechanical Dampers for Vehicle Suspension Systems' Vehicle System Dynamics, 18:4' 187 – 200

[25] Lallart and Guyomar (2008) 'An Optimized Self-powered Switching Circuit for Non-linear Energy Harvesting with Low Voltage Ouput', Smart Material and Structures. 17

[26] Kerber, Hurlebaus, Beadle and Stobener (2007) 'Control Concepts for an Active Vibration Isolation System' Science Direct, Mechanical Systems and Signal Processing

[27] Sam, Osman, and Ghani (2004) ‘A Class of PI Sliding Mode Control with Application to Active Suspension System’ Science Direct, Systems and Control Letters, 217-223

[28] Kim, Hwang, Kee, and Yi (2001) ‘Active Vibration Control of a Suspension System Using an Electromagnetic Damper’ Chonnam National University

[29] Xing, Xiong, and Price (2005) ‘Passive-active Vibration Isolation Systems to Produce Zero or Infinite Dynamic Modulus’ Science Direct, Journal of Sound and Vibration, 286, 615-636

[30] J.T. Scruggs (2009) ‘An Optimal Stochastic Control Theory for Distributed Energy Harvesting Networks’ Science Direct, Journal of Sound and Vibration, 320, 707-725

[31] Nayfeh, Zuo (2005) ‘Modified LMS Feed Forward Control for Vibration Isolation with Actuator Limits’ International Design Engineering Technical Conference, Long Beach

[32] Ryba, D. (1993) ‘Semi-active Damping with an Electromagnetic Force Generator’, Vehicle System Dynamics, 22: 2, 79-95

[33] D. Karnopp (1995) ‘Active and Semi-active Vibration Isolation’ ASME Conference, CA

[34] Nayfeh, Slotine, Zuo (2005) ‘Model Reaching Adaptive Control for Vibration Isolation’, IEEE Transactions on Control Systems Technology Vol. 13, NO. 4

[35] Huang, Lin (2003) ‘Adaptive Fuzzy Controller with Sliding Surface for Vehicle Suspension Control’ IEEE Transactions on Fuzzy Systems, Vol. 11 NO. 4

[36] Huang, Chen (2006) ‘Adaptive Sliding Controller with Self-tuning Fuzzy Compensation for Vehicle Suspension Control’ Science Direct, Mechatronics 607-622

[37] Alleyne, Hedrick (1995) ‘Nonlinear Adaptive Control of Active Suspensions’ IEEE Transactions on Control Systems Technology, Vol.3 NO. 1

[38] ELMadany, Abduljabbar (1999) ‘Linear Quadratic Gaussian Control of a Quarter-Car Suspension’, Vehicle Sysem Dynamics, 32:6, 479-497

[39] Sam, Ghani (2000) ‘LQR Controller for Active Car Suspension’ University of Teknologi Malaysia, IEEE